RADIAL FLOW ENERGY DISSIPATOR FOR CULVERT OUTLETS

by

Raymundo Aguirre
Walter L. Moore

Research Report Number 92-1

Performance of Circular Culverts on Steep Grades

Research Project 3-5-66-92

Conducted for

The Texas Highway Department

In Cooperation with the
U. S. Department of Transportation, Federal Highway Administration
Bureau of Public Roads

by

CENTER FOR HIGHWAY RESEARCH
THE UNIVERSITY OF TEXAS
AUSTIN, TEXAS

November, 1967

PREFACE

The research reported herein is a study of the performance of a new type of culvert flow energy dissipator in which flow parallel to the culvert axis is transformed into supercritical radial flow. Dissipation of energy is caused by the formation of a hydraulic jump which, due to the characteristics of radial flow, exhibits a degree of stability of position not found in the common parallel flow hydraulic jump on a horizontal basin floor. Experiments were conducted to determine the jump stability, velocity reduction and degree of angular uniformity of the radial flow attained from the proposed geometric schemes. A second report on this project entitled, "Culvert Outlet Energy Dissipator Incorporating Radial Flow and a Transverse Sill" will be issued in the near future.

The authors are grateful to numerous individuals for providing them with technical assistance and/or encouragement during all phases of the present investigation.

The authors thank Dr. Frank D. Masch for his interest and numerous helpful comments throughout this study. Thanks go to Dr. Clyde E. Lee and Dr. Milo W. Weaver for reviewing the present work and making many helpful comments.

The authors are grateful for the laboratory assistance provided by Mr. Ben Stanbury during the early stages of construction of the model, and Messrs. John U. Miller and John D. Christner during later construction and the collection and processing of data.

Acknowledgement is made to the Texas Highway Department and the U. S. Bureau of Public Roads for providing financial support for the project as well as numerous suggestions and comments during the progress of the investigation.

The opinions, findings, and conclusions expressed in this publication are those of the authors and not necessarily those of the Bureau of Public Roads.

Raymundo Aguirre
Walter L. Moore

ABSTRACT

A model study was performed on a new type of energy dissipator for culvert flow. In this structure, the culvert flow drops along a steep chute, which ends at its intersection with the horizontal bottom of the stilling basin. As the flow impinges on the horizontal bottom, it is caused to spread rapidly, thus avoiding separation from the flared wingwalls. At the same time, the flow is changed from parallel to radial flow, and again to parallel flow in the downstream channel.

The combination of this supercritical radial flow and the required tailwater depth results in the formation of a hydraulic jump whose leading edge occurs along a circular arc, thus it is referred to as a circular hydraulic jump. The required tailwater for such a hydraulic jump admits substantial variations while the position of the jump itself is varied by a relatively short distance.

The stability of jump position was investigated for several geometric arrangements which included variations in wingwall flare angle, channel width, and entrance channel bottom configuration. The largest change in tailwater depth for a given change in jump position was admitted by the basin with the longest flared wall region. The absolute tailwater depth required to hold the hydraulic jump at a given position within the stilling basin was also investigated. The smallest required tailwater depth was found for the basins with the larger wingwall flare angle.

Velocity measurements were made near the basin bottom, at different distances from the jump, in order to investigate the degree of angular uniformity of the flow and the efficiency of the stilling action. In all cases, higher velocities were found along the centerline than in any other region. In several cases the centerline velocity was low enough to suggest the feasibility of the proposed structure as an economical energy dissipator. In others, additional velocity reduction was considered desirable.

TABLE OF CONTENTS

LIST OF FIGURES

LIST OF SYMBOLS

b	Width of entrance channel
B	Width of downstream channel
c	Pressure head correction for bottom curvature
D	Diameter of circular culvert pipe
F_b	Nominal Froude number at the bottom of entrance channel drop
F_t	Froude number at the upstream end of the entrance channel vertical curve
g	Free-fall acceleration due to gravity force
L	Projected length of flaring wingwalls on a plane parallel to the centerline of the channel
L_x	Distance along the channel centerline, from leading edge of hydraulic jump to section of velocity measurement
p	Pressure on boundary of potential flow
p/γ	Pressure head on channel bottom
r	Radius of curvature of entrance channel bottom vertical curve
v	Measured velocity near bottom of channel
V_b	Nominal velocity at the bottom of entrance channel drop
$V_{\text{℄}}$	Measured velocity near bottom of channel and along the channel centerline
V_m	Mean velocity of flow in downstream channel
V_t	Velocity of flow at the upstream end of the entrance channel vertical curve

x	Distance along the centerline, from the upstream end of the flaring wingwalls to the leading edge of the hydraulic jump
x_u	Distance along the solid boundary, from intersection of solid boundaries to end of free streamline of potential flow
y_b	Nominal depth of flow at the bottom of entrance channel drop
y_t	Depth of flow at the upstream end of the entrance channel vertical curve
y_2	Downstream or sequent depth of flow at the hydraulic jump
y_u	Depth of flow in uniform region of potential flow
z	Height of drop of entrance channel bottom
α	Deflection angle between tangent to downstream end of entrance channel vertical curve and horizontal bottom
β	Angle between the two halves of any horizontal line projected on the curved portion of the entrance channel
Δ	Symbol which indicates a change in the quantity which it precedes
θ	Angle between flaring wingwall and the centerline of the channel
$\rho V^2/2$	Kinetic energy per unit volume of flow

Chapter I

INTRODUCTION

The usual single pipe or box culvert is considerably smaller in cross-sectional area than the channel immediately upstream and downstream from it. The reduced area indicates that relatively high flow velocities exist in the culvert. These high velocities are a major factor contributing to the potential for scour at culvert outlets. Even when flow in the culvert occurs at low velocity and within the range of subcritical flow, it will normally reach or exceed critical velocity at the end of the culvert barrel, unless flow in the outlet channel is deep enough to submerge critical depth in the culvert.

Downstream from the end of the culvert barrel, the flow tends to retain its confined shape and a separation zone usually results between the flow and the wingwalls. A considerable distance downstream from the end of the culvert, the flow finally reaches the full width of the channel and, unless tailwater is high, it will continue down the channel at high velocity with a high scouring potential.

Object

The present investigation is an exploratory model study of the performance of a proposed culvert outlet structure. It is

intended to investigate the feasibility of use of the proposed structure as a flow energy dissipator.

Such a structure permits the flow to drop along a steep slope into a horizontal stilling basin with flared wingwalls. As the flow impinges on the basin floor, high pressures are developed which cause the flow to spread rapidly and stay in contact with the wingwalls. Also, as a result of the immediate spreading action, the flow is transformed from parallel flow into radial flow.

The characteristics of radial flow are such that depth and Froude number change rapidly as the flow progresses downstream. Thus a hydraulic jump may form which admits a wide variation of tailwater depth, while the jump position is changed by only a short distance.

It was felt that the outlet structure proposed herein would overcome a number of undesirable characteristics of present basin designs. Since the flow spreads rapidly between wingwalls, formation of the hydraulic jump for a given tailwater level may occur closer to the end of the culvert barrel than for the case of parallel or nearly parallel flow. Such behavior would allow construction of a relatively short basin. Also, the proposed structure may provide a higher margin of safety, since tailwater for a given flow rate may be materially reduced without causing the jump to move downstream beyond the end of the stilling basin.

Another attractive aspect of the proposed structure would be its flat, horizontal basin bottom. This feature would simplify

construction, prevent accumulation of sediments and debris, and facilitate drainage after a storm. It was reasoned that velocities would need to be substantially reduced by the formation of the hydraulic jump before the flat basin bottom could be considered acceptable.

Scope and Limitations

The present study included investigation of several performance characteristics of the proposed structure. The stability of the hydraulic jump was determined by relating the jump position, the required tailwater depth, and the entering Froude number. Also, in order to study the degree of spreading and stilling action, velocity measurements were made within the region of the hydraulic jump, and depths of flow were measured along radial lines upstream of the jump.

The performance characteristics mentioned above were investigated for eight different geometric arrangements of the proposed structure. These included combinations of two wingwall flare angles, two entrance bottom configurations, and two widths of the downstream channel. For each geometric arrangement, the stability of the jump was tested at twelve values of the entering Froude number. To obtain the twelve values of Froude number, four flow rates were used and each flow rate was run at three different flow depths. The ranges used for flow rate, Froude number, wingwall

flare angle, ratio of downstream to entrance channel width were set in accordance with values that may be expected to occur under field conditions.

The present investigation was limited to a rectangular culvert section at the entrance of the proposed structure, and to a flat, horizontal stilling basin bottom.

Present Basin Designs

The study of the performance of different types of stilling basins at culvert outlets has been the object of numerous investigations. As a result, several standardized designs have been offered which make use of combinations of sills, baffles, impact walls, etc. to reduce the energy of the culvert flow. Usually each design is best suited for a certain given range of outlet flow conditions, and will be either unsafe or uneconomical if operated outside such range. Several of the presently existing designs will be described in the following paragraphs.

One of the simplest energy dissipators is the straight drop spillway, commonly installed in small drainage structures. One form of such structure is that known as the box inlet drop spillway, which is simply a rectangular box open at the top and at the downstream end (2)*. A design of this type of box has been

---

* Numbers in parentheses indicate the corresponding numbered reference in Bibliography.

developed by the U. S. Soil Conservation Service for general use. However, for culvert use, it appears applicable only where topography is steep enough to permit a straight drop at the culvert outlet.

Another simple form of energy dissipation results when the culvert flow is discharged at a downward angle into a depression in the outlet channel (4). Such depression would have an ungrouted rock-lined bottom sloping gradually downward and then more steeply upward to the outlet channel bottom elevation. The ungrouted bottom would permit complete drainage of the pool left after a flood. However, design information for this type of structure is not available.

A concrete stilling basin for pipe culvert outlets has been developed by the Public Works Department of New South Wales, Australia (1). A sketch of this basin is shown in Figure I. 1. The basin has vertical walls which flare out from the end of the pipe at an angle of 17^{o} from the centerline. The width of the basin varies from 1.17D (pipe diameter) at its upstream end to 3.67D at its downstream end. The length of the basin measured along the centerline is 4.17D. The bottom of the basin slopes downward from the end of the pipe at a slope of 1:4 (vertical to horizontal) for a distance of 2D and then continues horizontally for a distance of 1.5D. It then slopes upward at a slope of

1 : 1.5 for a distance of 0.5D and ends at a vertical sill 0.17D high. The height of the wingwalls varies from 1.25D at the end of the pipe to 1D at the downstream end of the basin.

Model tests of this basin indicate that the flow will reach the full width of 3.67D at the downstream end of the basin. Under low tailwater conditions, the basin will discharge at or near critical depth over the sill. The design of the P. W. D. basin was developed for short culverts on moderate slopes. It is recommended that use of this basin be limited to flows with specific energy less than 2D, which for the flow depth of D, corresponds to a Froude number of approximately 1.4. A possible objection to this basin lies in the difficulty of obtaining complete drainage of the bottom depression after a flood.

For culverts which are expected to operate at specific energy in excess of 2D, an impact type energy dissipator is recommended. This type of energy dissipator is built with a wall interposed across the flow, such that all or most of the flow is forced to change direction locally, and is then discharged in the original direction into a concrete basin.

One well known impact type energy dissipator is the Bradley-Peterka design of the U.S. Bureau of Reclamation Basin VI (5), shown in Figure I.2. This energy dissipator consists of a headwall at right angles with the culvert axis, and parallel training walls a distance of approximately 3D apart. Between the training walls, and a

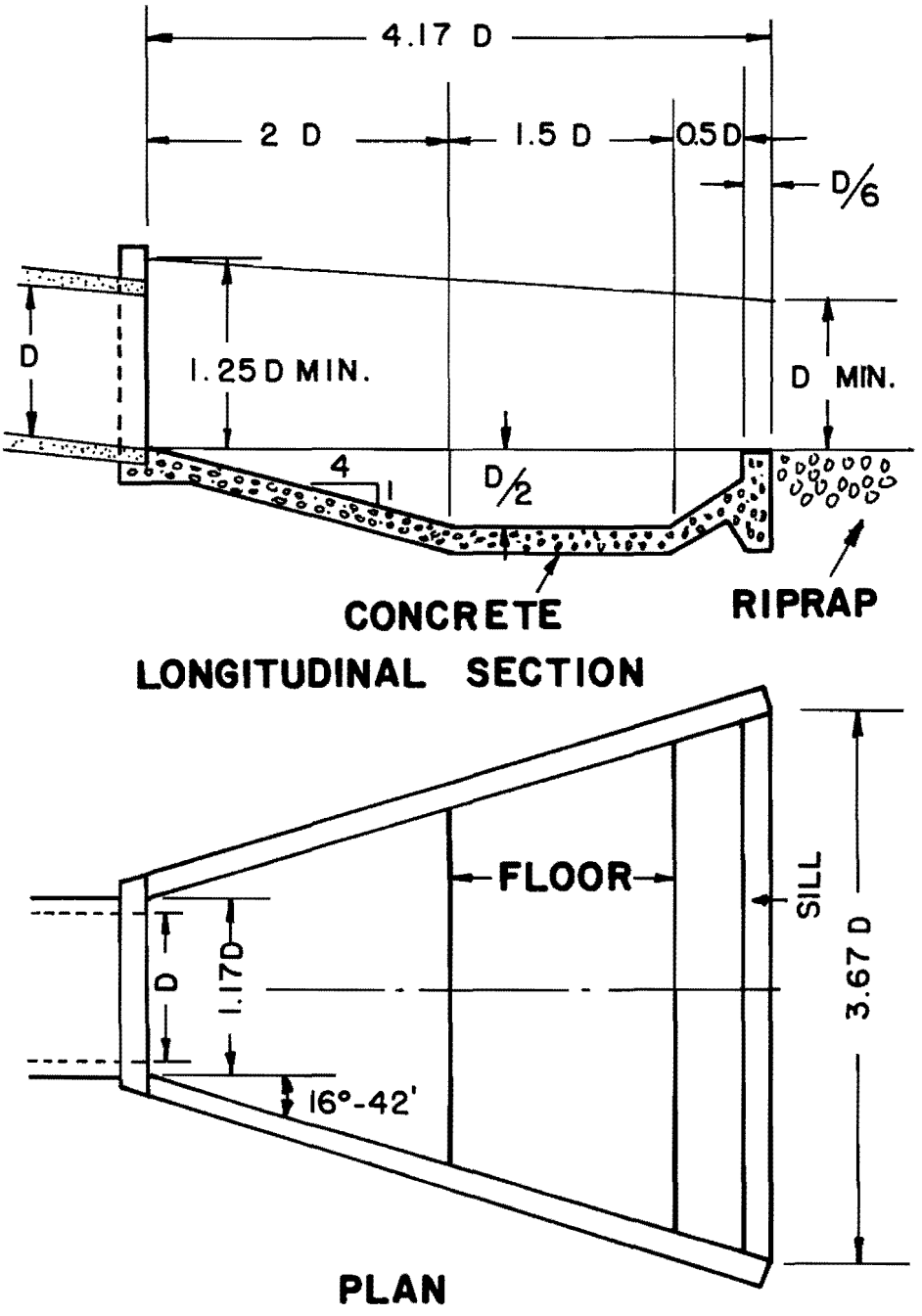

FIGURE I.1 – P.W.D. OUTLET STRUCTURE

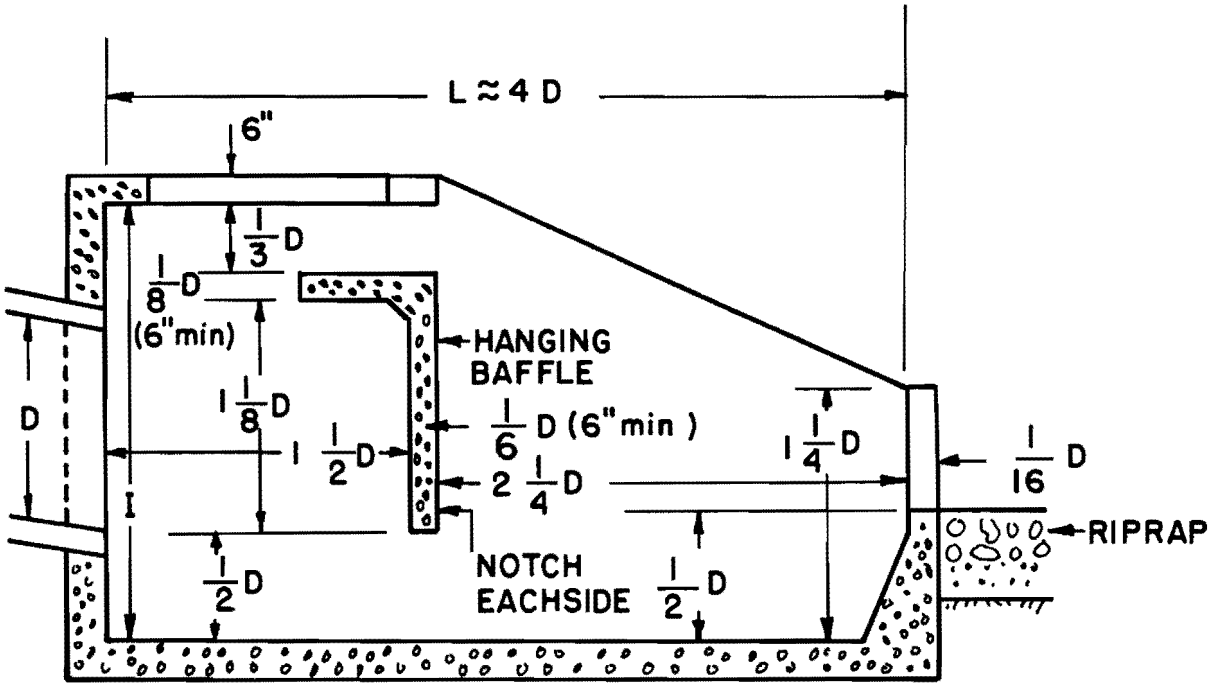

LONGITUDINAL SECTION

$H = 2\frac{1}{12}\,D$ (MIN.)

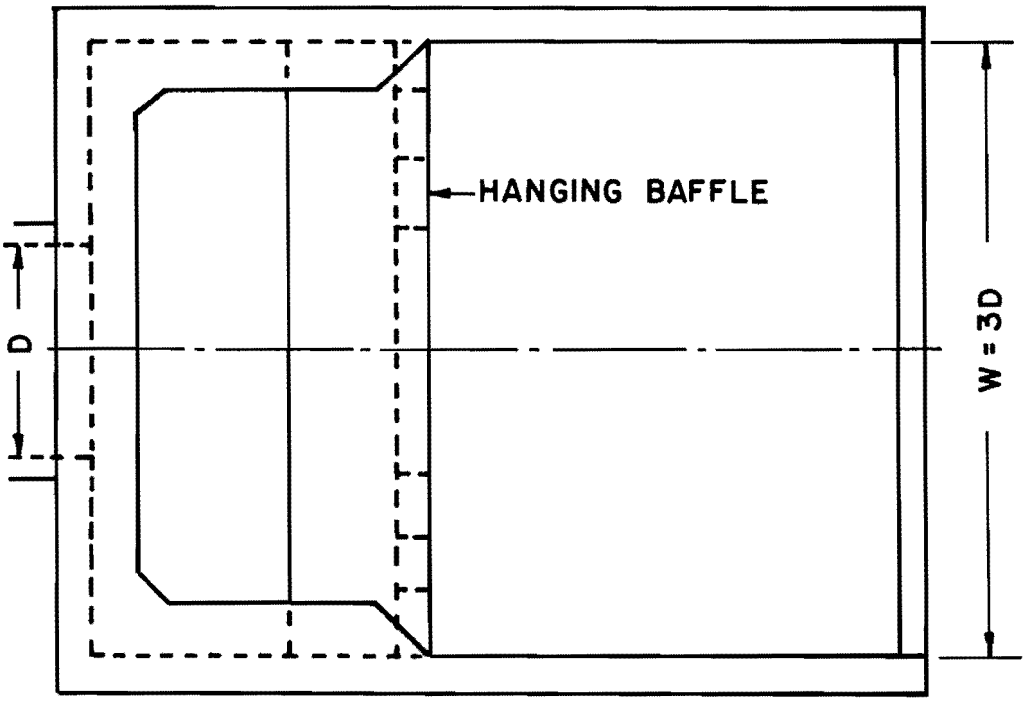

PLAN

FIGURE I.2 - BRADLEY-PETERKA BASIN VI

distance of 1.5D downstream from the end of the culvert, the basin has a hanging baffle notched at the bottom and with a deflector at the top to prevent overtopping. The distance between the lower edge of the baffle and the basin bottom is 0.5D. The basin bottom drops abruptly at the end of the pipe to 0.5D below the flow line of the culvert, and is horizontal throughout, except near the downstream end. There it slopes upward and ends at a vertical sill. The total height of the slope and vertical sill is 0.5D.

As mentioned above, this energy dissipator is particularly well adapted to flows with Froude numbers of 3 and greater, for which all of the flow will strike the transverse impact wall. At lower Froude numbers, only part of the flow strikes the wall, and for flows occurring at critical velocity near the culvert outlet (Froude number = 1) most of the flow passes under the wall. Even under such condition, the Bradley-Peterka basin still operates satisfactorily. However, in this range of outlet velocities, the P. W. D. basin discussed earlier is also adequate and is more economical to construct.

Another impact type energy dissipator uses two walls set across the bottom of a trapezoidal concrete outlet channel to induce energy dissipation. This structure, shown in Figure I.3, is known as the Contra Costa energy dissipator (8). Both transverse walls extend completely across the width of the bottom of the trapezoidal channel. The height of the front wall is one half

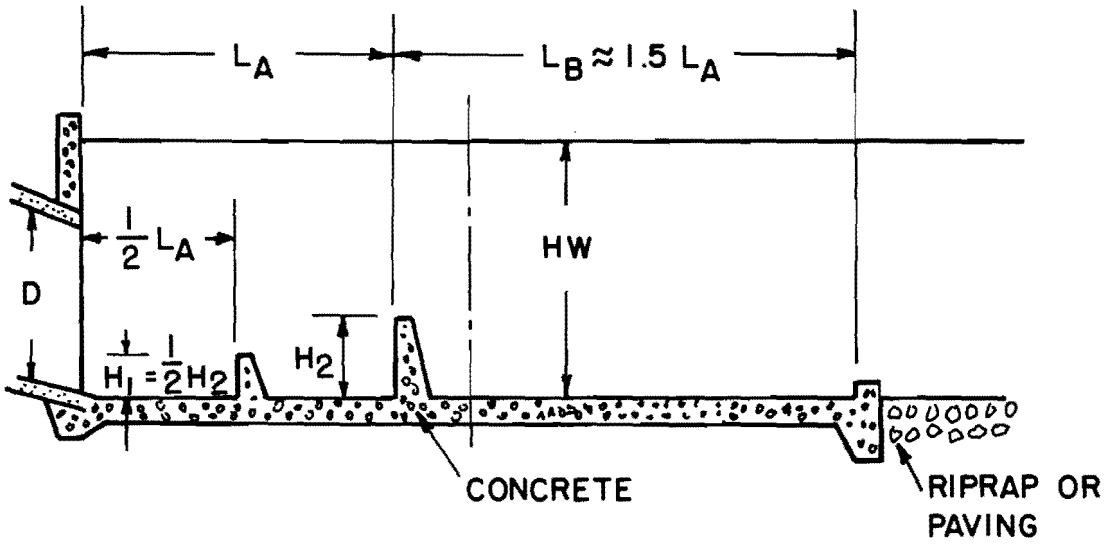

LOGITUDINAL SECTION

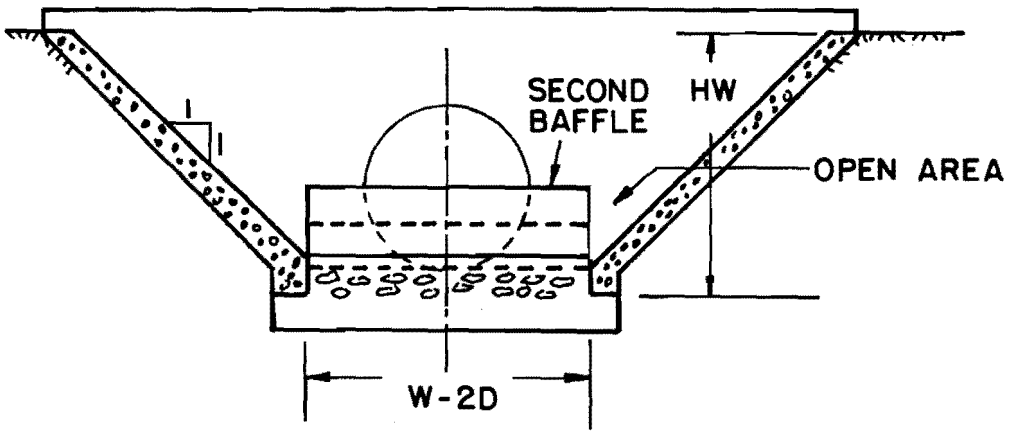

CHANNEL CROSS SECTION AND
END ELEVATION

FIGURE I.3 - CONTRA COSTA ENERGY DISSIPATOR

that of the back wall so that flow which is deflected upward by the first wall will still strike the second wall. The height of the back wall may be determined as a function of the flow rate, the pipe diameter and the slope of the culvert.

The distance from the end of the pipe to the back wall is found from the Froude number and depth of flow at the culvert outlet, and from the wall height. The front wall is placed halfway between the end of the pipe and the back wall. The total length of the concrete basin may be taken as 2.5 times the distance from the end of the pipe to the back wall. The bottom width of the trapezoidal outlet channel is 2 times the pipe diameter.

Laboratory tests of the Contra Costa energy dissipator have been made with satisfactory results for a wide range of outlet flow depths and Froude numbers. However, high Froude numbers were used only in conjunction with low outlet flow depths. At the maximum outlet flow depth tested of approximately 0.5D, the maximum Froude number used was 2.0. Field data on the operation of this structure are not available. It is, therefore, recommended that it be used only within the range of Froude number and outlet flow depth combinations for which laboratory data have been obtained.

A stilling basin structure which makes use of a hydraulic jump is the SAF (Saint Anthony Falls) basin (3). The SAF basin, shown in Figure I.4, consists of a steep chute which runs into a horizontal apron. The chute has chute blocks at its downstream end,

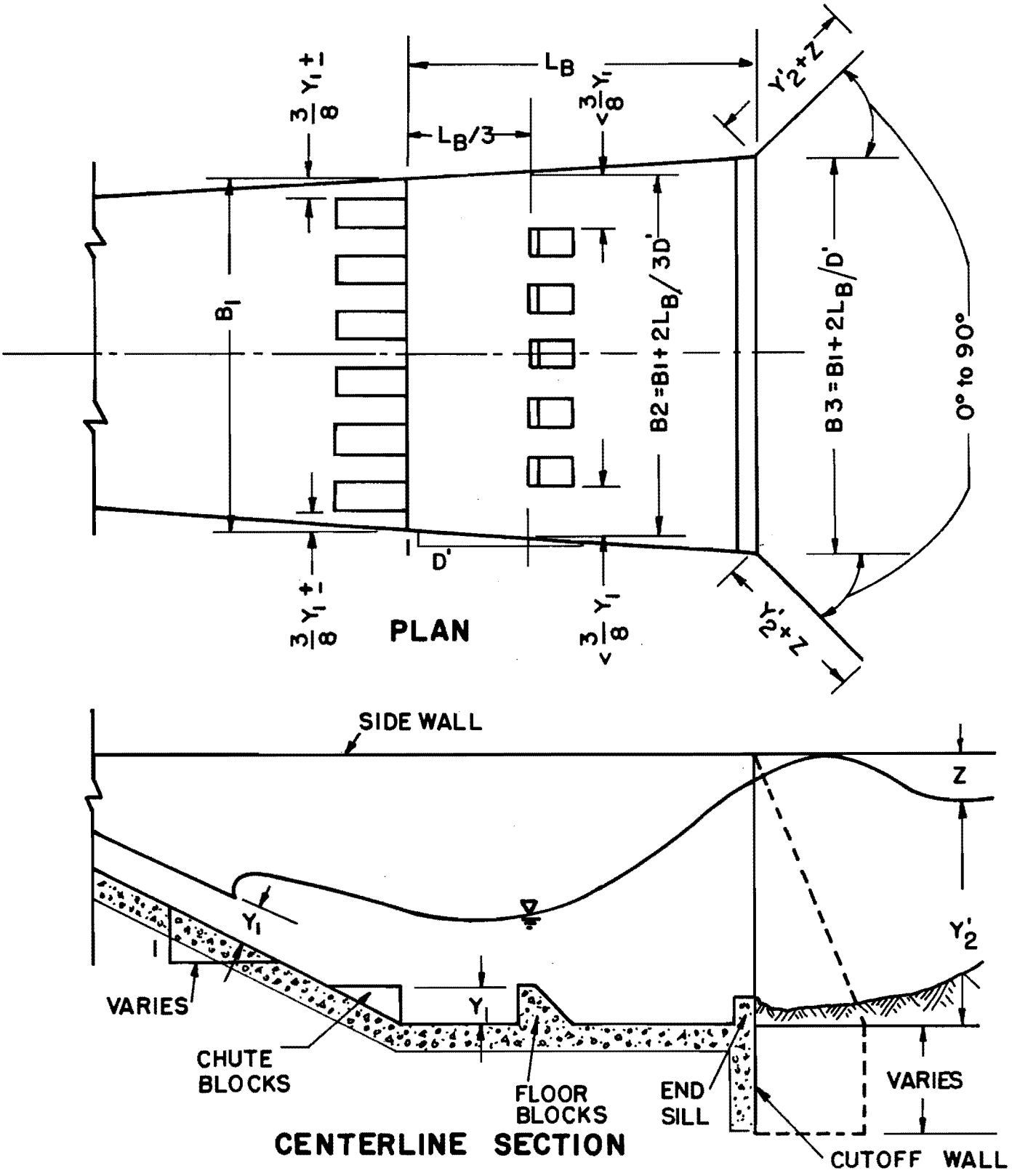

FIGURE I.4 - S.A.F. STILLING BASIN

whose dimensions and spacing are determined from the depth of flow at the end of the chute. The horizontal apron has baffle blocks of height equal to the flow depth at the end of the chute, and an end sill which extends for the full width of the basin. The basin training walls are straight and may be parallel or divergent. The width at the end of the basin may be varied according to field conditions.

The length of the horizontal apron is given as a function of the entering Froude number and the calculated sequent depth corresponding to the entrance depth. The distance from the end of the chute to the upstream face of the baffle blocks is given as one-third of the horizontal apron length. It is recommended that a vertical cut-off wall be used at the end of the concrete apron.

The stilling basin structures discussed in the preceding paragraphs, except for the SAF basin, do not require any particular depth of tailwater, since they do not depend on the formation of a hydraulic jump for their operation. For tailwater depths lower than critical depth at the downstream end of the basin, however, the basin will discharge at critical depth. For high flow rates, critical velocity, combined with a relatively shallow critical depth, may be high enough to cause scour of the channel bed downstream from the end of the basin. It is, therefore, recommended in various discussions of these structures (4) that some form of protection, such as riprap or paving, be used on the stream bed for an undetermined distance downstream of the end of the stilling basin.

It may be observed here that one undesirable characteristic of the basins with impact walls or blocks is their tendency to accumulate debris just upstream of such walls or blocks. For the Bradley-Peterka basin, floating debris may present a special problem, since all flow after impact must occur under the impact wall. Accumulation of debris in any of the impact-type basins may affect the flow area in such a manner that the energy-dissipating characteristics of the basin will be impaired, resulting in a greater scour potential than under normal operation.

The structure proposed herein is being studied without any type of impact obstacles in the region of flow. It is felt that this design will minimize the possibility of accumulation of debris in the basin, and at the same time, provide a more economical structure from the construction and maintenance point of view.

Free Surface Radial Flow

A study of free surface radial flow was made by Sadler and Higgins (11) in which the differential equation of the free surface was developed and used to predict hydraulic jump heights under conditions of axially symmetric flow. The basic equations used in the development of the free surface differential equation were the specific energy equation and the Chezy equation, used to evaluate friction losses. Thus,

$$E = Y + V^2/2g$$

and,

$$\frac{dE}{dR} = \frac{dY}{dR} + \frac{V}{g}\frac{dV}{dR} = S_o - S_f$$

where:

E = Specific energy of flow

V = Mean velocity of radial flow

R = Radius at any point of the radial flow field

Y = Depth of radial flow at radius R

S_o = Slope of bottom

S_f = Slope of total-head line = V^2/C^2Y

C = Chezy coefficient

From continuity:

$$V = \frac{Q}{2\pi RY}$$

and,

$$\frac{dV}{dR} = -\frac{Q}{2\pi RY}\left(\frac{1}{R} + \frac{1}{Y}\frac{dY}{dR}\right)$$

then,

$$S_f = \frac{Q^2}{4C^2\pi^2R^2Y^3}$$

$$\frac{dE}{dR} = S_o - \frac{Q^2}{4C^2\pi^2R^2Y^3} = \frac{dY}{dR} - \frac{Q}{2\pi RYg} \cdot \frac{Q}{2\pi RY}\left(\frac{1}{R} + \frac{1}{Y}\frac{dY}{dR}\right)$$

Let $M^2 = \frac{Q^2}{4\pi^2 g}$ and solve for $\frac{dY}{dR}$:

$$\frac{dY}{dR} = \frac{S_o + \frac{M^2}{R^2Y^3}\left(-\frac{g}{C^2} + \frac{Y}{R}\right)}{1 - \frac{M^2}{R^2Y^3}}$$

The Froude number defined by $F = V/\sqrt{gY}$ is introduced as:

$$F^2 = \frac{Q^2}{4\pi^2 g R^2 Y^3} = \frac{M^2}{R^2 Y^3}$$

and

$$\frac{dY}{dR} = \frac{S_o + F^2 \left(- \frac{g}{C^2} + \frac{Y}{R} \right)}{1 - F^2}$$

or

$$\frac{dY}{dR} = S_o + \frac{F^2}{F^2 - 1} \left(\frac{g}{C^2} - S_o - \frac{Y}{R} \right)$$

For a case of $S_o = 0$ and frictionless flow, which would be approximated by flow in which friction is negligible, the differential equation of the free surface becomes

$$\frac{dY}{dR} = \frac{F^2}{F^2 - 1} \left(- \frac{Y}{R} \right)$$

The frictionless flow differential equation indicates that for supercritical flow ($F>1$), the depth always decreases as the radius increases, and that at small values of R, the surface curve is steeper than at large values of R. The relatively large changes in the depth of the supercritical flow at small values of R permit substantial variations of the tailwater depth to occur while the radius of the resulting circular hydraulic jump is changed by a relatively small amount. It was this principle which led to the

expectation that the structure under investigation would exhibit a high degree of jump stability, especially when the jump occurred close to the point of onset of radial flow.

Analysis of Pressure at Basin Entrance

It was considered of interest to analyze more closely the pressure distribution on the bottom in the region where the sloping entrance chute intersects the horizontal basin bottom. In such region, as noted earlier, pressures build up causing rapid spreading of the flow in the stilling basin.

The maximum pressure which can be attained is stagnation pressure at the line of intersection between the sloping chute and the horizontal bottom. Since the buildup of pressure spreads both up and downstream from the point of maximum pressure, it was felt that the intersection between the sloping chute and the horizontal bottom should be placed a certain distance downstream from the end of the parallel entrance training walls, that is, the flaring wall region. In this manner, a portion of the pressure buildup upstream of the point of stagnation would be used in spreading the flow. It was, therefore, desired to estimate the distance over which a relatively high pressure persists in order to make efficient use of this potential spreading force.

In order to study the distribution of pressure, an analysis was made of a two-dimensional potential flow bounded on one side by two straight, intersecting solid boundaries, and on the other by

two straight solid boundaries connected to each other by a free streamline. A diagram of the flow is shown in Figure I.5. Gravitational acceleration was not considered in this flow. This particular flow configuration was used as a simulation of a free surface flow which would be uniform throughout, except in the region near the boundary intersection. Such boundary intersection would correspond to the intersection of a steep chute and a horizontal bottom.

The position of the free streamline was established by conformal transformation methods with application of the Schwarz-Christoffel theorem (12). Details of this solution are given in the Appendix. Solution for interior streamlines was performed by means of relaxation techniques.

There exists an infinite number of solutions for this general flow configuration, each one depending on the value assigned to the ratio of free streamline velocity to uniform velocity at the upstream and downstream ends of the flow field. Each solution yields a particular free streamline which ends at a given value of the ratio x_u/y_u. The parameters x_u and y_u are defined in Figure 1.5.

It was not considered essential to establish any one value of the ratio x_u/y_u for the present pressure distribution analysis. Instead, it was desired to use a value which would be representative of the range of flow conditions expected in the model studies.

The solution of the flow field for one such value is presented in Figure I.6. Also plotted in Figure I.6 is the pressure increment along the bottom boundaries. It may be appreciated that the pressure varies nearly linearly between the end of uniform flow and the point of stagnation.

Several factors were present which were expected to cause differences between the pressure distribution of the potential flow herein analyzed and that of the model flow. Among these are the effect of gravity, the convex curvature of the bottom of the entrance channel, which causes a decrease of pressure on the bottom; the flaring wingwalls, which allow the flow to spread, thus resulting in smaller flow depths downstream of the slope break than those of the potential flow analysis; and boundary resistance which causes a vertical variation in the velocity distribution of the approaching flow.

The actual pressure head distribution on the bottom in the region of the intersection of the steep chute and the horizontal bottom was determined experimentally. A representative distribution is shown in Figure I.7. It should be noticed that the ordinates of Figure I.7 represent relative pressure heads which include gravity effects. As expected, the convex curvature of the entrance channel bottom caused a reduction of pressure on the bottom of the entrance channel. The point of maximum pressure was moved downstream from the point of stagnation, which indicated

that the end of the sloping chute should not be placed as far into the flared wall region as might be inferred from the potential flow analysis.

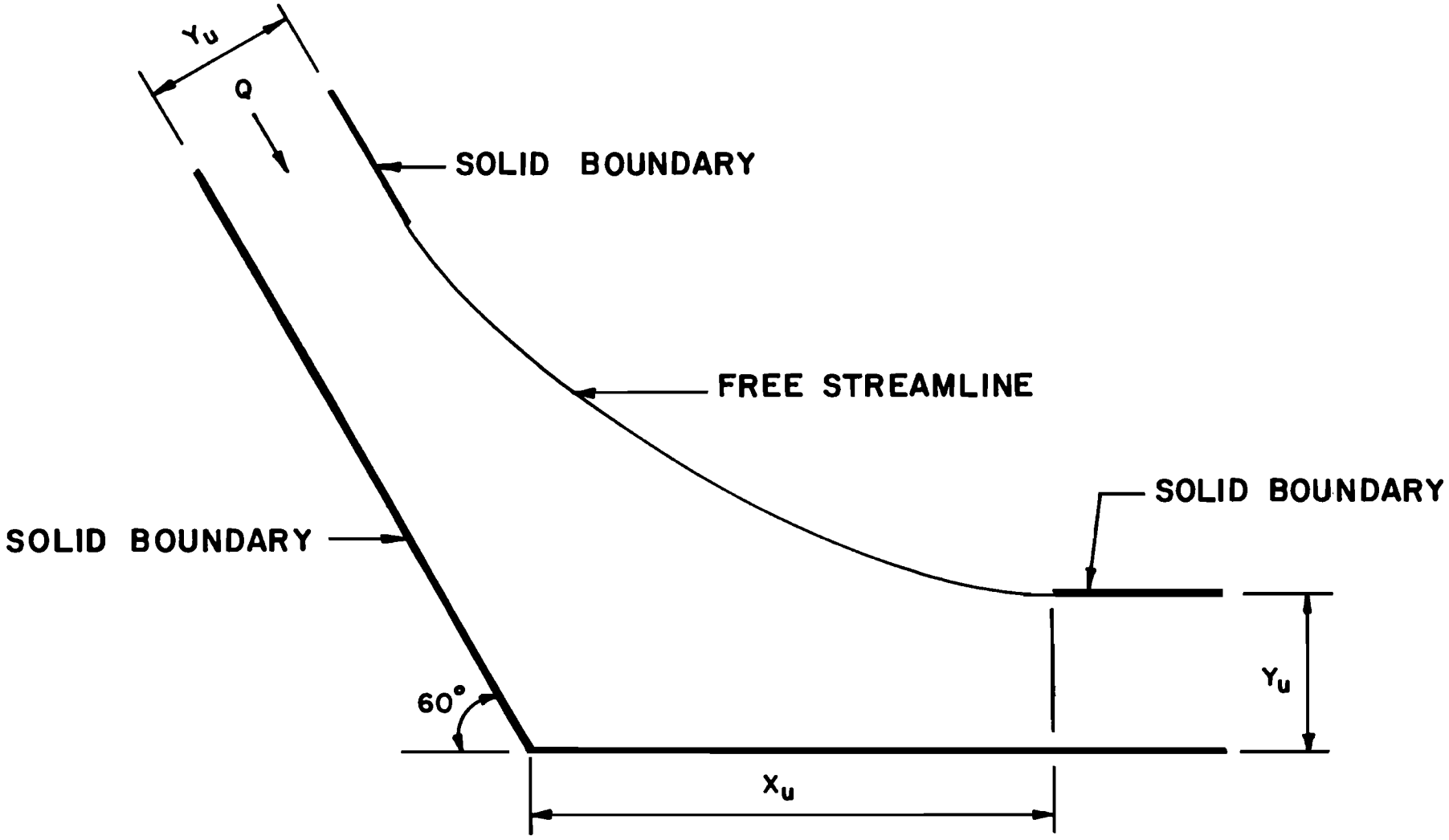

FIGURE I.5 - POTENTIAL FLOW AT BOUNDARY INTERSECTION

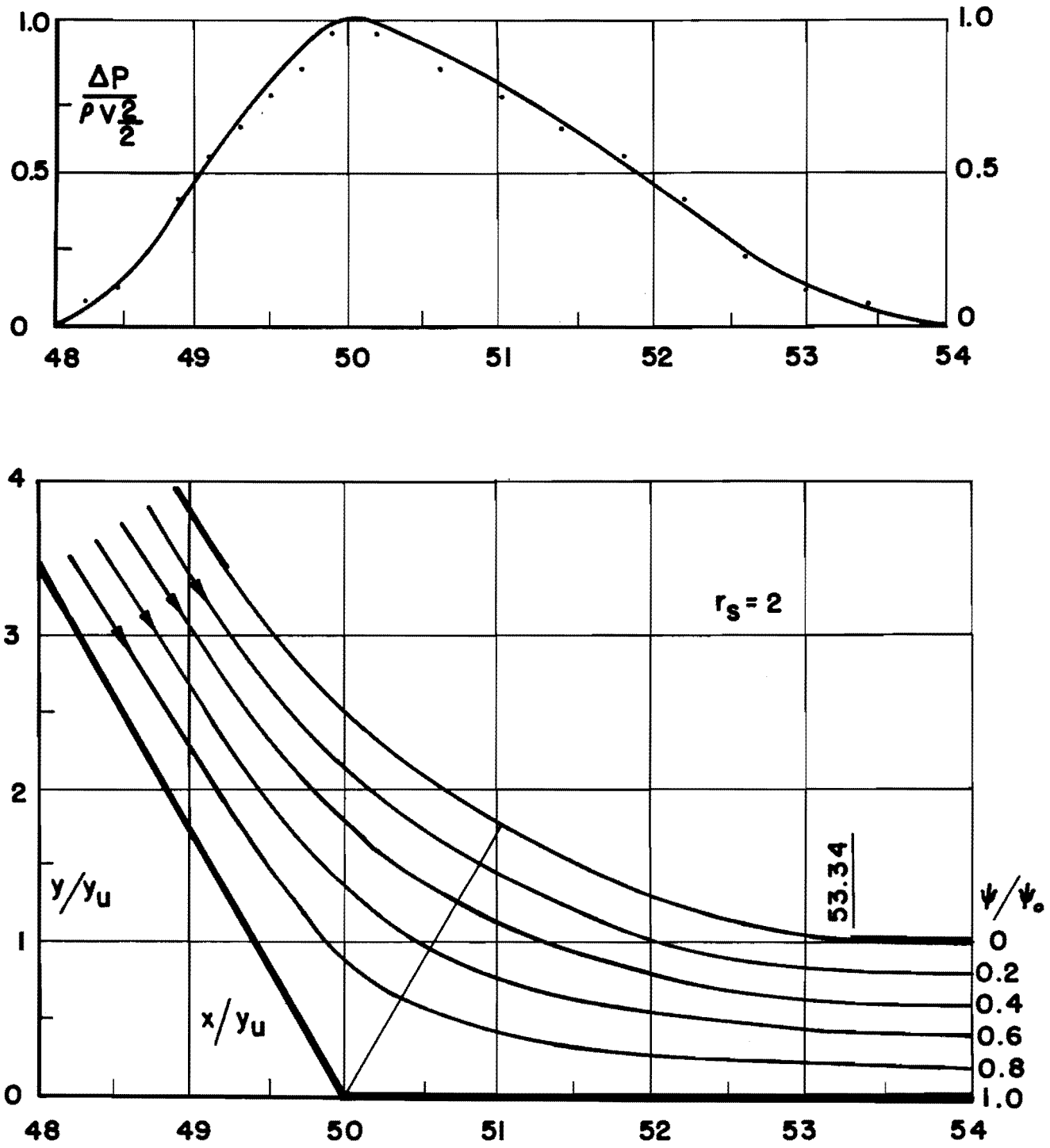

FIGURE I.6-STREAMLINES AND PRESSURE ALONG LOWER BOUNDARY OF POTENTIAL FLOW IN REGION OF BOUNDARY INTERSECTION

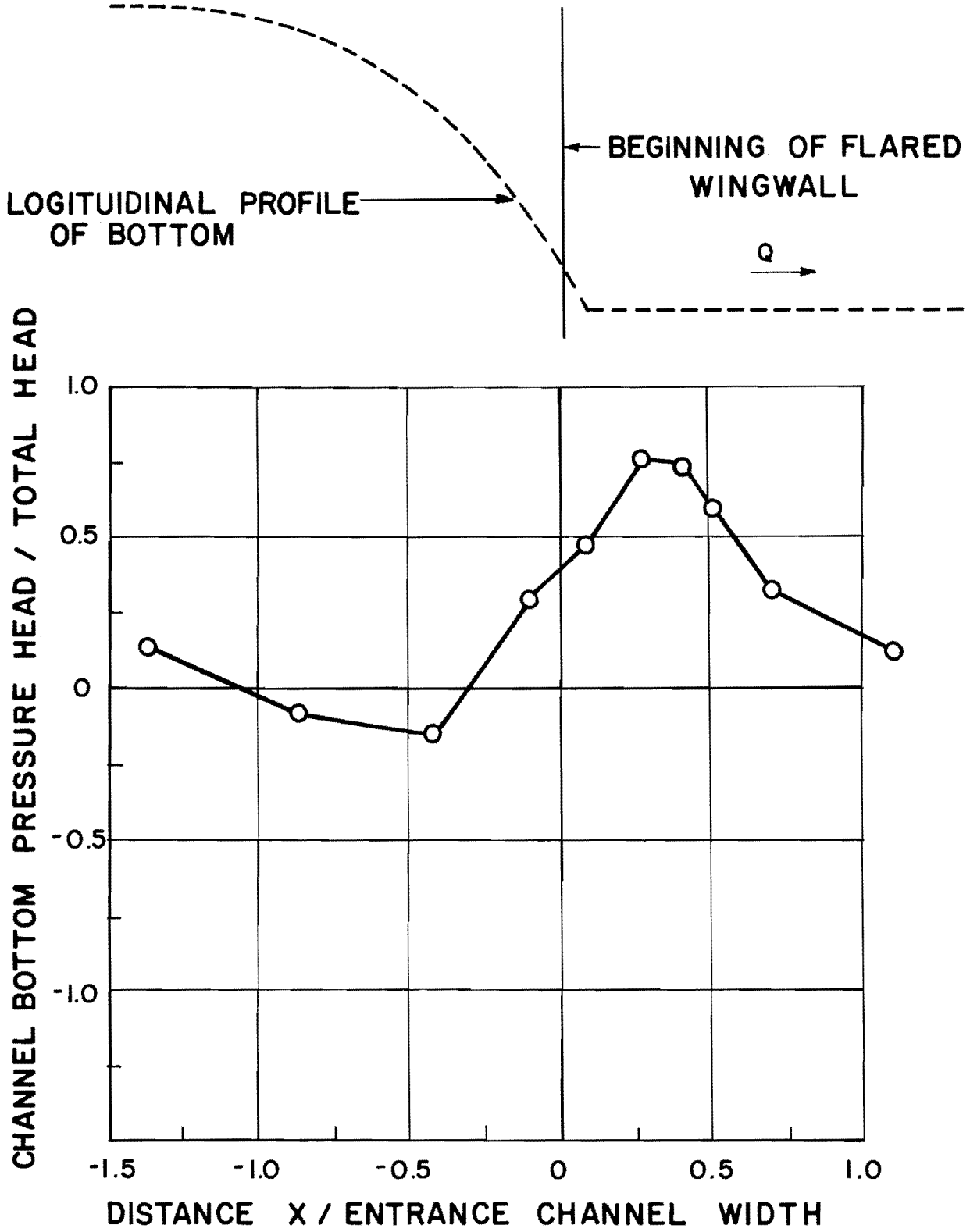

FIGURE 1.7 DISTRIBUTION OF PRESSURE ON BOTTOM OF ENTRANCE CHANNEL AND BASIN.

Chapter II

EXPERIMENTAL PROGRAM

Once the initial general layout of the energy dissipator was developed, it became necessary to formulate an experimental program compatible with object and scope of the present study. In order to form significant dimensionless parameters, dimensional analysis of the variables in the problem was performed. The values and ranges of the significant dimensionless parameters were then selected, and a model was designed and constructed in such a manner that experimentation could be carried out according to the program that had been established.

Analysis of Variables

Analysis of the problem pointed out several variables which were expected to be of significance. With tailwater as the dependent variable, these may be expressed as:

$$y_2 = f(V_t, y_t, x, B, b, z, r, g, \theta, \alpha, \beta)$$

where:

y_2 = Downstream or sequent depth of hydraulic jump.

V_t = Mean velocity of flow at the upstream end of the vertical curve in the entrance channel. This point is designated at P.C. in Figure II.1.

y_t = Depth of flow measured at the same section where V_t occurs.

g = Acceleration due to gravitational attraction.

x, B, b, z, r, θ, α, β, are defined in Figure II.1.

From the significant variables that were selected the following dimensionless variables were obtained:

$$\frac{y_2}{y_t} , F_t , \frac{x}{y_t} , \frac{y_t}{b} , \frac{B}{b} , \beta, \theta$$

where:

$F_t = V_t/\sqrt{g \cdot y_t}$ = Froude number at the upstream end of the vertical curve in the entrance channel.

It was decided to keep z, r, and α constant throughout this study, therefore they do not appear in any form in the group of dimensionless variables given above.

Indirectly, the variable z was included by combining it with the variables V_t and y_t to yield two new variables V_b and y_b. These are nominal calculated values of velocity and depth at the end of a drop of the entrance channel bottom through a vertical distance z. The calculation was based on a constant energy level, i.e., that existing at the point where V_t and y_t occur. However, since it was planned to keep z constant, the validity of eliminating z as a significant variable by the combination previously described is not being confirmed herein. It was decided to explore both V_t, y_y and V_b, y_b, with the restriction that any results obtained by using V_b, y_b would not necessarily apply to values of z other than that used in the present investigation.

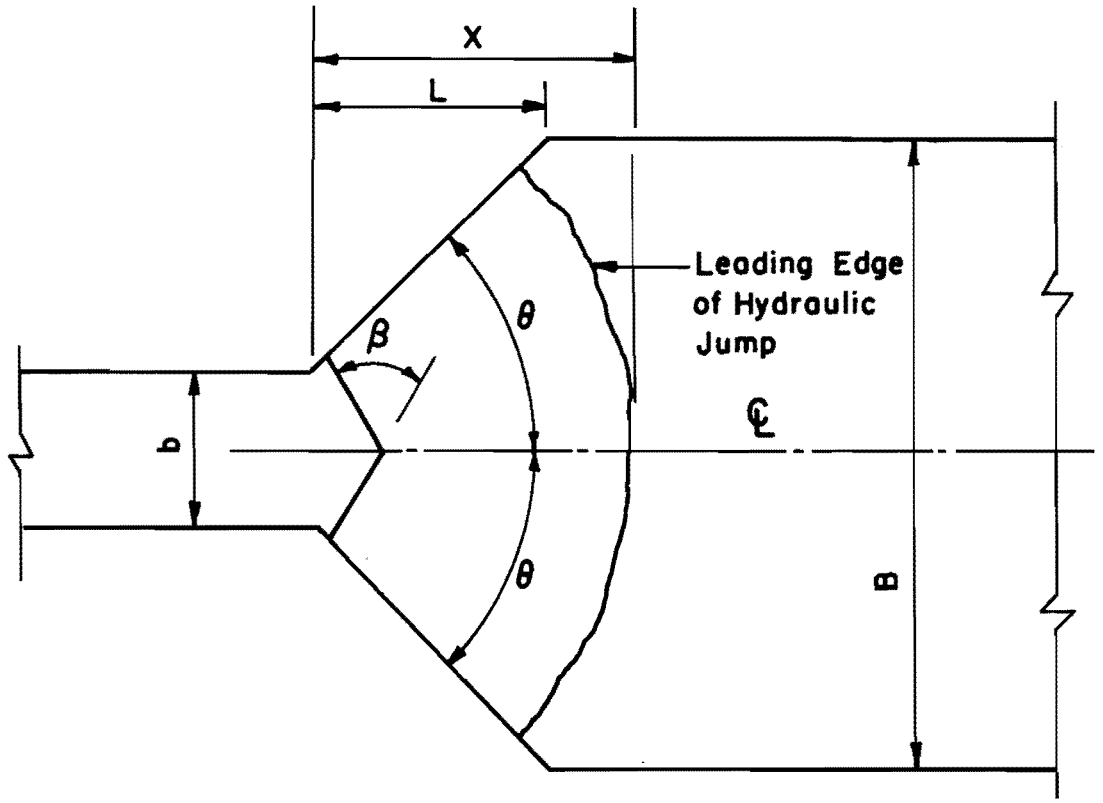

PLAN

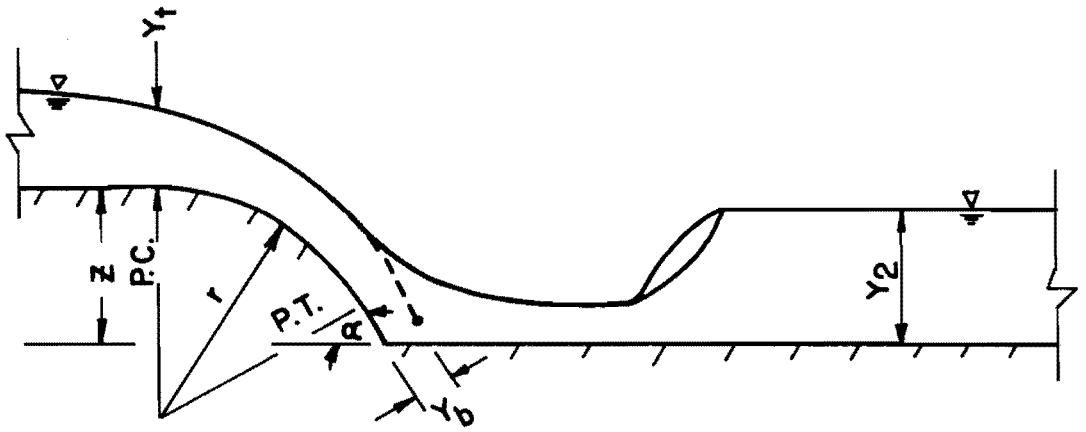

℄ ELEVATION

FIGURE II.1 DIAGRAM OF STILLING BASIN SHOWING DEFINITION OF PARAMETERS

Two fluid properties which have not been listed among the significant variables but need to be considered are viscosity and density. Flow in the prototype structure treated in the present problem will be governed by gravity forces, while viscous forces are expected to be relatively unimportant. In the model, gravity forces must also govern the flow field, and viscous forces must remain unimportant in order to attain dynamic similarity between model and prototype. The criterion used to determine the relative importance of viscosity is Reynolds number. If the minimum Reynolds numbers found in the prototype and model indicate that turbulent flow occurs in both, and the Reynolds numbers are sufficiently high, viscous effects may be considered negligible in model and prototype. Preliminary analysis of the model yielded a minimum value of Reynolds number of approximately 1×10^5, which indicates that viscous effects in the model may be considered negligible.

Density will become important if it is desired to obtain pressures on the prototype structure from pressure measurements on the model. In the case of dynamic pressures, the Euler number for any two points on the prototype and the corresponding points on the model must be the same. Since the Euler number is a function of density, it is evident that the density of the fluid used in the model and that expected in the prototype must be known when prototype pressures are obtained from model measurements.

On the other hand, density is not significant in the determination of the ratio of the initial depth to the sequent depth of a hydraulic jump.

Selection of Ranges and Values of Variables

The selected values of the dimensionless variables involving basin geometry were set from practical construction considerations. It was desired to choose values which would lead to a design that was simple and economical to construct and would be applicable to normal field conditions encountered. Values of dimensionless variables which involve flow dimensions at the culvert outlet were also set in accordance with those found in normal field operation of culverts on steep grades.

The radius of curvature r was set from an estimate of the pressure on the bottom along the vertical curve. It was desired to limit negative pressure head to a minimum of approximately $-1.5y_t$ at the maximum value of F_t. Negative pressure head on the bottom was estimated as follows (6):

$$p/\gamma = y_t - c$$

where: p/γ = pressure head on the channel bottom

c = pressure head correction for curvature, obtained from:

$$c = \frac{y_t V_t^2}{gr} = \frac{y_t}{r} \cdot F_t^2$$

then: $$r = \frac{y_t^2 F_t^2}{c}$$

Let: $$p/\gamma = -1.5y_t$$

then: $$c = y_t - p/\gamma = y_t + 1.5y_t = 2.5y_t$$

and: $$r = \frac{y_t^2 F_t^2}{2.5y_t} = \frac{y_t F_t^2}{2.5}$$

Estimated values: Maximum $F_t \simeq 3$

at $y_t \simeq 0.2'$

then: $$r = \frac{(0.2)(3^2)}{2.5} = 0.72: \quad \text{Use} \quad r = 0.75'$$

Upon this basis, the minimum radius of curvature was found and established as the value to be used throughout the present investigation. The same basis could be used for determining the minimum radius of a vertical curve for other flow conditions at the end of the culvert. The relation $r = Y_t F_t^2/2.5$ should be applicable for the anticipated range of conditions encountered in other models or for prototype conditions. It is possible that negative pressures of larger magnitude could be tolerated leading to a smaller radius of curve, but the radius determined by this relation will give satisfactory performance.

The value of α was set from a combination of the distance z and the radius of curvature r. In order to obtain the most efficient spreading action, it was deemed desirable to make α as large as possible, within the limits set by the established value of z. However, it was also desired to have a short tangent at the

lower end of the vertical curve. From these considerations, the value of was set at 60° for the complete investigation.

The experimental program which finally evolved called for eight different combinations of the geometric variables, composed from the following specific values:

$$\theta = 30°, 45°$$

$$\beta = 0°, 60°$$

$$B/b = 4, 6$$

The exact range of F_t used for each geometric combination varied from approximately 1.5 to 3.1. The lower limit was the minimum value of F_t which could be obtained in the model. Values of y_t/b ranged from approximately 0.4 to 0.6. The range of x/y_t varied according to the geometric arrangement of the basin. The minimum value of x for each run was such that the leading edge of the jump was immediately downstream of the falling jet. Maximum x was taken at a point where the jump was completely outside the flared wingwalls. These limits yielded values of x/y_t ranging from approximately 1.3 to 11.5.

Design and Construction of Model.

The model used in the present investigation consisted of a horizontal bottom stilling basin and downstream channel, an entrance channel with a curved bottom and a stilling and control tank. A sectional diagram of the model is shown in Figure II.2, and a view of the model and instrumentation is given in Figure II.3.

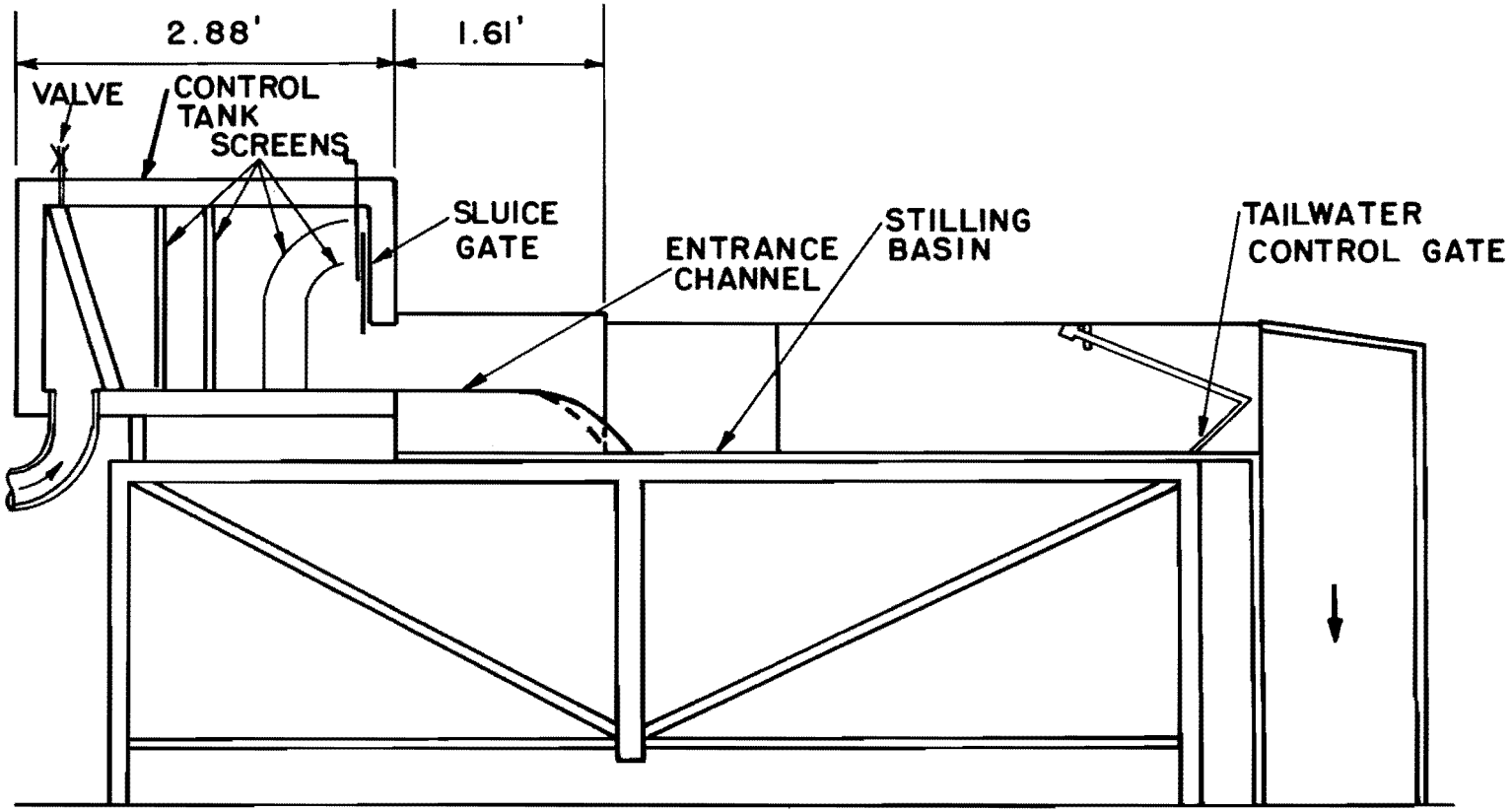

FIGURE II.2 SECTIONAL DIAGRAM OF APPARATUS.

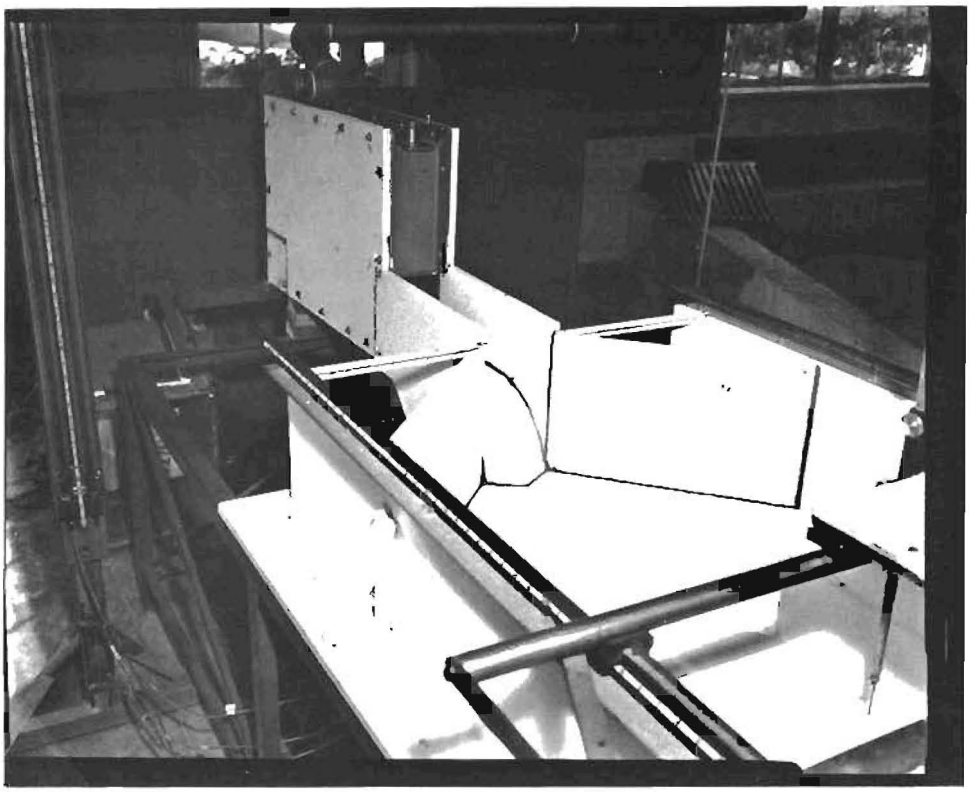

FIGURE II.3 ENERGY DISSIPATOR MODEL AND INSTRUMENTATION

The stilling basin and downstream channel had a 3/4 inch plywood horizontal bottom and vertical sides. The sides of the channel were parallel and varied in length from 46 inches to 26 inches, depending on the angle of the stilling basin walls and the width of the channel. Two fixed channel walls were 36 inches apart, and two removable walls were used to make the channel 24 inches wide when desired. A flap gate 36 inches long was placed at the end of the channel to permit control of the tailwater depth.

The upstream portion of the stilling basin had flaring walls set at angles of either 30^{o} or 45^{o} measured from the channel centerline. The distance between the flaring walls varied from 6 inches at the end of the entrance channel to 36 inches at their intersection with the parallel channel walls. The joints between the horizontal bottom and vertical walls and between flaring and parallel walls were caulked and secured with wood screws. All plywood surfaces were waterproofed and painted.

The entrance channel had 3/4 inch plywood sides enclosing one of the two removable bottoms shown in Figure II.4. Both removable bottoms consisted of 3/4 inch plywood sides which were used as templates set 6 inches outside to outside. These templates formed a horizontal bottom 6 inches above the stilling basin bottom. Downstream from the horizontal portion and tangent to it, the templates formed a circular vertical curve with a 9 inch radius and a 60^{o} deflection angle. A short tangent connected the downstream

end of the vertical curve with the horizontal basin floor. The space between templates was spanned with wire mesh on which a paste of white cement and marble powder was placed and finished to a smooth surface.

One of the removable bottoms had its surface finished in such a manner that, at any point along its surface, a transverse horizontal line would be a straight line. The other bottom had a sheet metal template which formed an identical vertical curve and end tangent as the plywood templates. This metal template was placed along the centerline of the bottom, with its point of curvature and its point of tangency at the same elevation as the corresponding points on the side templates. It was displaced downstream a distance such that, when projected on a horizontal plane, a horizontal line connecting any point on the center template to a corresponding point on the outside of the side template would form an angle of 30° with a horizontal straight transverse line. Thus two such horizontal lines from corresponding points on the side templates would intersect at the center template forming a 60° deflection angle.

The removable bottom was placed between the entrance channel sides and secured in place. The bottom was placed so that the downstream end of the slope at the two vertical planes formed by the outside faces of the plywood templates was 1/2 inch, measured parallel to the channel centerline, downstream from the intersection

of the entrance channel walls and the flaring basin walls. The position of either removable bottom, relative to the inside face of the flared wingwalls, is shown by the dashed lines in Figure II.4. Joints between the removable entrance channel bottom and basin bottom, entrance channel walls and control tank outlet were caulked and smoothly finished.

The stilling and control tank was a 6 inch wide box with four sides made from structural steel channel and two from 3/4 inch plywood, as shown in Figure II.2. The inlet to the tank was through the bottom, adjacent to the back of the tank, and consisted of a 4 inch diameter pipe welded to the steel channel at one end and threaded at the other. The tank outlet consisted of a 6 inch wide by 6 1/4 inch high opening in the front face of the tank. To control depth of flow out of the tank, a sluice gate was provided at the tank outlet. The sluice gate was built from 1/8 inch thick brass plate. Vertical movement of the gate was controlled by means of a lead screw which projected through the top of the tank. The stem was held in position by a special water-sealing fitting.

Stilling action in the tank was provided by five wire mesh screens placed as shown in Figure II.2. All screens were secured to one of the plywood sides. A valve was placed on the tank top, near the back, to assure atmospheric pressure over the water surface in the tank, when the tank was operated at a depth smaller than the tank height.

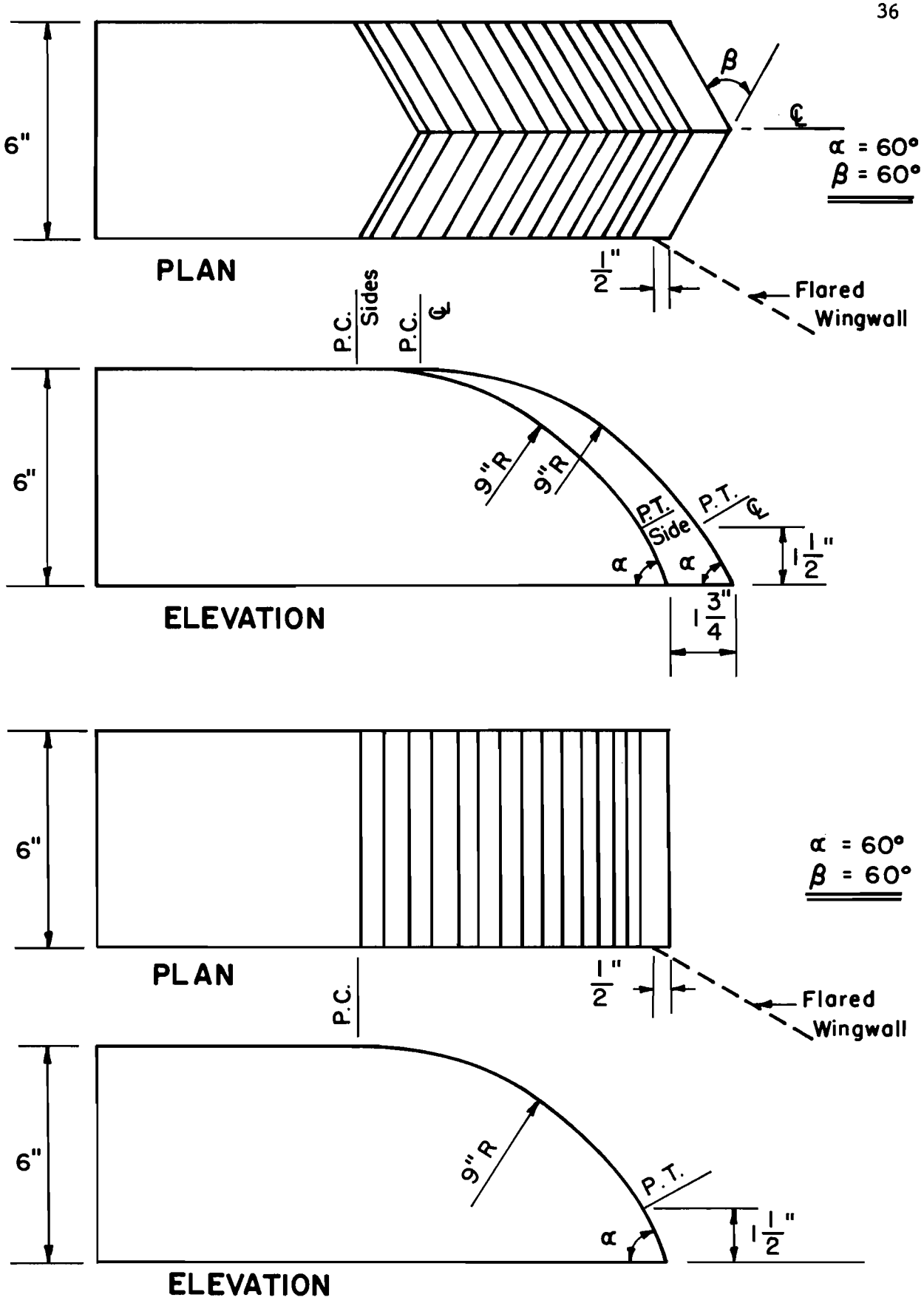

FIGURE II.4 - DETAILS OF REMOVABLE ENTRANCE CHANNEL BOTTOMS

An instrument carriage was provided and placed on two tracks made from round steel bars. The bars were bolted on structural steel angles which were supported by the vertical plywood walls on the 36 inch channel. The carriage consisted of two separate frames, both made of a combination of steel pipe and structural steel shapes. The bottom frame was placed directly on the side tracks and had longitudinal movement. The top frame was placed on the steel pipe sides of the bottom frame, which served as tracks for transverse movement.

A Lory Type "A" point gage was mounted on the top frame of the instrument carriage for measurements of water depths and location of jump position. Velocity measurements were made by means of a Prandtl-type Pitot tube, also mounted on the top frame of the instrument carriage. Tailwater depth measurements were made with a piezometer tap placed in the downstream channel bottom, 8 inches upstream of the control gate and on the centerline. The tap was connected to an open manometer secured on one of the channel sides.

In the vicinity of the basin entrance, eleven piezometers were placed along the channel centerline. Seven piezometers were in the horizontal basin bottom, and four in the removable entrance channel bottom with $\beta = 0$. All eleven piezometers were connected to a common open manometer with flexible plastic tubing. Clamps were used to shut off piezometer connections.

The model was connected to the laboratory constant head tank. A 3 inch gate valve was used to regulate the flow rate, which was measured by means of a Venturi-orifice type meter connected to a differential water manometer.

Experimental Procedure

Experiments were conducted for eight different geometric arrangements of the energy dissipator structure. As mentioned earlier, the three geometric parameters varied were θ, β, and B/b. The combination of geometric parameters used and the designation given to each combination are given in Table 1. A view of the entrance channel and basin layout for one of these arrangements is given in Figure II.5.

TABLE 1

DESIGNATION AND CHARACTERISTICS OF THE GEOMETRIC ARRANGEMENTS

Designation	B/b	β, Deg.	θ, Deg.
66030	6	60	30
46030	4	60	30
60030	6	0	30
40030	4	0	30
66045	6	60	45
46045	4	60	45
60045	6	0	45
40045	4	0	45

In general, each arrangement was tested at four different flow rates. At each flow rate, three depths of flow y_t were used, such that twelve values of the Froude number F_t were obtained. The largest value of y_t at each flow rate was obtained by permitting the flow to pass free of the control tank sluice gate. The two smaller depths were regulated by use of the sluice gate, thus at these depths the same values of y_t could be obtained for any of the four flow rates used. Table 1.a gives values of the flow rates Q, the corresponding $Q/b^{2.5}$, depth of flow y_t, and Froude number.

TABLE 1.a

Q, cfs	$Q/b^{2.5}$	y_t, ft.	F_t
0.76	4.31	0.195	3.13
		0.225	2.52
		0.310*	1.56
0.72	4.09	0.195	2.98
		0.225	2.41
		0.300*	1.54
0.67	3.80	0.195	2.78
		0.225	2.24
		0.285*	1.55
0.64	3.64	0.195	2.64
		0.225	2.13
		0.275*	1.57

*Variable for different runs

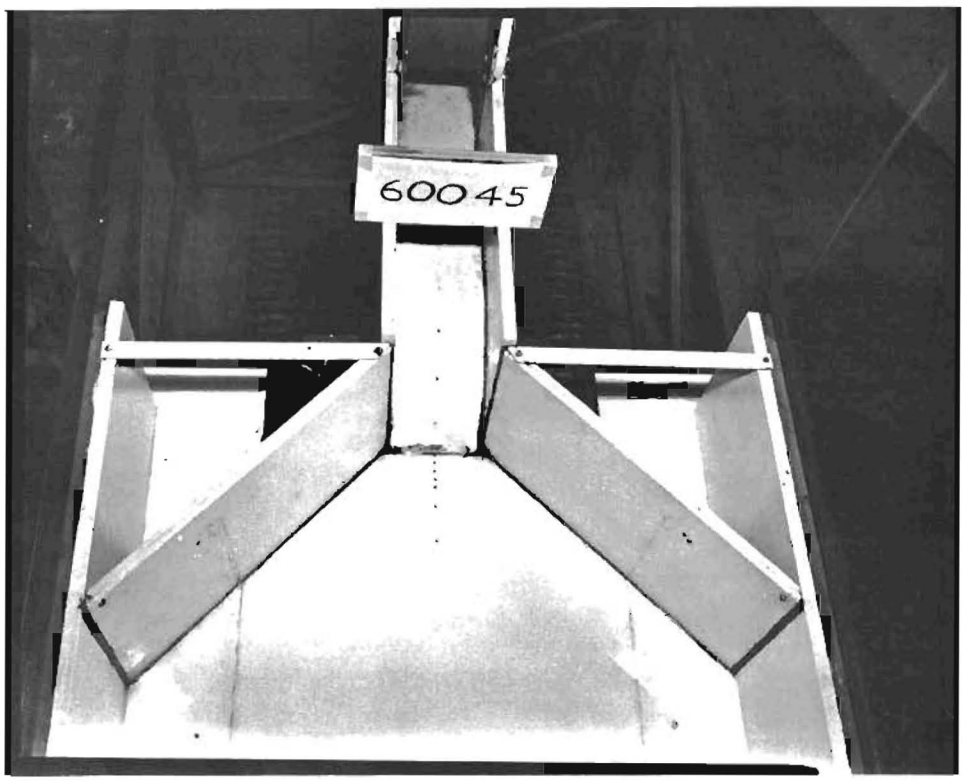

FIGURE II.5 ENTRANCE CHANNEL AND STILLING BASIN LAYOUT

Measurements were made to determine jump stability and velocity distributions for the eight different arrangements. Water surface profiles in the basin were taken for the four cases of B/b = 6. Also, bottom pressure measurements were made along the entrance channel and the upstream portion of the stilling basin for Arrangement No. 40045.

The stability of the hydraulic jump was determined in terms of the longitudinal change in position corresponding to a change in tailwater depth. The position of the jump was defined by the distance along the basin centerline from a section at the beginning of the flared wingwalls to the leading edge of the jump, denoted as x.

Measurement of the jump position was accomplished by placing the point gage supported on the instrument carriage directly over the leading edge of the jump. The position was indicated on a calibrated tape placed on the side of one of the longitudinal tracks, and on which a reading corresponding to the reference section (x = 0) had been taken previously. The point gage was kept on the channel centerline, for which a reference reading on a tape placed along the front transverse track had also been taken.

The leading edge of the jump exhibited a considerable degree of longitudinal fluctuation. In determining the jump position, it was attempted to obtain a visual temporal average of the position for each tailwater setting. The tape on which the jump position

was indicated was read to the nearest 0.01 ft., but the actual average position was determined to approximately 0.04 ft.

For each reading of jump position, a tailwater depth measurement was made by means of a piezometer installed through the bottom of the channel. The piezometer tap was connected to a manometer which was read to the nearest ±0.002 ft. The tailwater depth was varied from maximum to minimum in amounts that would yield approximately even increments of x. An average of about 10 readings were taken from the highest to the lowest depth.

Velocity measurements were made within the region covered by the hydraulic jump to obtain an indication of the efficiency of the spreading action and the degree of velocity reduction in the jump. Velocity was measured with the Pitot tube placed parallel to the channel centerline at 0.03 ft. from the bottom, which was approximately 8 to 10 percent of the tailwater depth. Points of velocity measurement are graphically shown in Figure II.6, a and b. Before velocity measurements at a given Froude number were started, the jump was stabilized at x = 1.00 ft. for arrangements with B/b = 6, and at x = 0.80 ft. for those with B/b = 4. Measurements for all arrangements, except No. 46030, were taken at three different sections set at 1.00 ft., 1.50 ft., and 2.00 ft. downstream from the jump position. At each section, velocity was measured at the centerline and symmetrically at 0.40 ft. and 0.80 ft. from the centerline for B/b = 4. For B/b = 6,

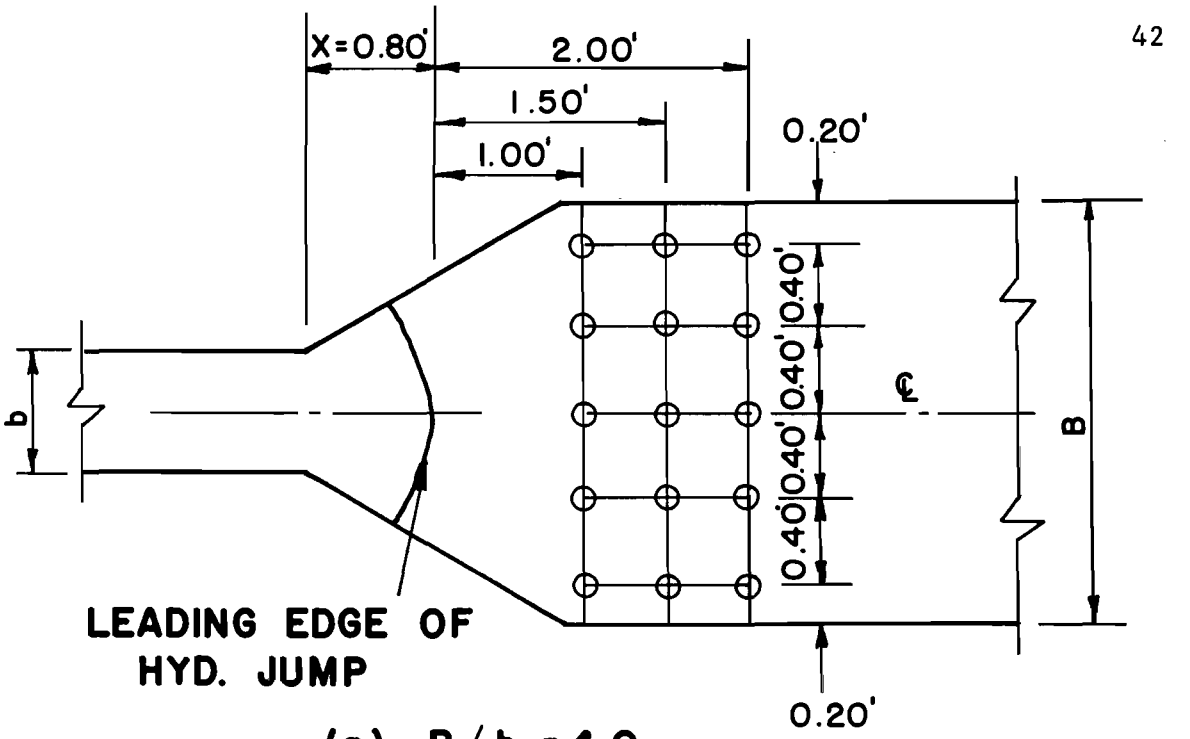

(a) B / b = 4.0

⊕ POINTS OF VELOCITY MEASUREMENT

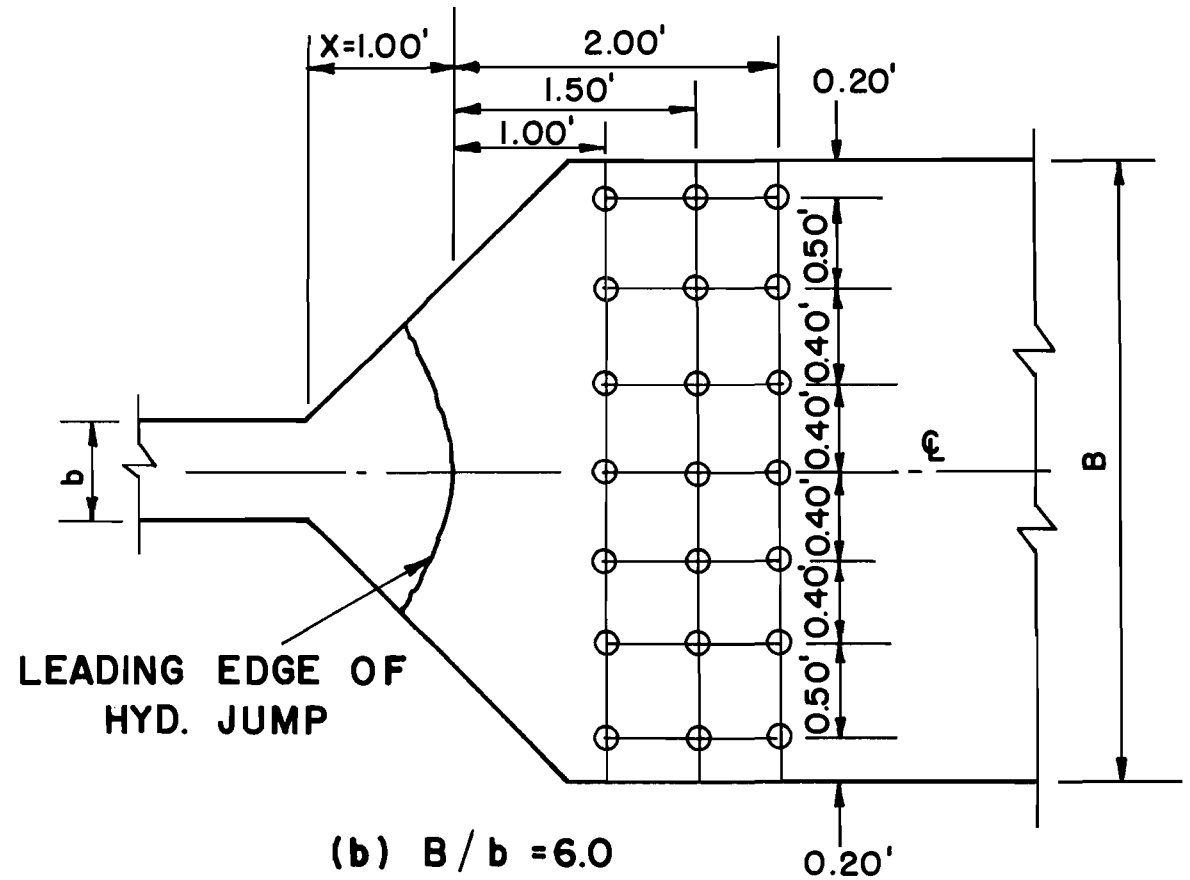

(b) B / b = 6.0

FIGURE II. 6 - LOCATION OF VELOCITY MEASUREMENTS

readings were also taken at 1.30 ft. from the centerline. The same points were used at each transverse section for Arrangement 46030, but for this arrangement the jump and the point of the transverse sections of velocity measurements were varied over a wider range, and were set at distances given at multiples of y_t and y_2. respectively.

Velocity was measured by means of a Pitot tube which was connected to a differential water manometer. The difference in the water column levels was read to the nearest ± 0.001 ft.

In order to determine the degree of angular uniformity of the supercritical flow in the basin, water depth measurements were made along radial lines having the same vertex as the wingwalls. Water depth was measured for arrangements with B/b - 6. The radial lines used for reference were the centerline and symmetrical lines 15° and 30° from the centerline for $\theta = 30^{\circ}$, and 15°, 30°, and 45° for $\theta = 45^{\circ}$. Measurements were taken at straight transverse sections usually set 0.20 ft. apart. A Lory Type "A" point gage was used to determine the water depths. The accuracy of depth measurements varied according to the stability and smoothness of the water surface. Along the wingwalls, where a high wave formed, readings were made to ± 0.03 ft. Downstream of the wave, the water depth was determined to ± 0.005 ft. Depth along the upstream portion of the centerline was read to ± 0.002 ft. Downstream the surface became rough and readings were made to ± 0.01 ft. Along the other radial lines, depth was determined with ± 0.002 ft. at most points along each line.

Chapter III

ANALYSIS OF RESULTS

Stability of the Hydraulic Jump

One performance characteristic that was investigated for the structure under consideration is the degree of stability of the jump position for a variable tailwater depth. The stability was determined in terms of the change in tailwater depth necessary to produce a given change in the position of the hydraulic jump, indicated by the distance x. An increment in this distance corresponds to a decrement in tailwater depth, when all other variables remain constant.

It was expected from analysis of the problem that for a given basin and channel geometry, the required depth of tailwater to stabilize the jump at a distance x would depend on V_t, y_t, and g. These variables and the entrance channel width b were combined to form the dimensionless variables y_2/y_t, x/y_t, F_t, and y_t/b. Use of dimensionless variables is desirable because such variables permit combination of several variables into one, making analysis of results simpler.

In accordance with the experimental procedure that was established for investigation of the jump stability, the parameters x and y_2 were varied over a certain range while V_t and y_t were held constant. This procedure yielded functions of x/y_t vs. y_2/y_t for several constant values of F_t and y_t/b. By varying the total

discharge rate, and keeping the same values of y_t used for the previous discharge rate, additional functions of x/y_t vs. y_2/y_t were obtained for a different set of values of F_t, but at the same values of y_t/b. Thus, twelve different values of F_t were investigated for each geometrical arrangement of the stilling basin. The functions obtained for each arrangement are graphically shown in Figures III.1 through III.8.

The degree of stability of the hydraulic jump at a given point is indicated by the absolute value of the slope of each curve of x/y_t vs. y_2/y_t, or that of a tangent at such given point. It may be observed that all the curves obtained show an approximately constant slope at small values of x/y_t. As x/y_t is increased, the absolute value of the slope decreases, and in some cases the curve becomes nearly horizontal, depending on how far the jump was moved downstream from the end of the flared wingwalls. It is expected that all curves would have become nearly horizontal if, in all cases, the jump had been moved sufficiently far downstream.

Analysis of the curves of x/y_t vs. y_2/y_t shows that the hydraulic jump is highly stable within the region of the basin with flared wingwalls. This behavior had been expected from a preliminary study of radial flow characteristics (11), which showed that for identical bottom slope and surface conditions, in radial flow the Froude number and depth of flow within a short radial length would vary much more than they would in the same

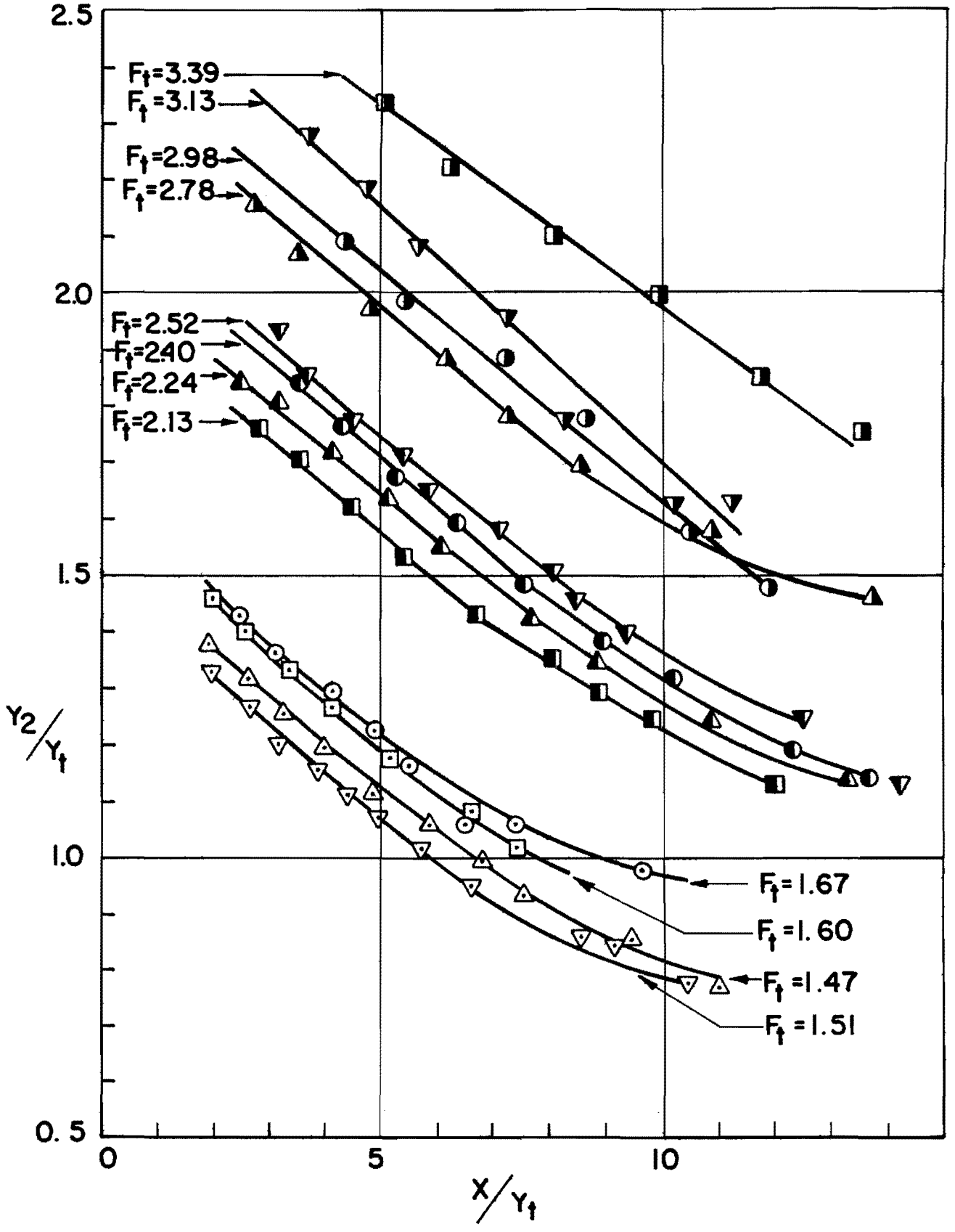

FIGURE III.1 - VARIATION OF Y_2/Y_f vs. X/Y_f FOR ARRANGEMENT NO. 66030

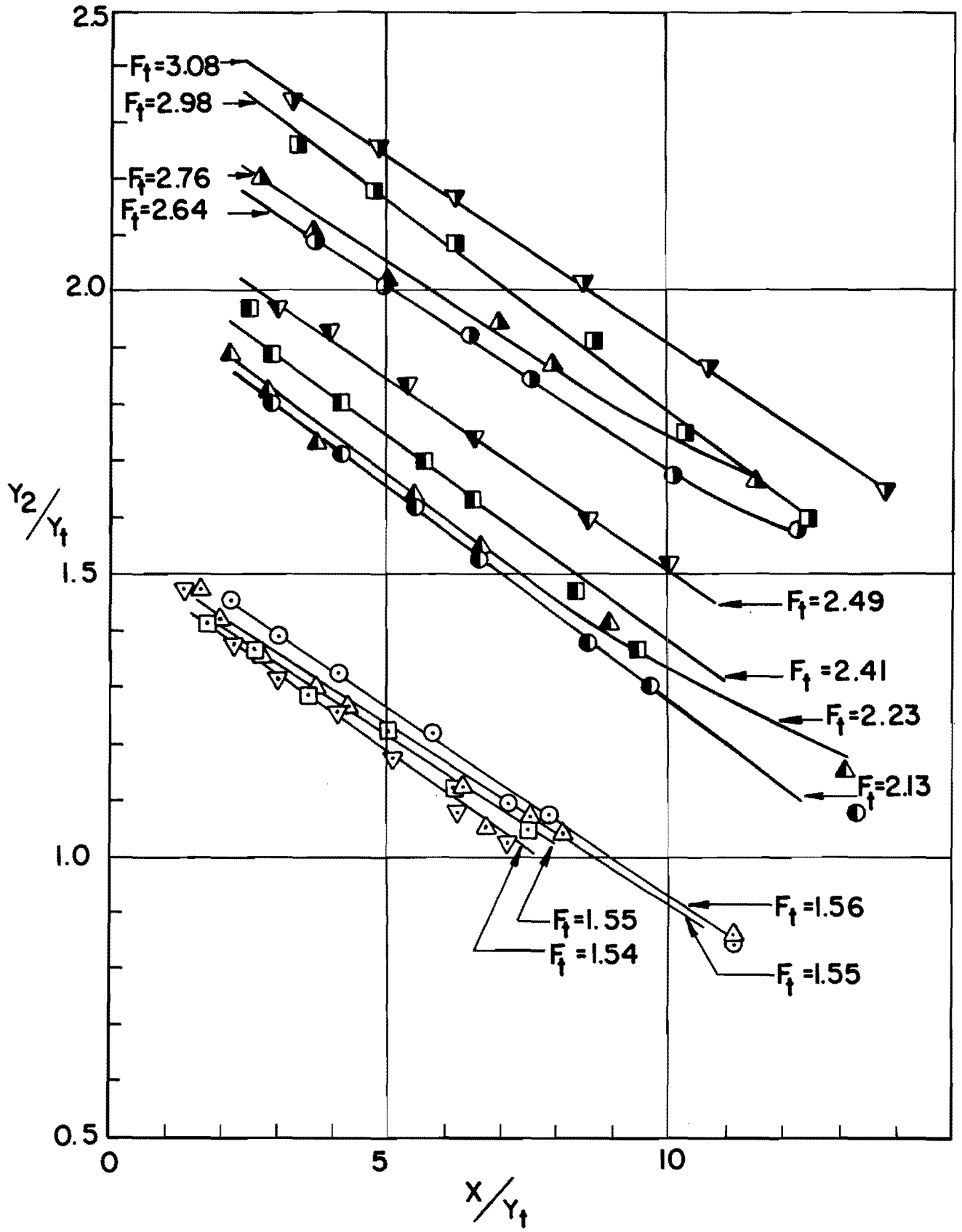

FIGURE III. 2 - VARIATION OF Y_2/Y_t vs. X/Y_t FOR ARRANGEMENT NO. 46030

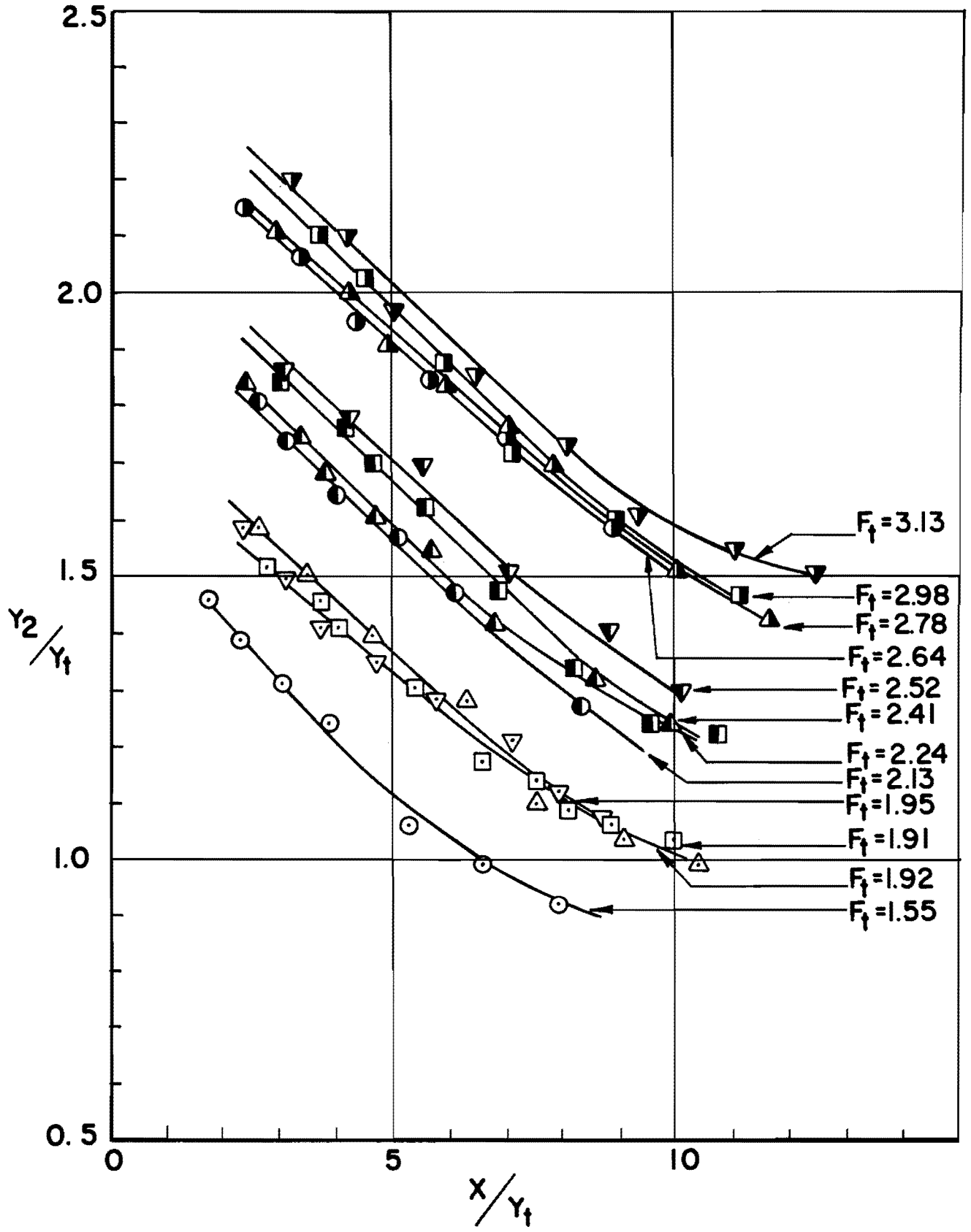

FIGURE. III 3 - VARIATION OF Y_2/Y_t vs. X/Y_t FOR ARRANGEMENT NO. 60030

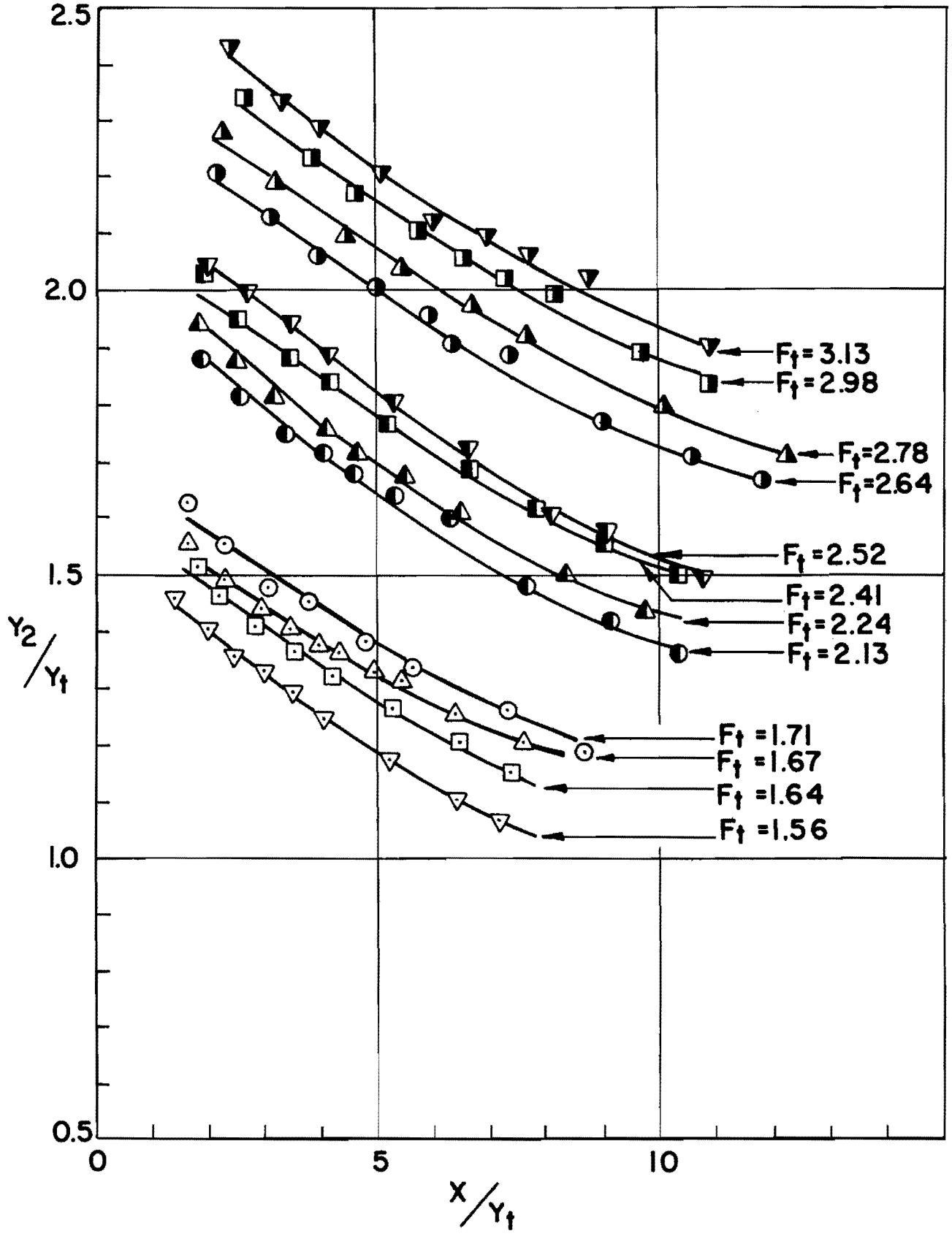

FIGURE III.4 - VARIATION OF Y_2/Y_t vs. X/Y_t FOR ARRANGEMENT NO. 40030

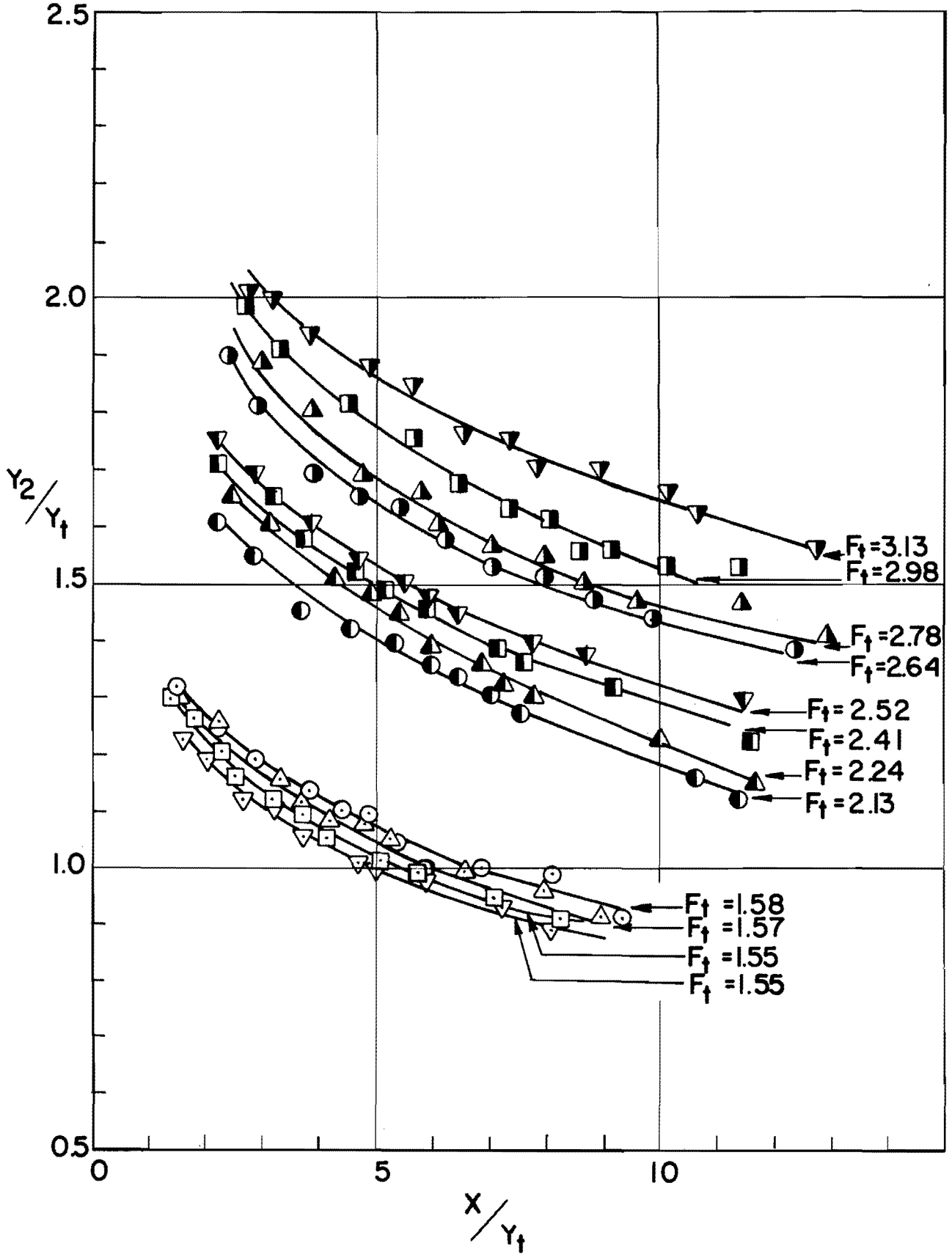

FIGURE III.5 - VARIATION OF Y_2/Y_t vs. X/Y_t FOR ARRANGEMENT NO. 66045

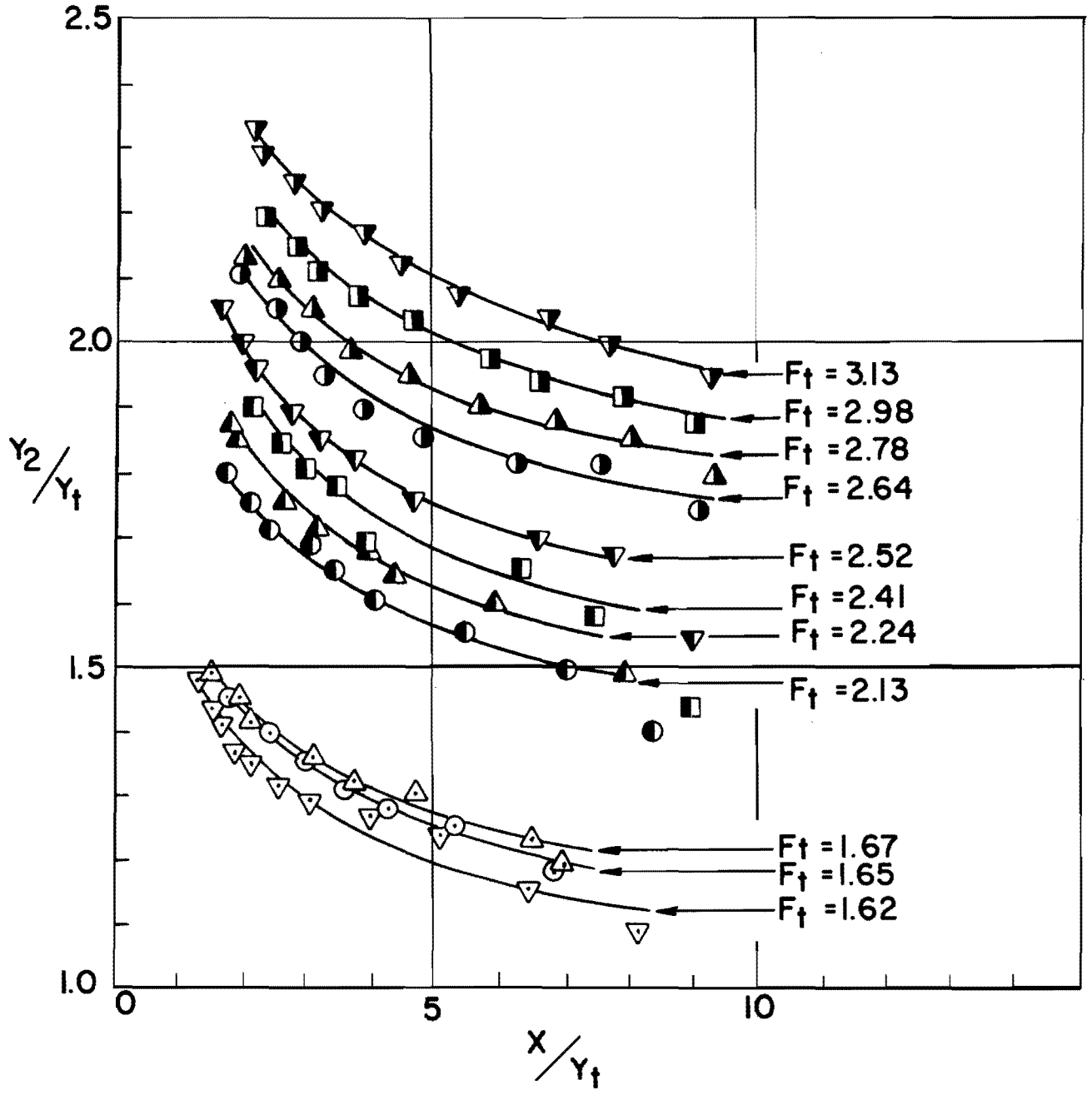

FIGURE III.6 - VARIATION OF Y_2/Y_t vs. X/Y_t FOR ARRANGEMENT NO. 46045

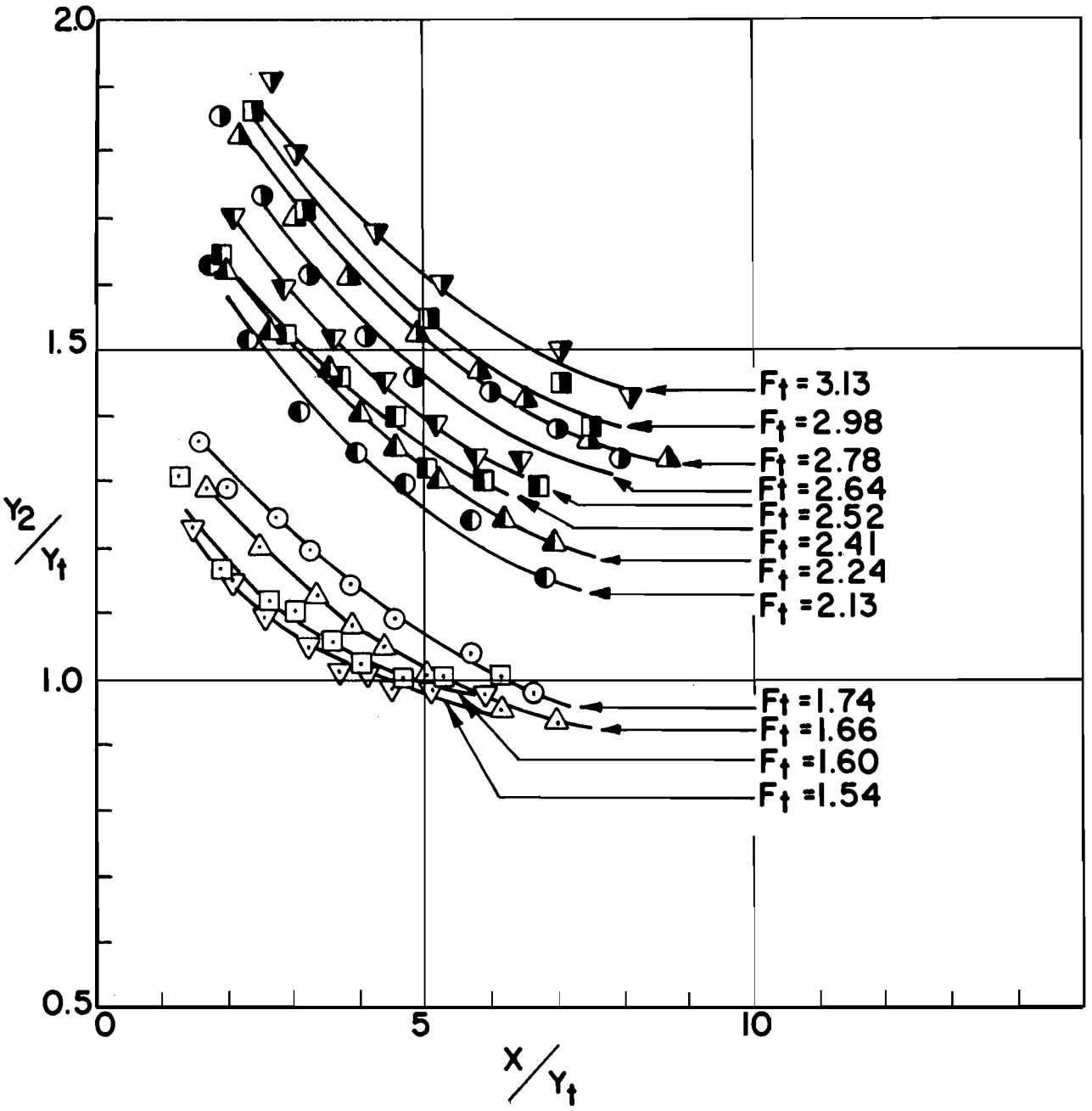

FIGURE III.7 - VARIATION OF Y_2/Y_t vs. X/Y_t FOR ARRANGEMENT NO. 60045

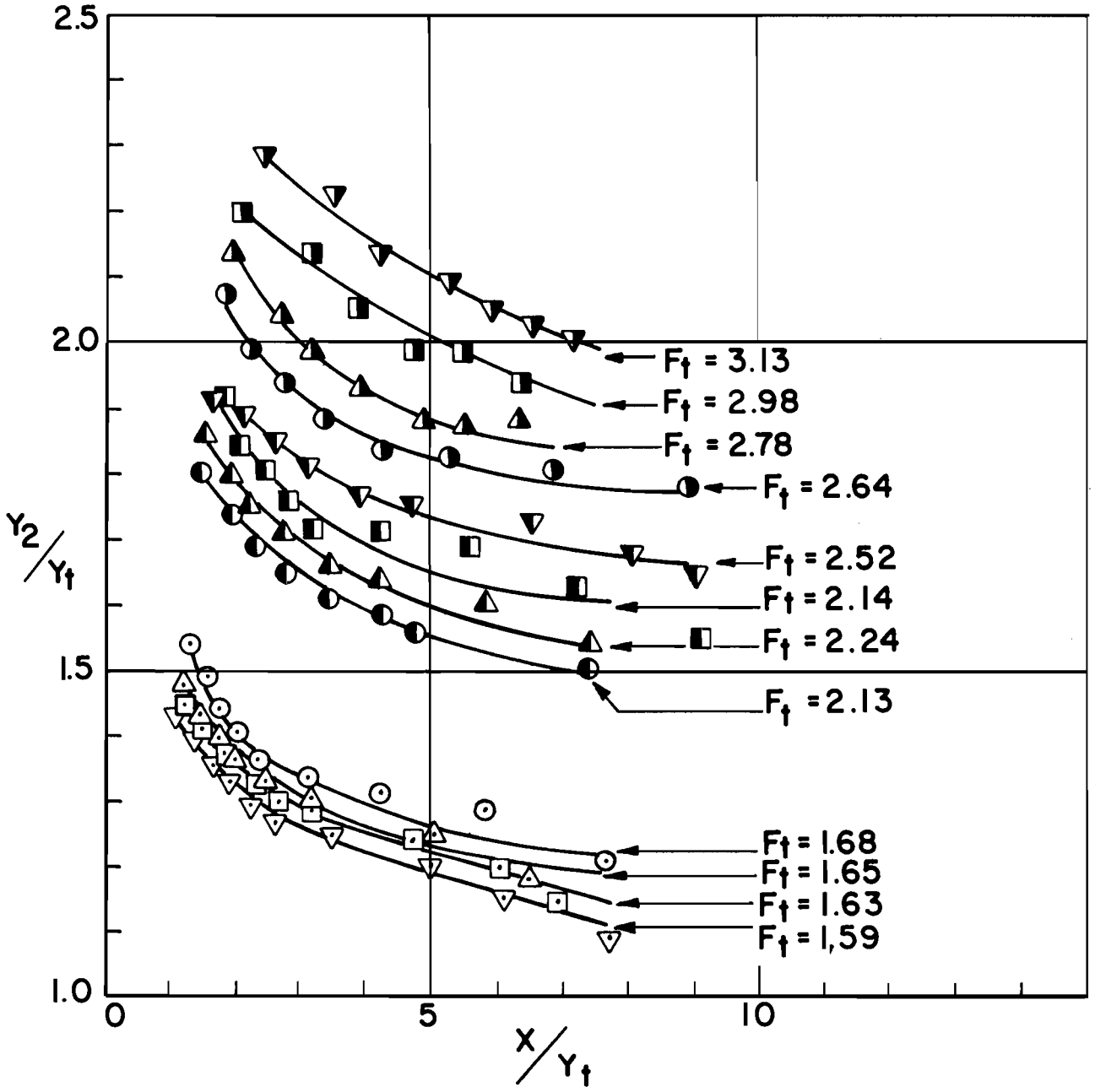

FIGURE III.8 - VARIATION OF Y_2/Y_t vs. X/Y_t FOR ARRANGEMENT NO. 40045

length of a uniform channel. This variation in radial flow may be such that both, Froude number and depth of flow, decrease as flow progresses downstream. In a uniform channel of horizontal or mild slope, as supercritical flow progresses downstream, its Froude number will decrease, but its depth must necessarily increase. The two conditions of radial flow just described, i.e., greater variation in Froude number and flow depth and the fact that both can decrease conjunctively permit the required sequent depth y_2 to decrease sharply within a short length of basin.

Since flow in the structure under investigation does not represent a case of true axially symmetric radial flow, flow in the basin area did not attain complete angular symmetry. However, the degree of radial dispersion of the flow was sufficient to eliminate the problem of separation at the wingwalls, immediately downstream from the culvert outlet, and to permit the stability characteristics inherent to radial flow to be retained to a considerable degree by the quasi-radial flow in the stilling basin structure. A view of a representative flow in the stilling basin is shown in Figure III.9. The percentage change of tailwater depth y_2 required for the jump to move downstream into the region with parallel wingwalls varied for each geometric arrangement. It was in all cases greater for the longer basins. The approximate average variation of y_2 was in the order of $0.5y_t$ as x/y_t varied from a value of 2.5 to 10.0.

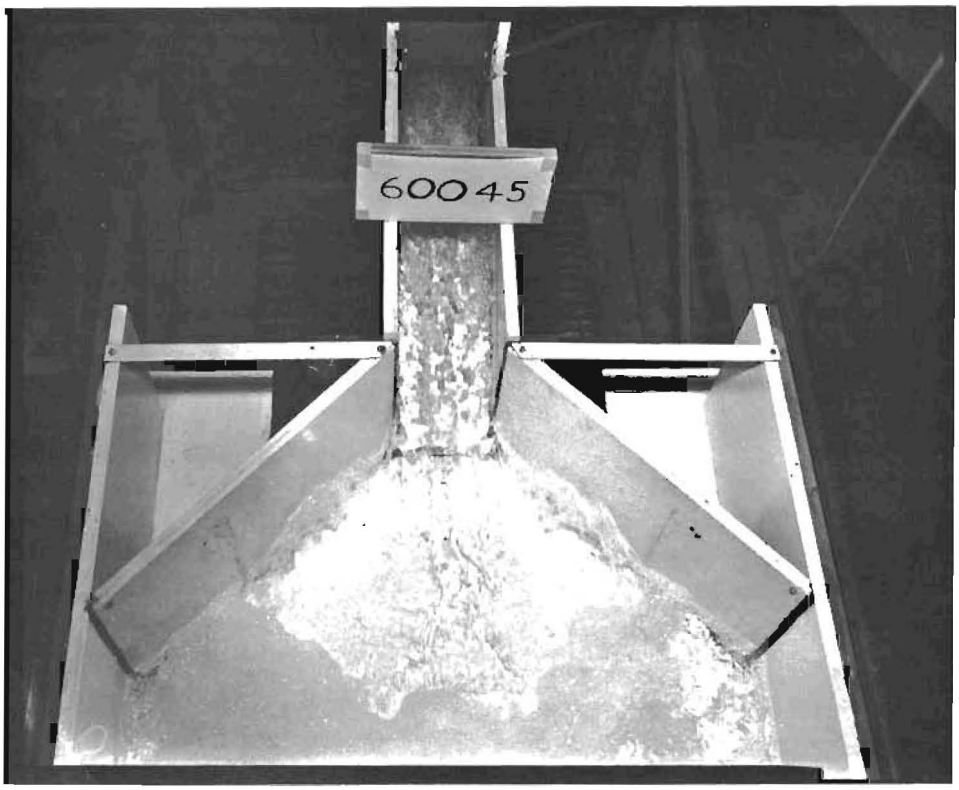

FIGURE III.9 FORMATION OF HYDRAULIC JUMP IN STILLING BASIN

As the jump moved into the zone with parallel training walls, the absolute value of the slope of the y_2/y_t vs. x/y_t function decreased rapidly, but it did not sharply reach the limiting minimum value corresponding to the parallel channel. Instead, there was a transition in which flow was being transformed from radial flow to parallel flow. This transformation required a certain length of basin since radial flow continued in its radial direction until it encountered a sufficient lateral pressure-momentum buildup to force it to change to a direction parallel to the channel centerline. The basin length required for the transformation from radial to parallel flow manifests itself as the increment of x/y_t required for the slope of the y_2/y_t vs. x/y_t function to change from the initial constant value to nearly horizontal.

Another variation of the same three parameters involved in the functions discussed in the previous paragraphs is that of y_2/y_t vs. F_t at particular constant values of x/y_t. It was considered of interest to investigate this variation in order to compare it, at a given value of x/y_t, with the same type of variation for a two-dimensional hydraulic jump. The values of y_2/y_t vs. F_t for each constant x/y_t were graphically determined for the curves plotted in Figures III.1 through III.8. The values thus obtained were interpolated from the plotted curves, and should not be interpreted as original data. Curves of y_2/y_t vs. F_t for each geometric arrangement of the stilling basin are given in Figures III.10

through III.17. Also shown in each one of these figures is the corresponding curve which would be obtained from a two-dimensional hydraulic jump with initial depth equal to depth y_t.

In general, there are twelve plotted points for each one of these curves, of which the highest four values of Froude number correspond to a constant value of y_t/b of 0.39, and the middle four values to a constant y_t/b of 0.45. The lowest four values of Froude number are in all cases approximately constant and do not correspond to a constant y_t/b. These lowest four points cover a range of y_t/b from 0.50 to 0.60.

Since, in the present program, high values of F_t were restricted to low values of y_t/b, no direct comparison can be made between values of y_2/y_t at a constant F_t and variable y_t/b. However, it may be observed from Figures III.10 through III.17 that in general, within the range of y_t/b investigated, the values of y_2/y_t vs. F_t define a straight line for each value of x/y_t without undue scatter of points. Each straight line was established by the method of least squares.

It may also be noticed that each group of four points corresponding to a constant y_t/b in most cases defines a short curve with a smaller slope than that of the straight line. If this tendency should continue for a greater range of F_t at each y_t/b value, it would indicate that, at a constant x/y_t and F_t, a certain range of values of y_2/y_t would be possible. However, in order to verify

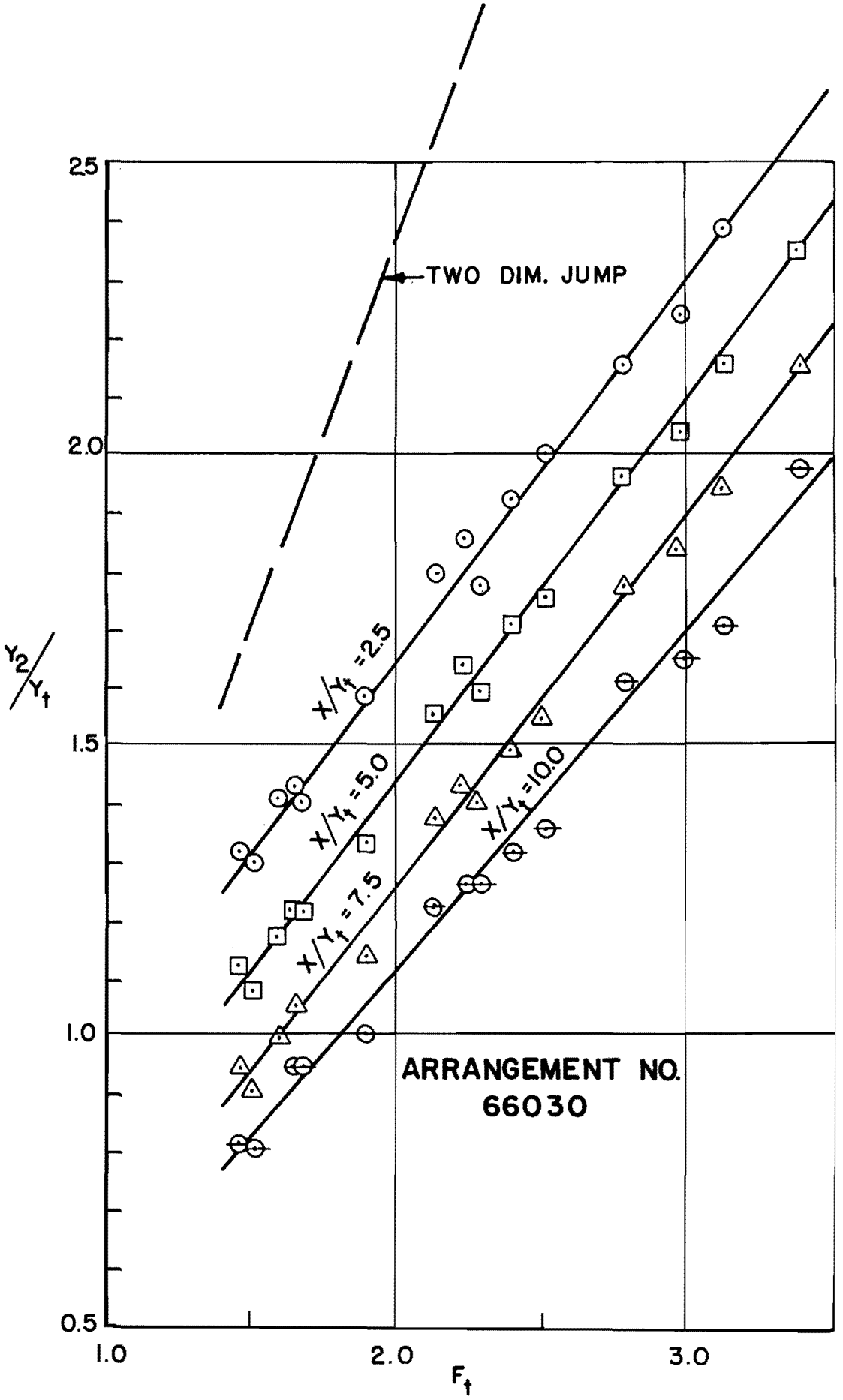

FIGURE III.10- VARIATION OF Y_2/Y_t vs. F_t

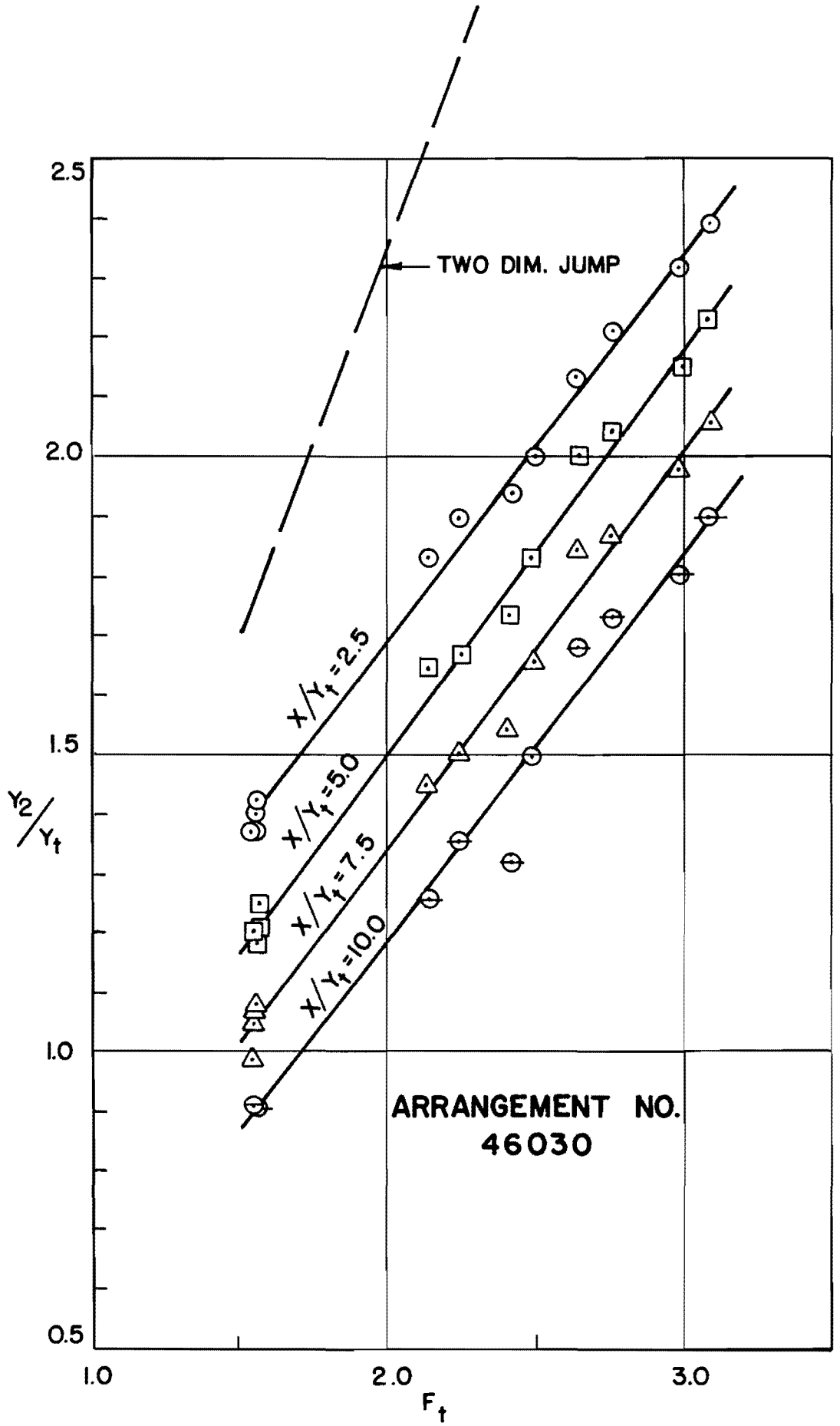

FIGURE III.11- VARIATION OF Y_2/Y_t vs. F_t

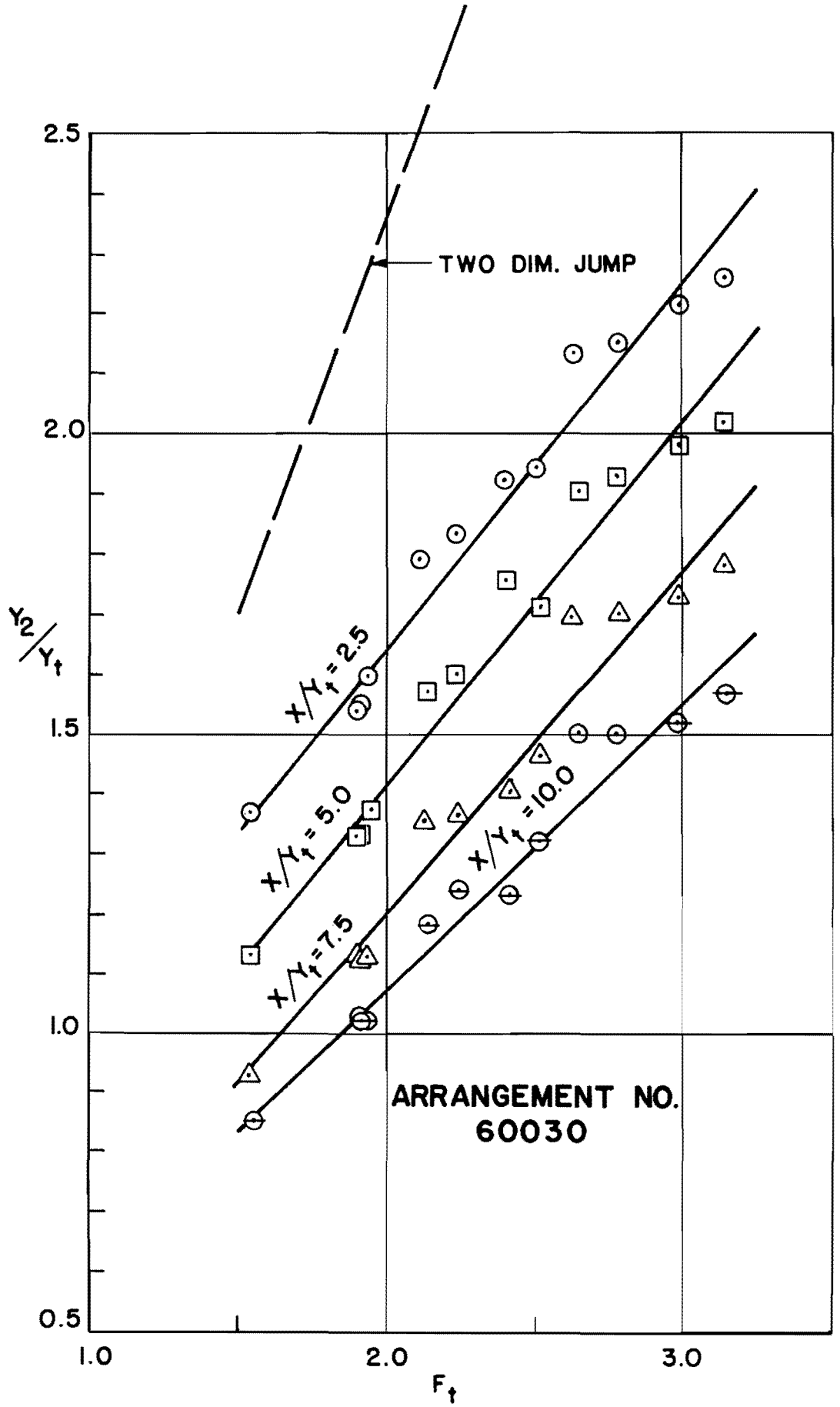

FIGURE III.12- VARIATION OF Y_2/Y_t vs. F_t

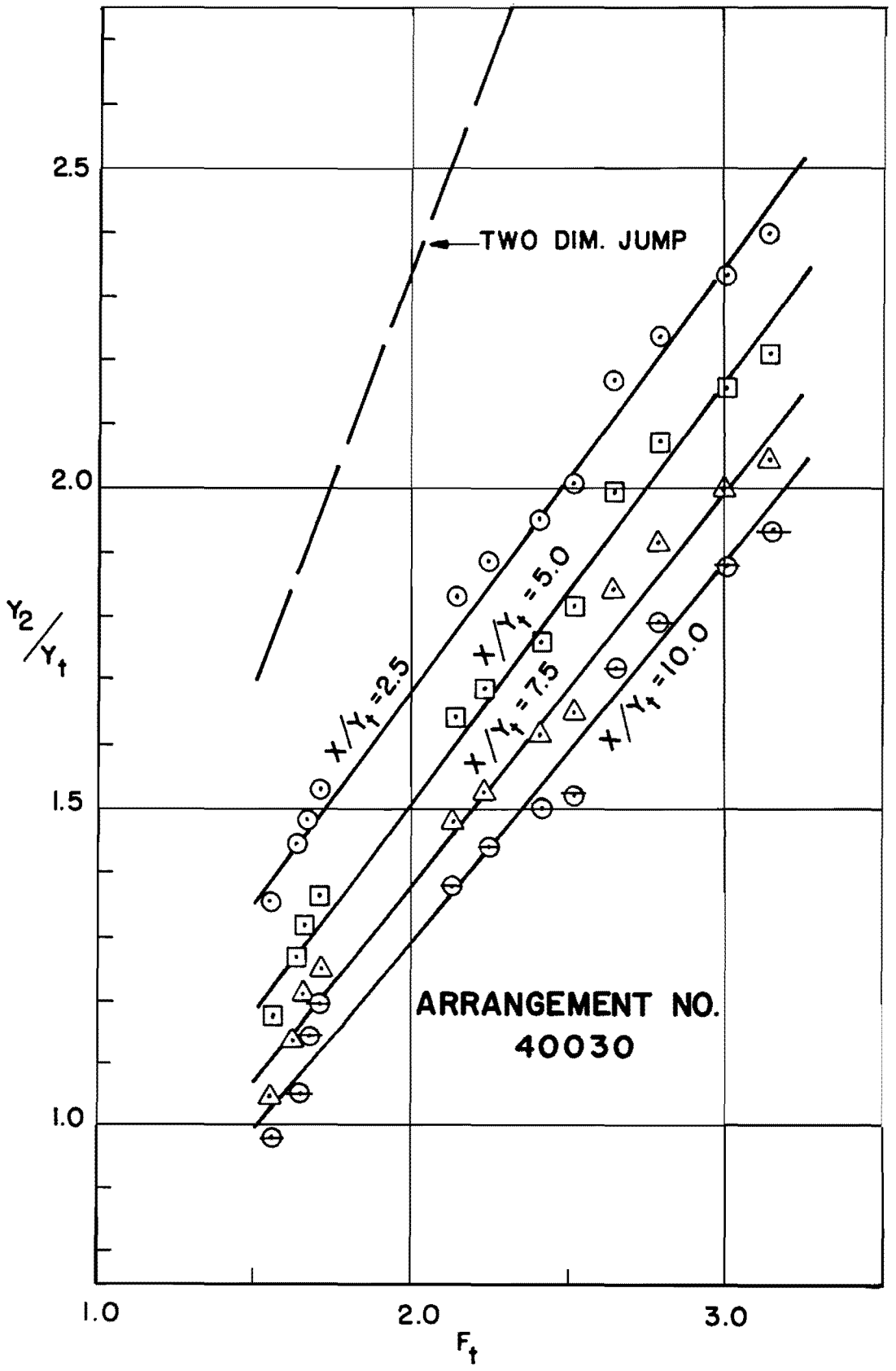

FIGURE III.13 - VARIATION OF Y_2/Y_t vs. F_t

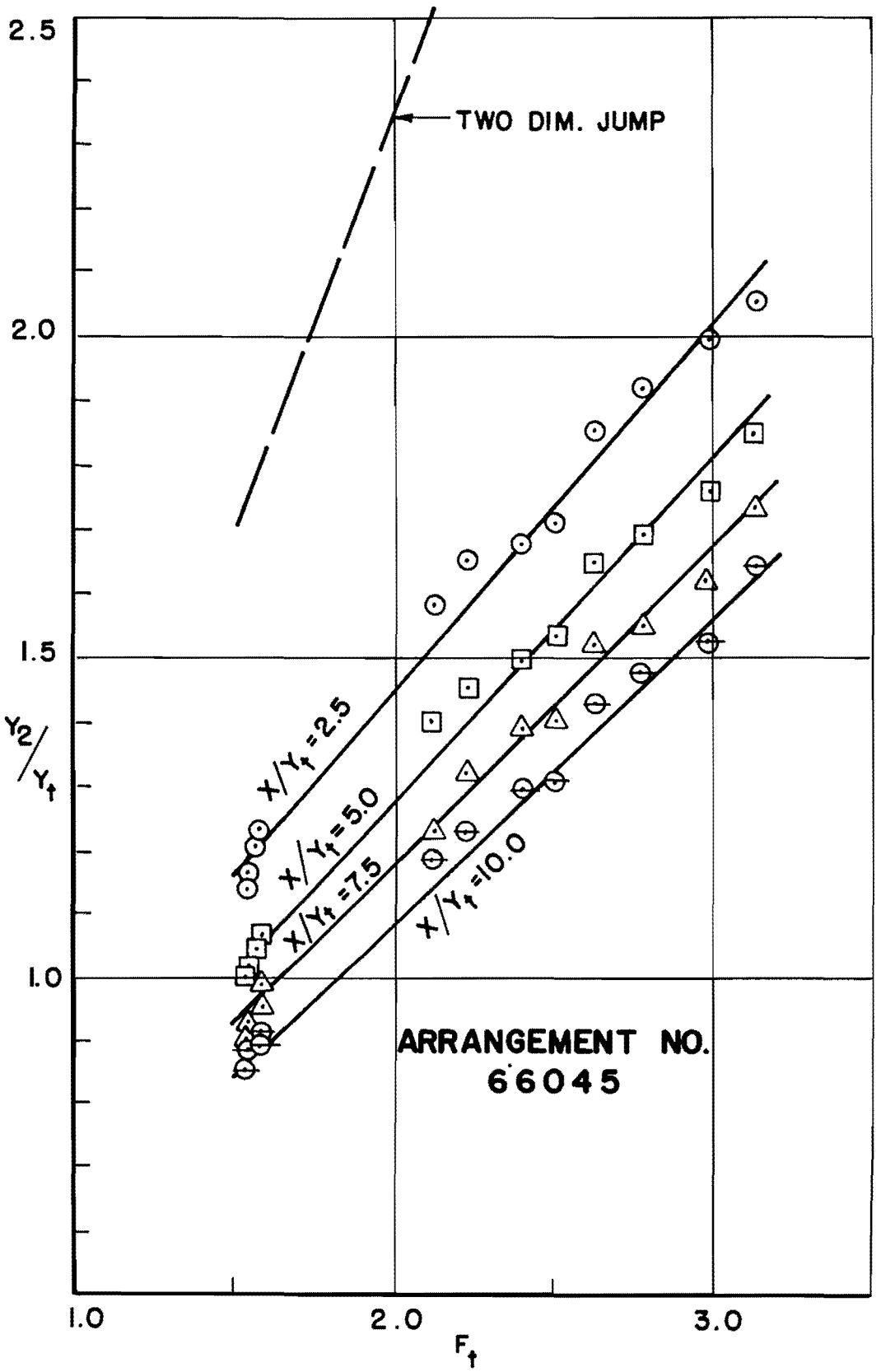

FIGURE III.14 - VARIATION OF Y_2/Y_1 vs. F_1

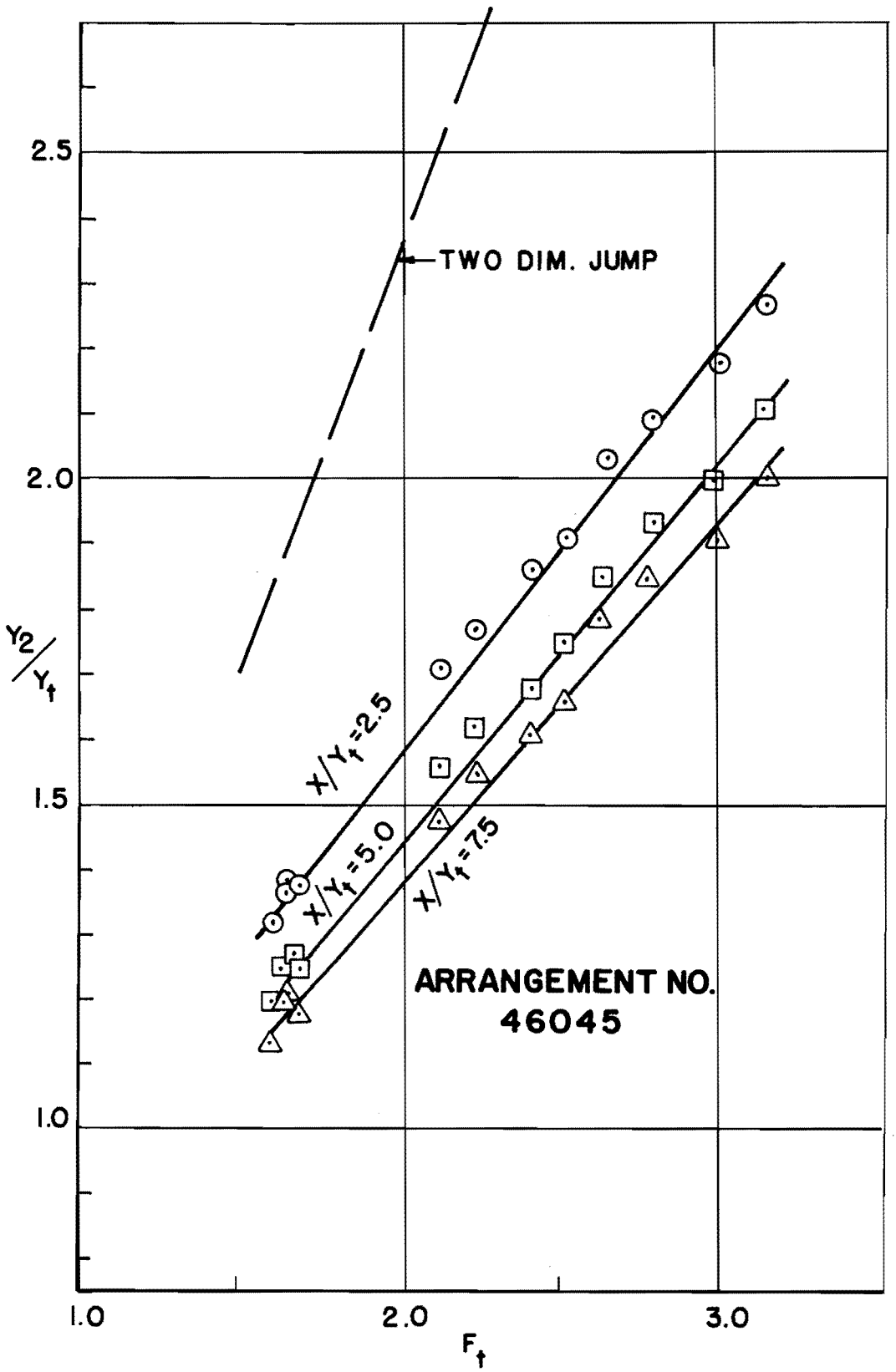

FIGURE III.15 - VARIATION OF Y_2/Y_f vs. F_f

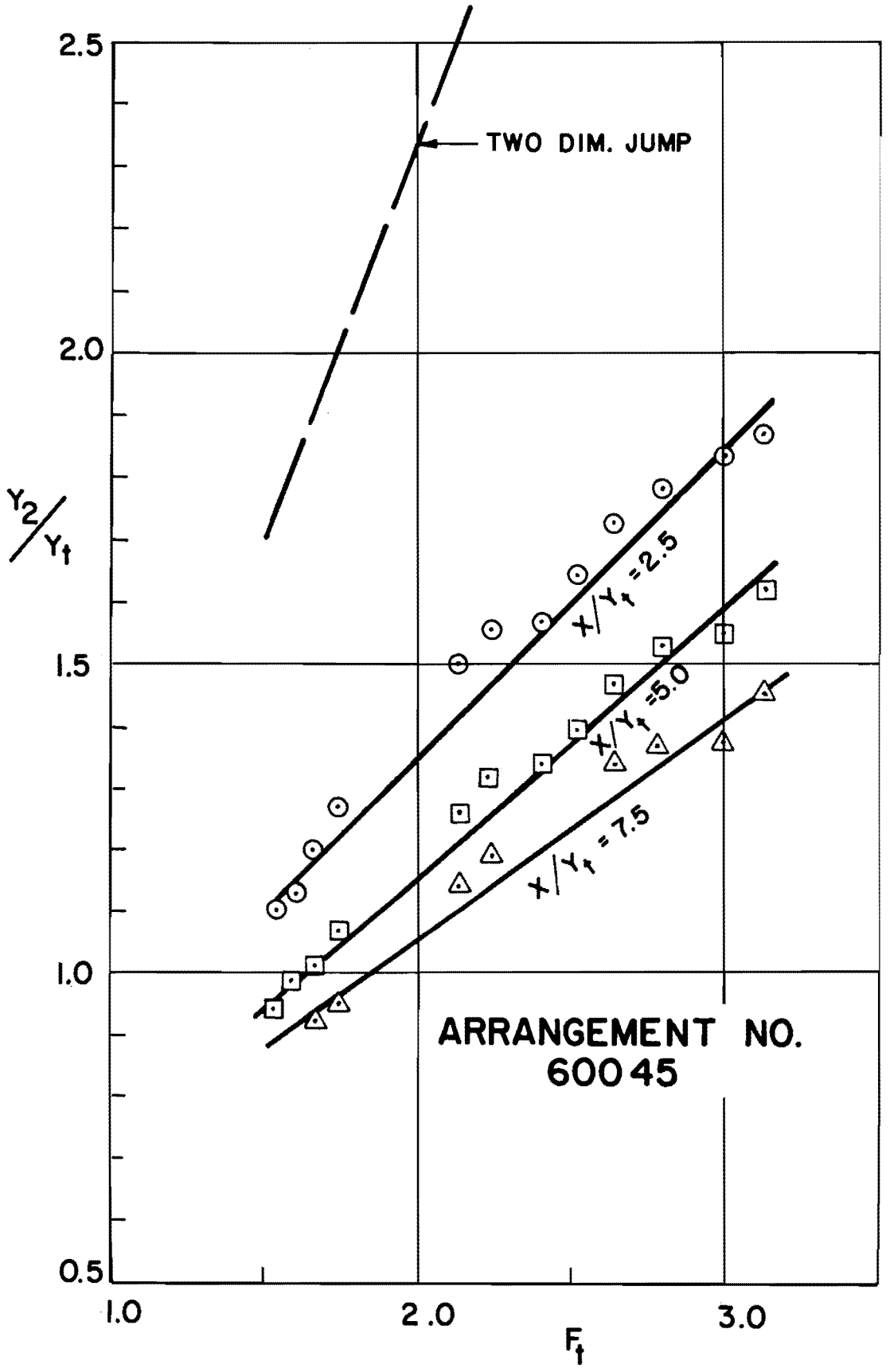

FIGURE III. 16 VARIATION OF Y_2/Y_t vs. F_t

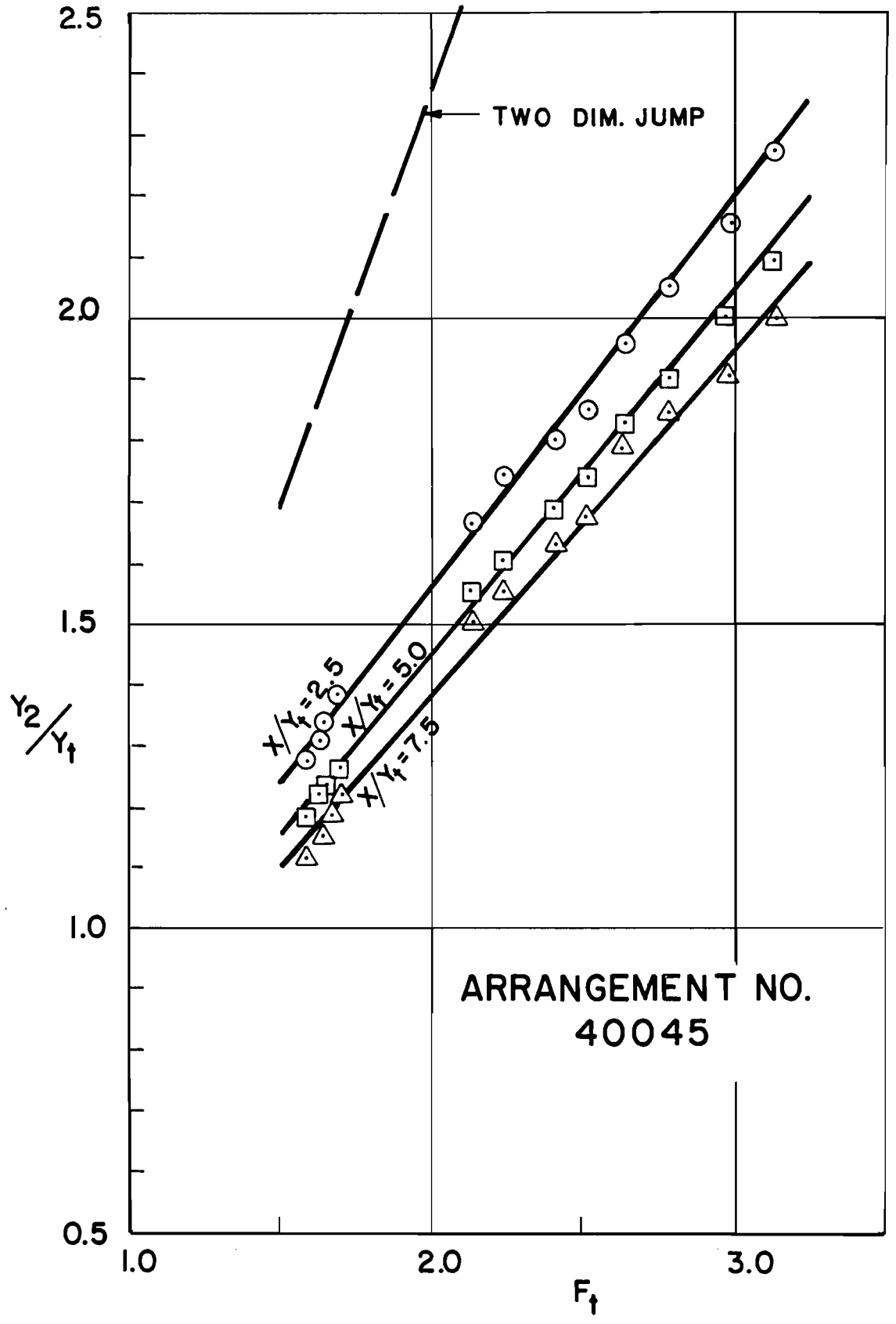

FIGURE III. 17 VARIATION OF Y_2/Y_1 vs. F_1

this tendency, much more extensive testing would be required covering a greater range of F_t at each particular value of y_t/b, and probably also a greater range of values of y_t/b.

A comparison of the relative jump stability characteristics of each of the geometric arrangements used can be made from the y_2/y_t vs. F_t functions established for each basin. At a constant value of F_t, the difference in y_2/y_t between any two of the constant x/y_t curves may be obtained for each basin. The geometric arrangement which yields the largest difference in y_2/y_t will be considered to have the highest degree of jump stability within the range of the two x/y_t values used. This comparison was performed at a value of F_t = 2, and the results are given in Table 2.

TABLE 2

DETERMINATION OF JUMP STABILITY

	Limits of x/y_t Range		
	2.5 to 5.0	2.5 to 7.5	
Arrangement	$\Delta y_2/y_t$	$\Delta y_2/y_t$	L/b
66030	0.20	0.39	4.30
46030	0.18	0.35	2.58
60030	0.22	0.44	4.30
40030	0.17	0.31	2.58
66045	0.17	0.27	2.50
46045	0.15	0.21	1.50
60045	0.21	0.31	2.50
40045	0.11	0.16	1.50

The parameter L/b is introduced at this time because of its apparent relationship to the degree of jump stability. However, L/b is not independent of variables introduced in the dimensional analysis. Its value is obtained from the combination $L/b = (1/2)(B/b - 1) \cot \theta$. It becomes evident then, that whatever influence L/b may be found to have on the jump stability is the result of the combined effect of B/b and θ.

The values given in Table 2 and plotted in Figure III.18 indicate that the basins with the highest degree of jump stability are Arrangements 60030 and 66030, which also have the largest values of L/b. In the second range of x/y_t considered, that is, for x/y_t from 2.5 to 7.5, it is evident that the jump must be moved farther downstream than in the first range. As the jump moves downstream, it may reach the parallel wall region of the shorter basins at $x/y_t = 7.5$, whereas at the same value of x/y_t it would still be within the flared wall region of the longer basins. It was noticed earlier that the jump stability is higher in the flared wall region than in the parallel wall portion of the basin. This same behavior is made evident by the general relationship between $\Delta y_2/y_t$ and L/b observed from the values of Table 2.

Another comparison of relative tailwater requirements for the different geometric arrangements may be made in terms of the absolute values of y_2/y_t at one given value of x/y_t, and the complete range of F_t. This is not a comparison of the sensitiveness

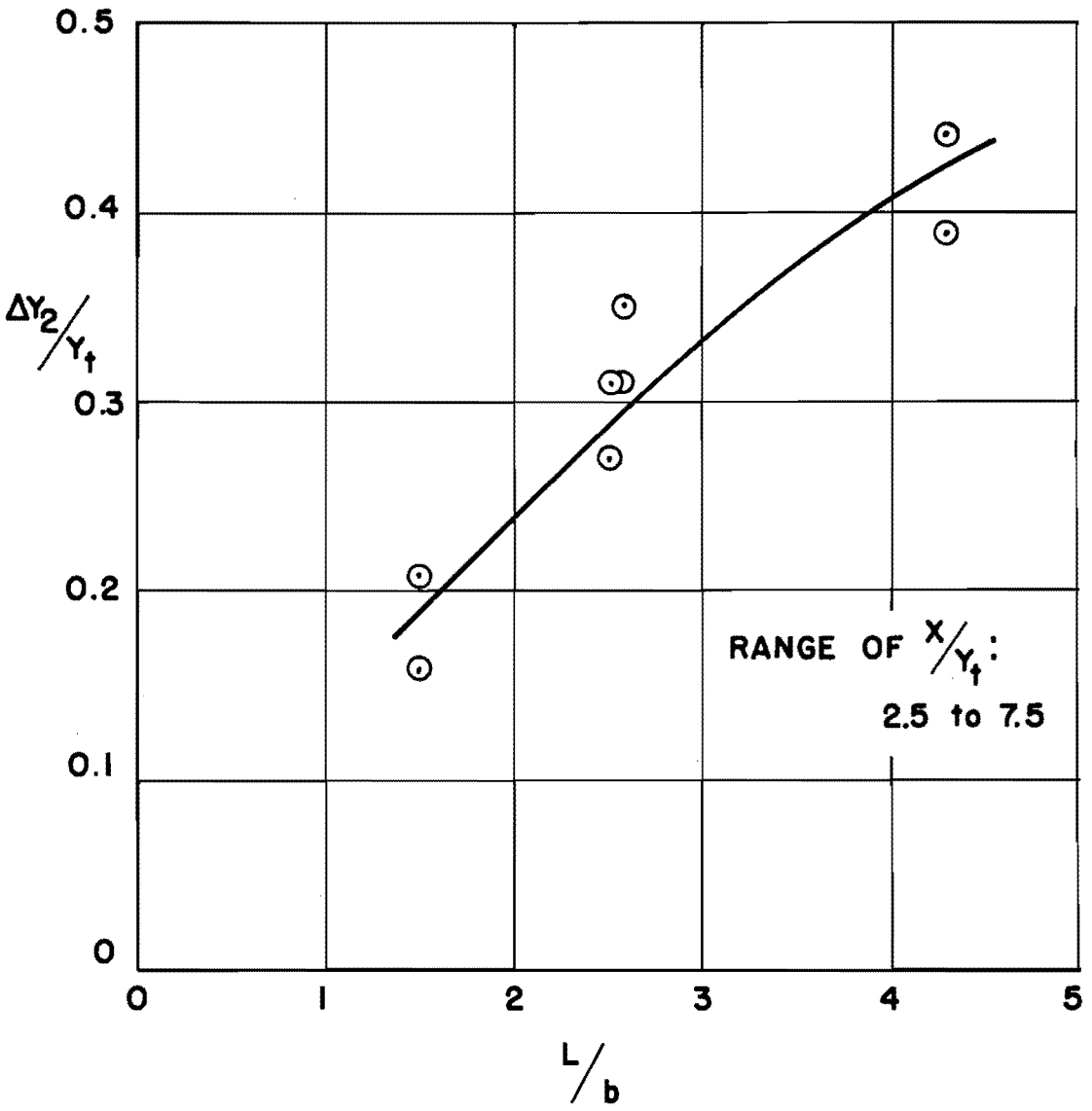

FIGURE III.18 – VARIATION OF $\Delta Y_2 / Y_t$ vs. L/b

of the hydraulic jump to changes in tailwater level, but rather one to explore the absolute tailwater depth requirements of each arrangement.

From a comparison of the y_2/y_t vs. F_t curves of all the arrangements tested, it was found that the arrangement which required the least relative tailwater depth at all values of x/y_t was 60045, followed by 66045. In general, tailwater requirements at small values of x/y_t were lower for arrangements with $\theta = 45^o$. At values of x/y_t of 5 and larger, it was found that the lowest y_2/y_t requirements corresponded to arrangements with B/b of 6. Also, lower tailwater at all values of x/y_t was required for $\beta = 0$ when B/b = 6. At B/b = 4, $\theta = 30^o$ and large values of x/y_t, lower tailwater was required for $\beta = 60^o$, while at $\theta = 45^o$, no difference was found between the tailwater requirements of either value of β. In Table 3, the different arrangements are listed in order of increasing required tailwater depth for different values of x/y_t.

From the behavior outlined above, it may be observed that generally, better or equal performance is obtained from the entrance channel bottom with $\beta = 0$ than from the channel with $\beta = 60^o$. The required y_2/y_t for the jump to form near the basin entrance appears to be affected more strongly by the wingwall flare angle θ than by the entrance channel angle β. Since the wingwall angle θ affects the degree of spreading of the flow, it becomes apparent from the results for $x/y_t < 5$ that better spreading action is obtained when the flare angle θ is 45^o.

TABLE 3

LISTING OF GEOMETRIC ARRANGEMENTS
ACCORDING TO TAILWATER REQUIREMENTS

$x/y_t < 5$		$x/y_t \geq 5$	
Order of Increasing y_2/y_t	Arrangement Designation	Order of Increasing y_2/y_t	Arrangement Designation
1	60045	1	60045
2	66045	2	66045
3 - 4	46045	3	60030
3 - 4	40045	4	66030
5 - 6	60030	5 - 6	46045
5 - 6	66030	5 - 6	40045
7 - 8	46030	7	46030
7 - 8	40030	8	40030

At large values of x/y_t and B/b = 4, the jump forms either in or near the downstream channel with parallel wingwalls. In this region, the jump becomes less stable and therefore the required tailwater depth is increased. For the present case, then, the effect of the parameter B/b becomes dominant over the effect of the angle 0, with the result that, at large values of x/y_t, lower tailwater is required by the arrangements with B/b = 6.

Since the selection of the value of B/b to be used in a given prototype structure is not entirely up to the designer, but

rather is fixed to a large extent by natural channel conditions and required culvert size, two arrangements of the present structure may be mentioned as having the lowest tailwater depth requirements, depending on whether a large or small value of B/b is to be used. If the value of B/b is in the order of 6, the lowest tailwater depth required to stabilize the jump at any value of x/y_t is obtained with Arrangement 60045. When the value of B/b is in the order of 4, the lowest required tailwater depth for all values of x/y_t is given by Arrangements 40045 and 46045. From a construction point of view, the entrance channel with $\beta = 0$ appears simpler and thus more economical to construct; therefore, according to the foregoing considerations, for a situation of B/b in the order of 4, Arrangement 40045 would be the preferable choice.

It was mentioned earlier that the height of drop of the entrance channel, denoted as z, was considered a significant parameter in the present study. According to this consideration, the results presented in the foregoing pages would be quantitatively different for values of z other than that used herein. This appears reasonable since a set of constant values of y_t and V_t will yield different values of velocity and depth of flow at the basin entrance as the height of drop of the entrance channel is varied.

In order to investigate the significance of nominal values of depth and velocity of flow at the basin entrance, calculations

for such values were performed according to a procedure described earlier. Thus, values of y_b and V_b were obtained for each set of y_t and V_t. From each combination of y_b and V_b, the corresponding value of F_b was calculated. Results obtained were plotted in the form of functions of y_2/y_b vs. x/y_b for each value of F_b. Since the values of y_2 and x are the same as those used in the previous analysis, the general shape of each of the y_2/y_b vs. x/y_b curves is the same as that found for the corresponding y_2/y_t vs. x/y_t curve. The same general pattern is also evident in that higher y_2/y_b values at a given x/y_b are obtained as F_b is increased.

From the plotted curves of y_2/y_b vs. x/y_b, values of y_2/y_b were obtained for each F_b at constant values of x/y_b. The functions of y_2/y_b vs. F_b thus obtained are given in Figures III.19 through III.26. As in the case of y_2/y_t vs. F_t, the plotted points may be represented by a straight line for each value of x/y_b. In this case, however, each point corresponds to a particular value of y_b/b, since identical values of y_t occurring at different velocities V_t will yield different values of y_b.

A comparison of jump stability for the different geometric arrangements, similar to the one made previously, was performed in terms of the change effected in y_2/y_b by a change in x/y_b at a given value of F_b. This comparison was made at a value of $F_b = 3.5$, and the results obtained are given in Table 4.

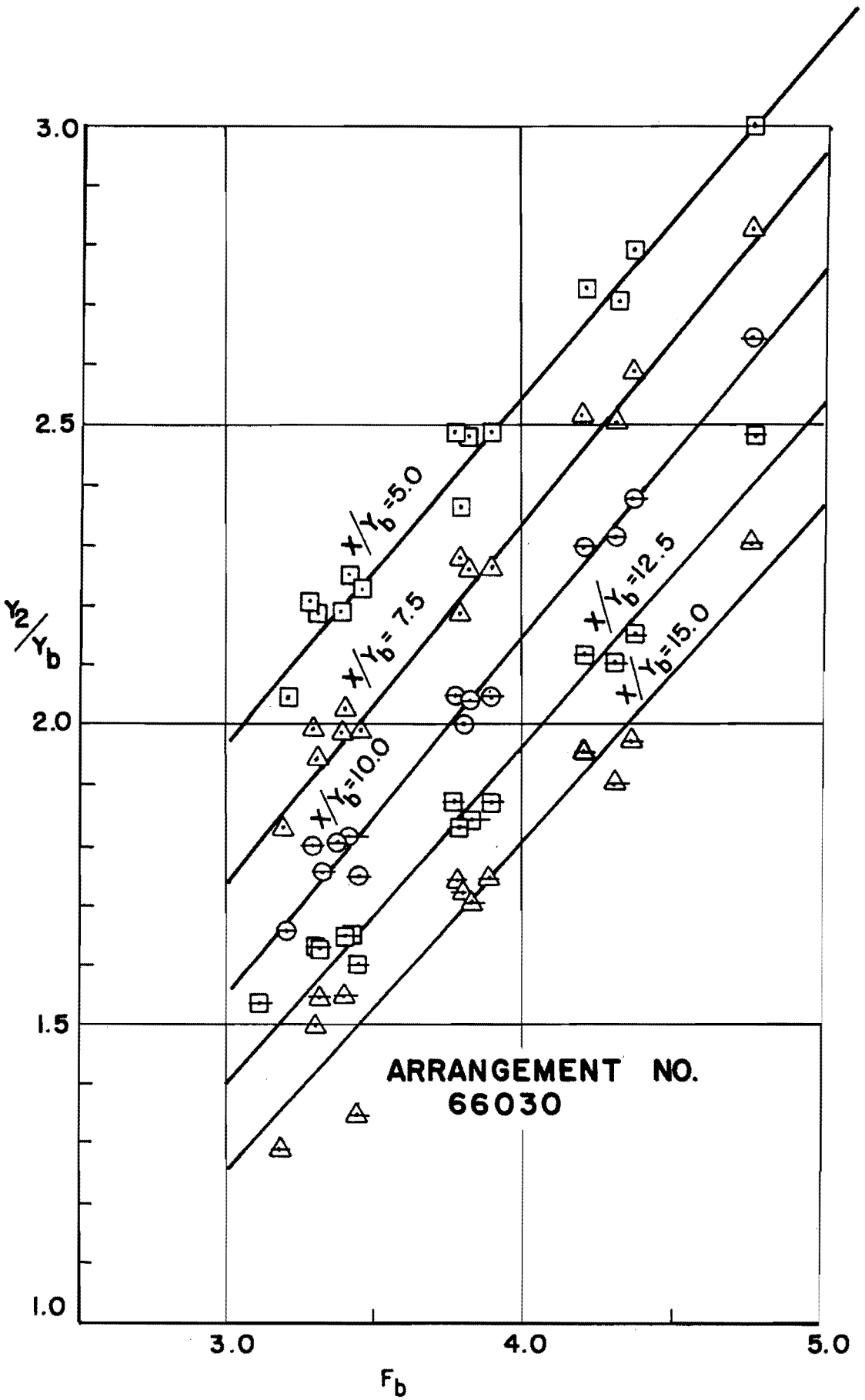

FIGURE III.19 - VARIATION OF Y_2/Y_b vs. F_b

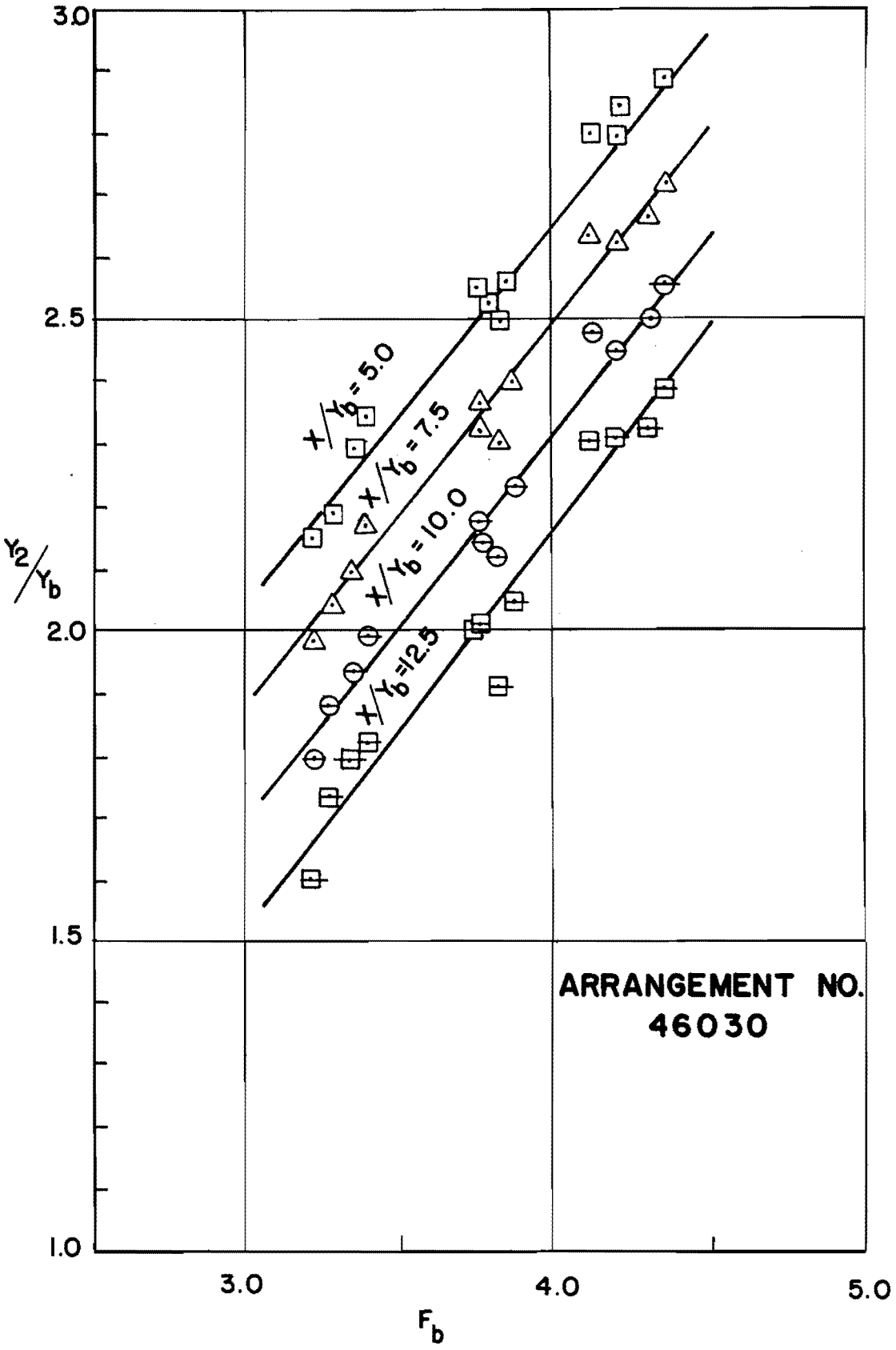

FIGURE III.20 - VARIATION OF Y_2/Y_b vs. F_b

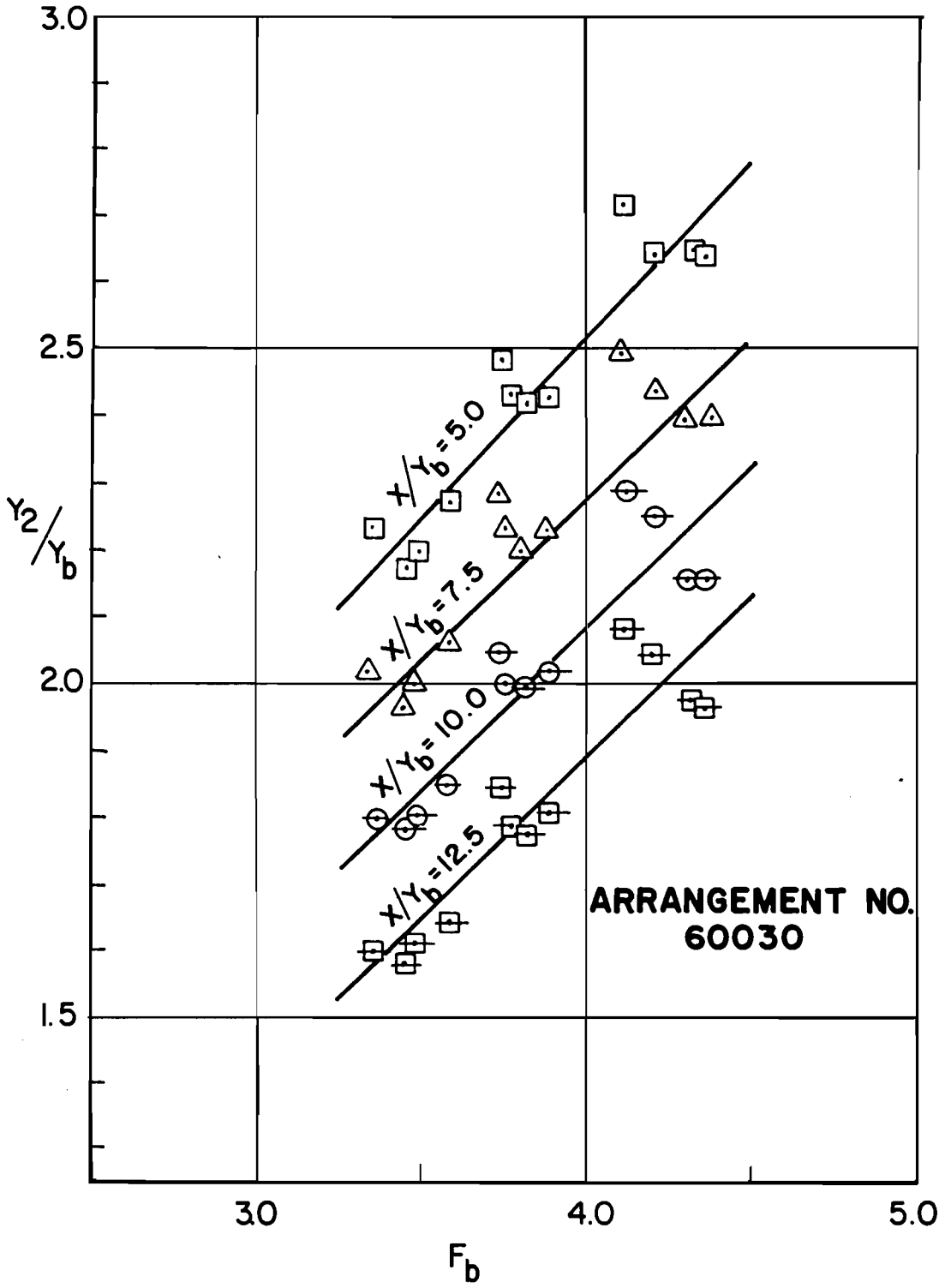

FIGURE III. 21- VARIATION OF Y_2/Y_b vs. F_b

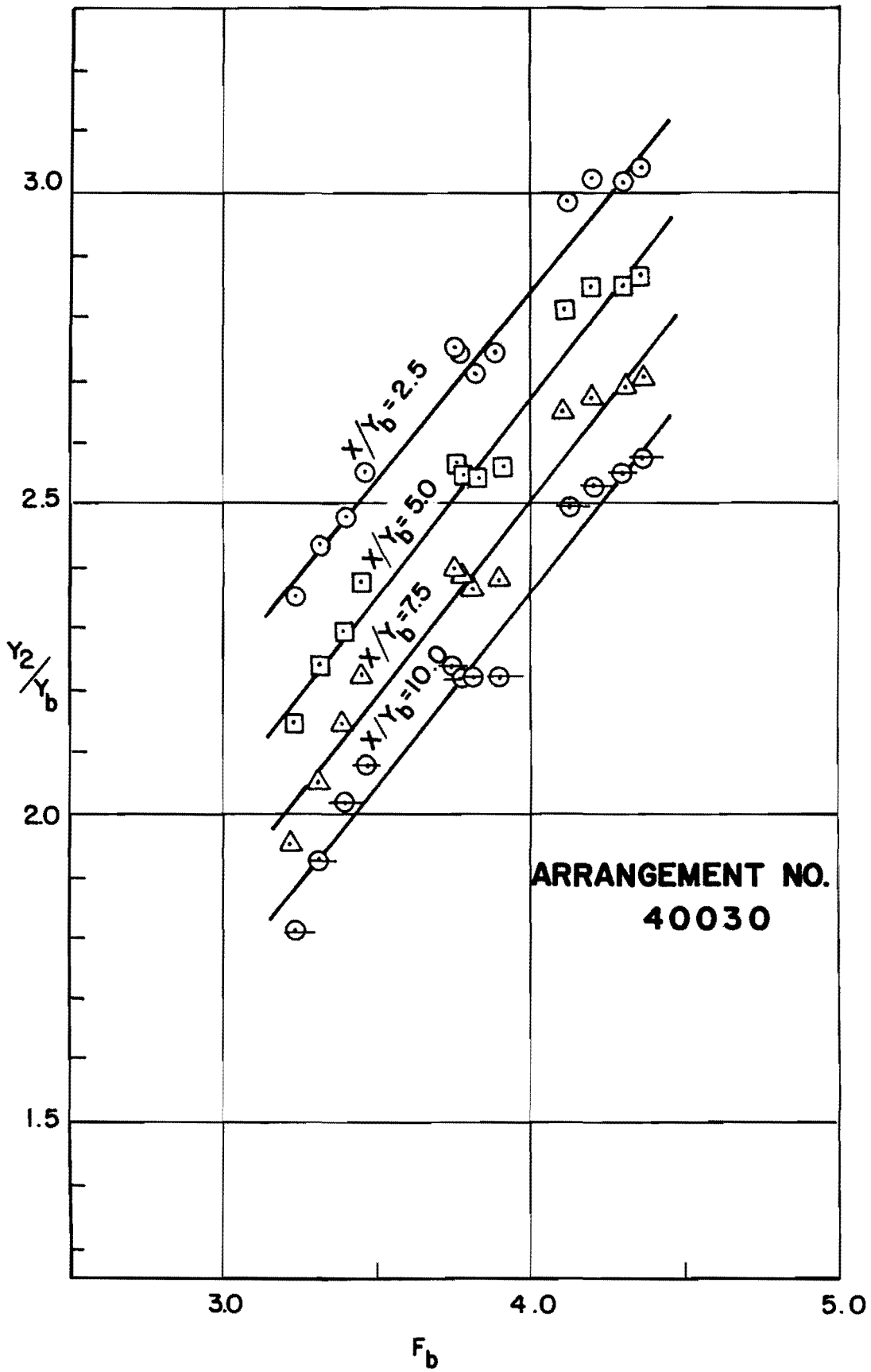

FIGURE III.22- VARIATION OF Y_2/Y_b vs. F_b

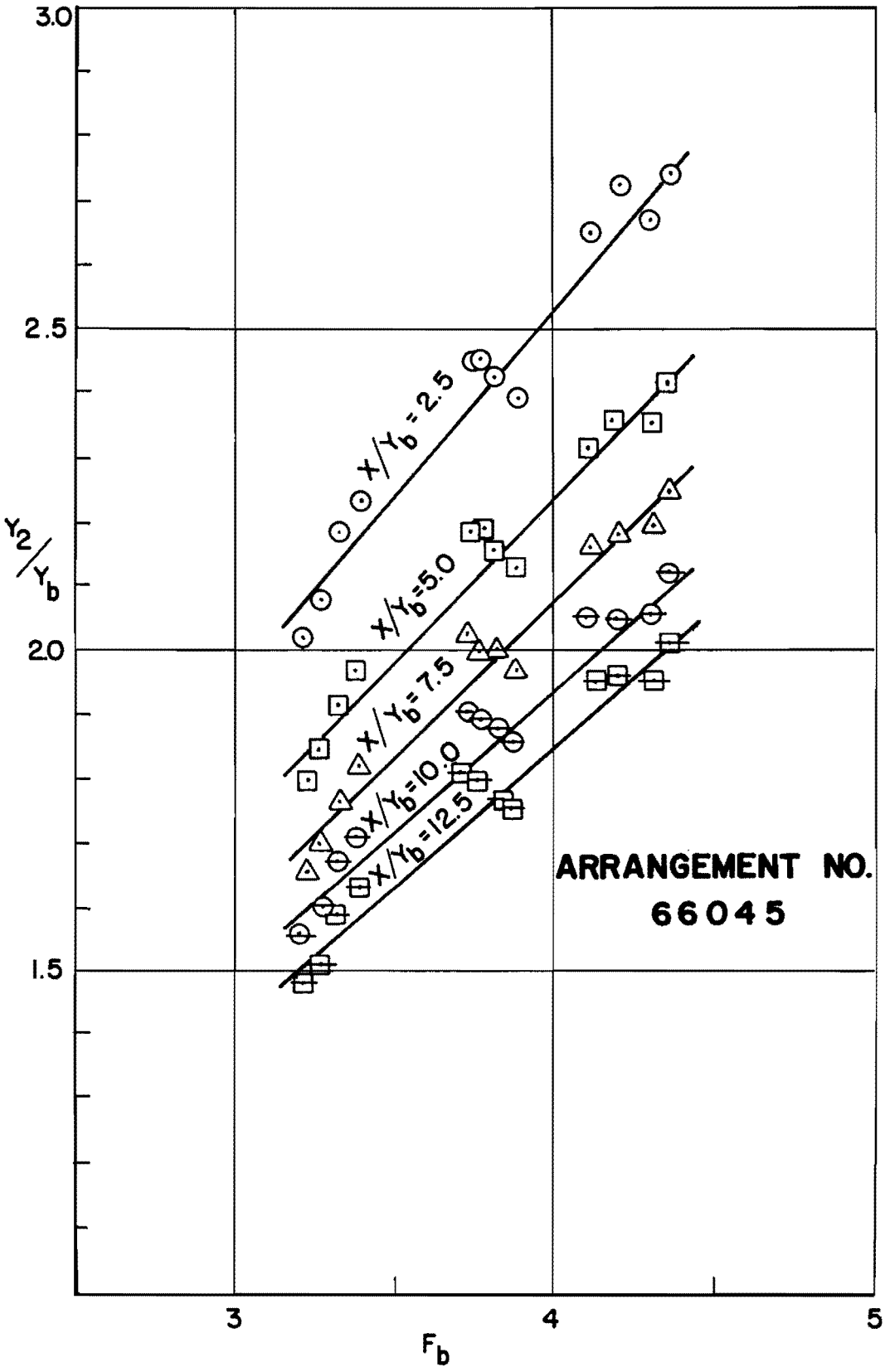

FIGURE III.23 - VARIATION OF Y_2/Y_b vs. F_b

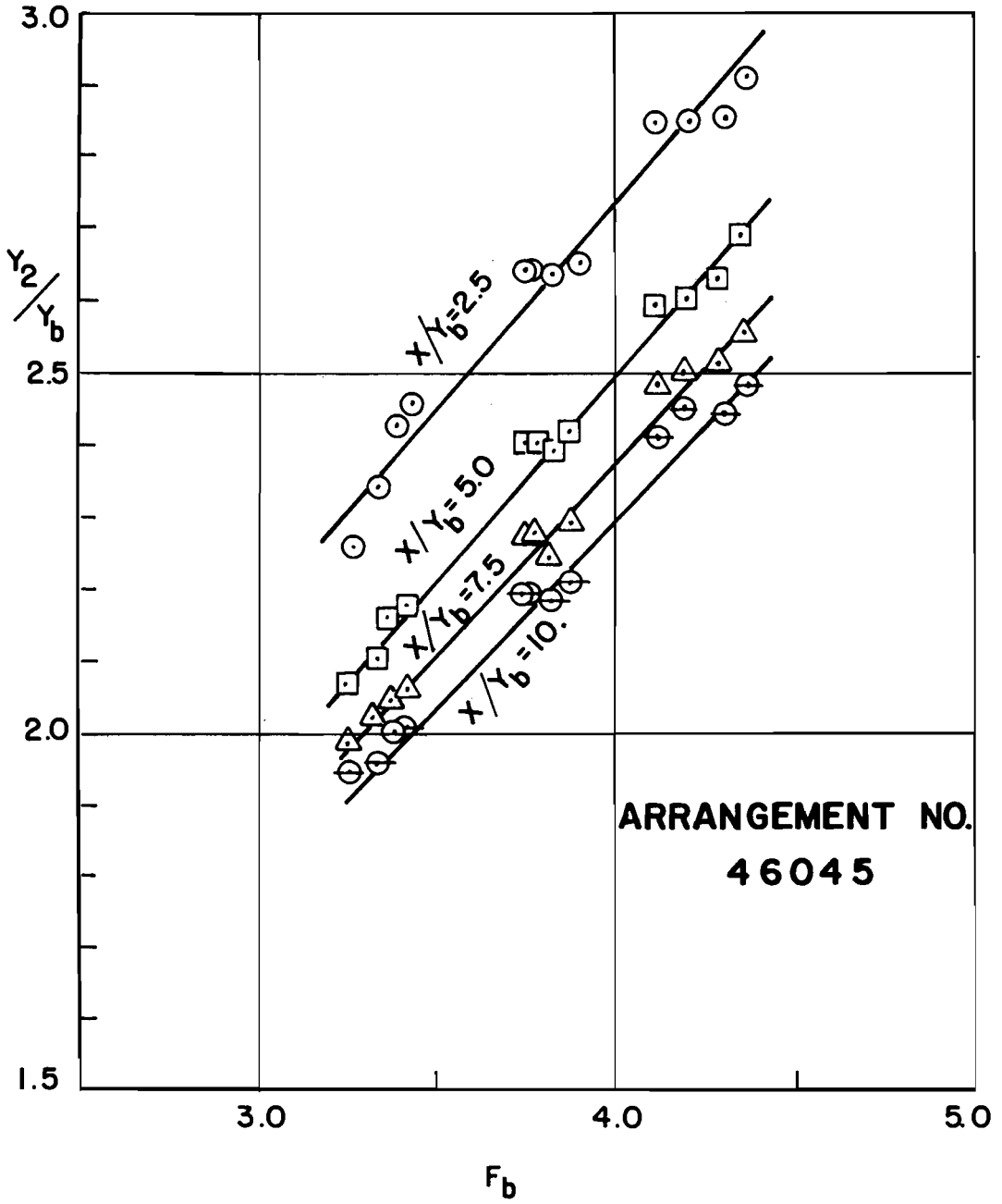

FIGURE III.24 - VARIATION OF Y_2/Y_b vs. F_b

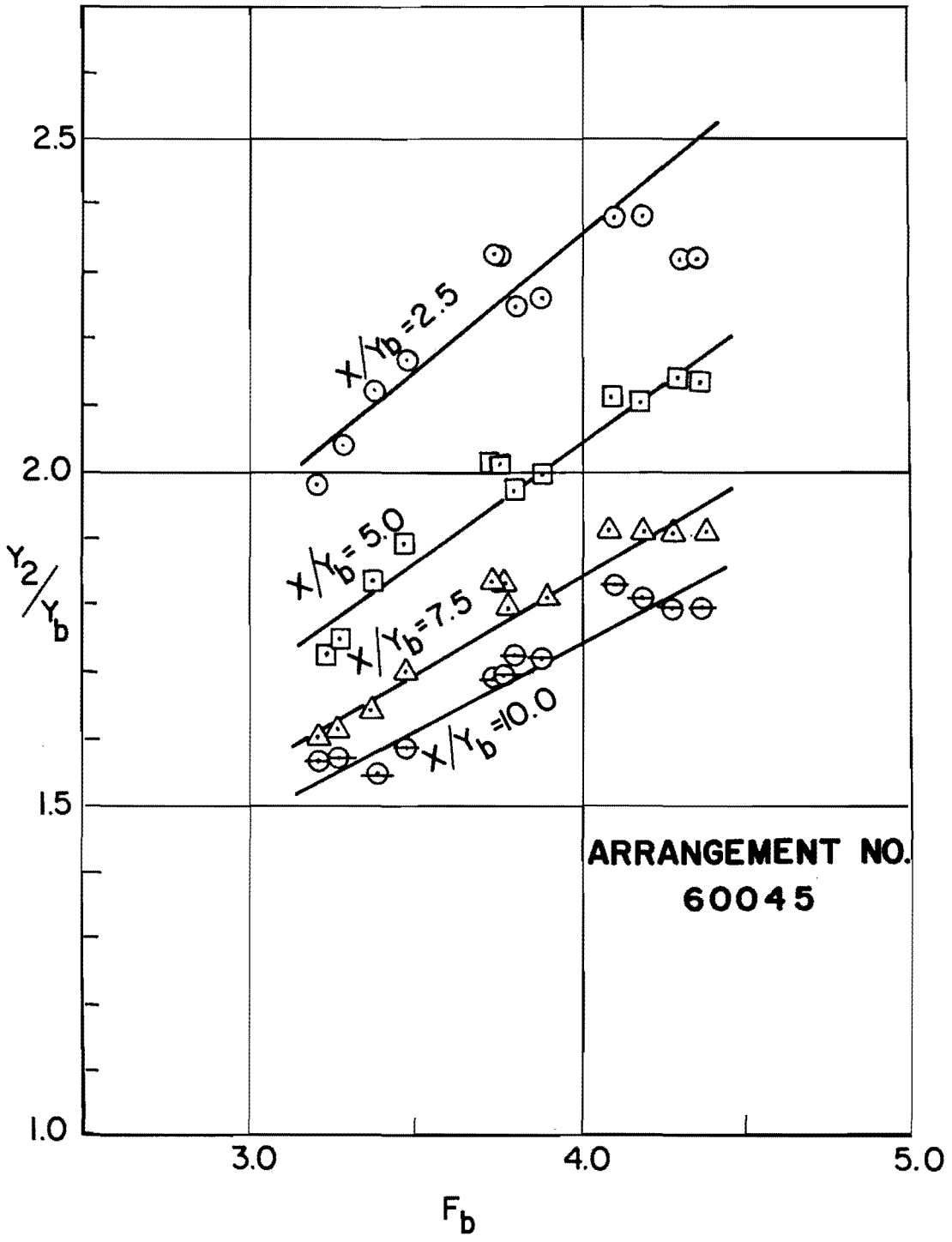

FIGURE III. 25 - VARIATION OF Y_2/Y_b vs. F_b

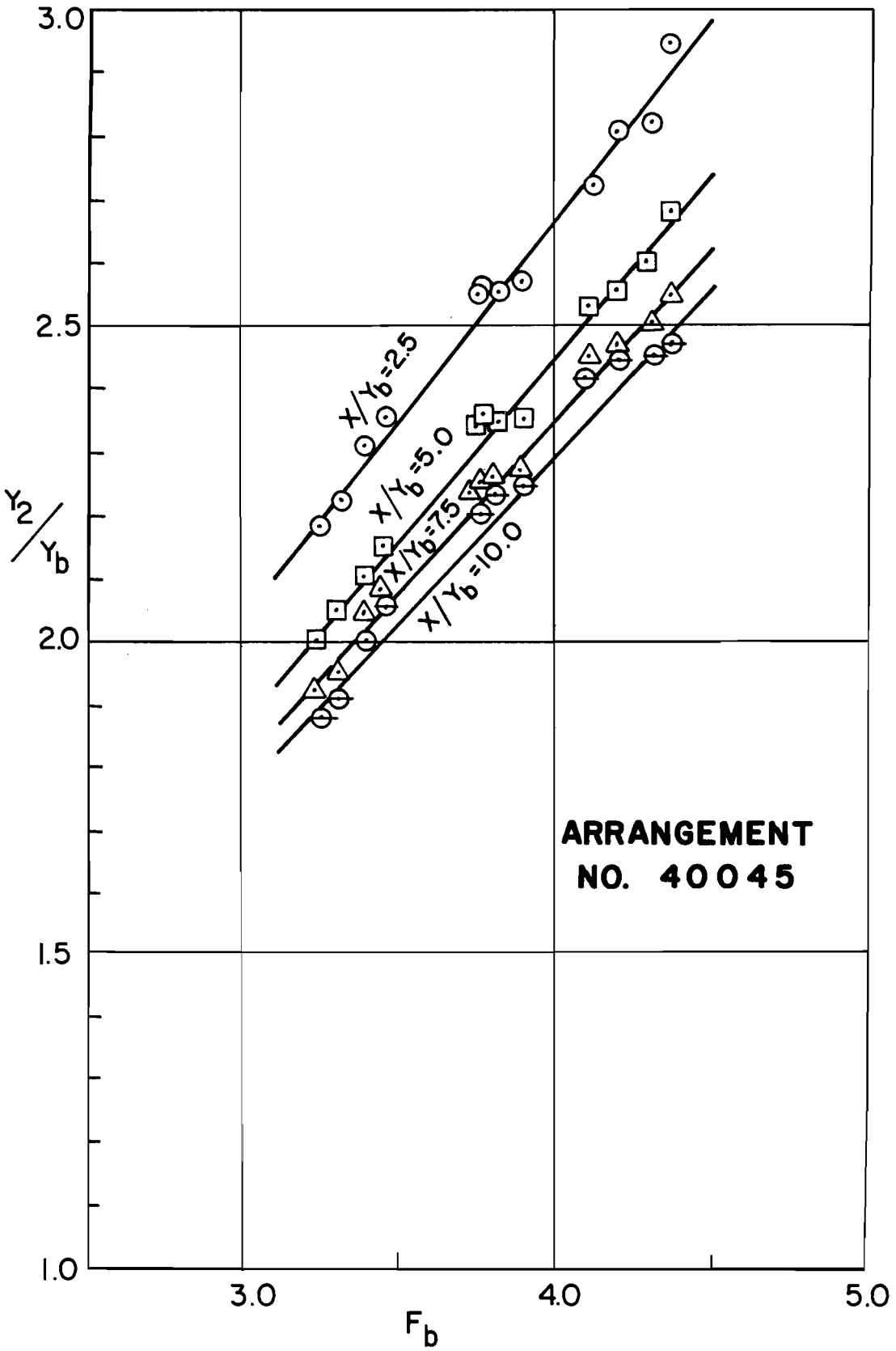

FIGURE III.26 - VARIATION OF Y_2/Y_b vs. F_b

TABLE 4

COMPARISON OF JUMP STABILITY

	Limits of x/y_b Range		
	5.0 to 7.5	5.0 to 10.0	
Arrangement	$\Delta y_2/y_b$	$\Delta y_2/y_b$	L/b
66030	0.21	0.40	4.30
46030	0.17	0.34	2.58
60030	0.21	0.41	4.30
40030	0.16	0.30	2.58
66045	0.15	0.36	2.50
46045	0.11	0.17	1.50
60045	0.16	0.25	2.50
40045	0.08	0.12	1.50

The results given in Table 4 agree in general with those found from the previous comparison in terms of $\Delta y_2/y_t$. It is again indicated that the basins with highest degree of jump stability are Arrangements 60030 and 66030, which, as pointed out earlier, correspond to the largest value of L/b. Also, the lowest degree of jump stability was found for the basins with the smallest L/b value.

Results in terms of y_b and V_b may not, at this time, be made general for values of z/b other than that used in the present study. If the height of drop z/b is changed while the values of r/b and α, the relative vertical curve radius and deflection angle respectively,

are kept constant, it becomes necessary to change the relative length of tangent leading into the stilling basin. This change in relative tangent length may affect the bottom pressure distribution near the basin entrance to such an extent that, at a given value of F_b, the relation obtained for y_2/y_b vs. x/y_b may vary as the value of z/b is varied. The validity of this supposition has not been ascertained herein, since a constant value of z/b was used throughout the present investigation. If the effect of the difference in pressure distribution for different values of z/b were subsequently found to be negligible as far as relations of y_2/y_b vs. x/y_b are concerned, such relations would be of more general use than the y_2/y_t vs. x/y_t functions, since the former would not be restricted to one particular value of z/b.

Velocity Distribution and Reduction

Velocity measurements were made near the bottom of the downstream channel to determine the transverse velocity distribution and the efficiency of stilling action, as measured by the degree of velocity reduction. Velocities were obtained at various sections with particular values of L_x, the distance along the centerline from the leading edge of the hydraulic jump downstream to the section of velocity measurement. The general procedure followed was to set the flow at a given value of F_t and to stabilize the jump at a value of x. Under such conditions, velocity was measured at three different sections as shown in Figure II.6 for each value of F_t used.

The velocity distributions obtained showed generally that the measured velocity near the sides of the channel was very low, while at the center of the channel it varied according to the distance from the leading edge of the jump to the point of measurement. Figure III.27 shows two representative distributions of measured velocity at values of L_x/b of 2 and 3.

It should be observed that since the Pitot tube was placed in a longitudinal position, the measured velocity at some points may be lower than the true velocity. Along the centerline and the lines of points immediately next to and on either side of the centerline, the resultant velocity was nearly parallel to the Pitot tube. At these points the measured velocity coincided with the true velocity within a range of approximately $\pm$0.05 fps.

Along the outside lines of points, and especially for arrangements with B/b of 6, most longitudinal measurements appeared to yield zero velocity. It was observed that eddies formed near the channel walls, which indicated the occurrence of velocities not measured by the Pitot tube in its longitudinal position. Thus at several of these points the Pitot tube was rotated 360^{o} about each point so that the resultant velocity could be determined. The maximum resultant velocity found at any of the points investigated was approximately 0.7 fps. For the present model, such velocity was in the order of $1V_m$.

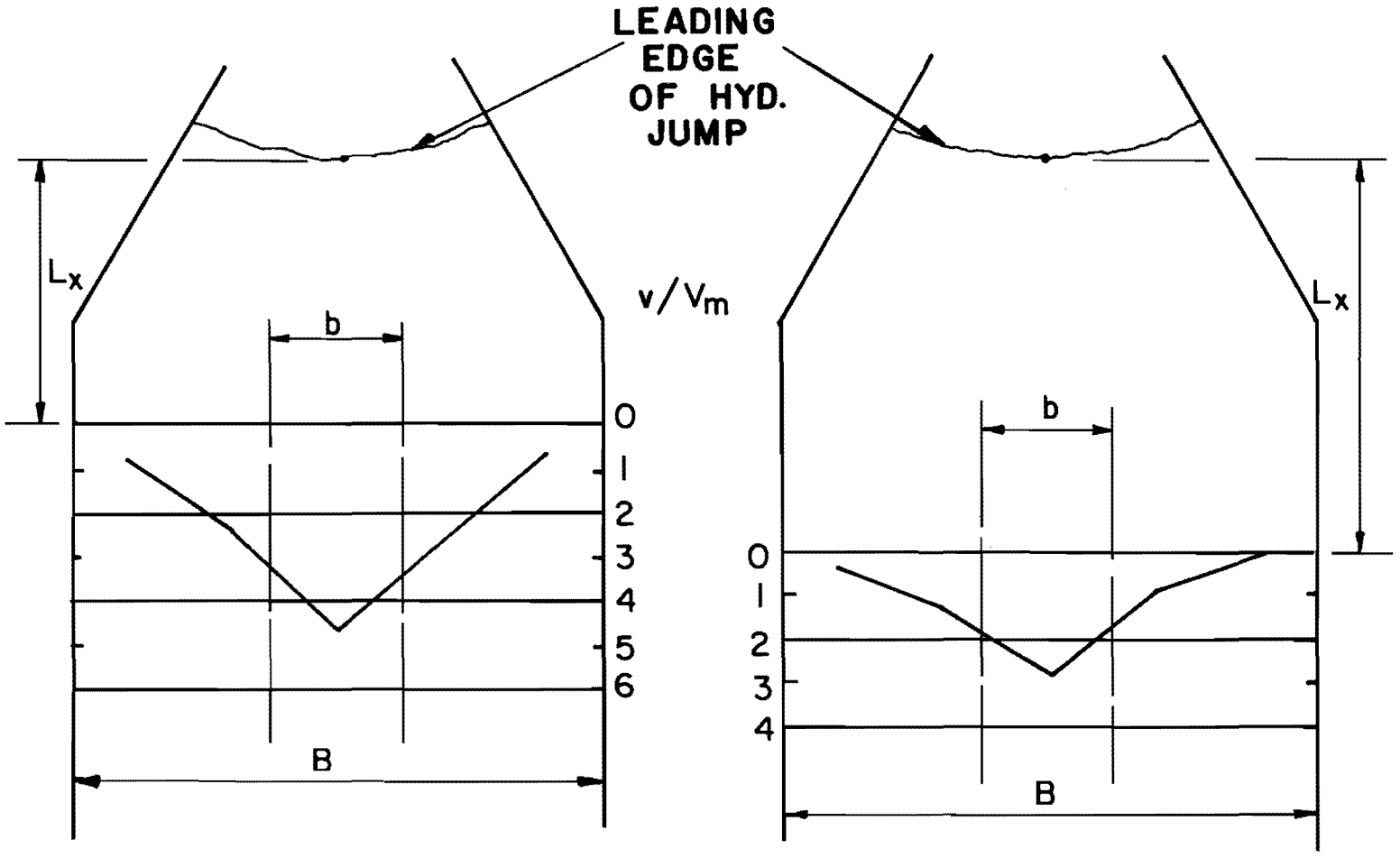

FIGURE III.27 - VELOCITY VARIATION ACROSS CHANNEL WIDTH

In all cases the highest velocity was found at the centerline of each section. At the section nearest the leading edge of the jump, the velocity at the center varied withing the range of 3 to 7 times V_m. Generally, this was equivalent to a velocity ranging from 50 to 85 percent of V_t, the velocity at the beginning of the vertical curve drop. At the middle section, it varied from approximately 2 to 5 times the mean channel velocity, which is equivalent to 30 to 60 percent of V_t. It is considered that centerline velocities at these two sections may be sufficiently high to cause scour of certain unprotected channel beds.

At the section farthest downstream from the leading edge of the jump, the centerline velocity varied from approximately 1 to 4 times the mean channel velocity. This range corresponds to approximately 15 to 50 percent of V_t. For arrangements in the lower portion of this range, such as Arrangement 40030, the concrete bottom slab of a prototype may in many instances be safely ended at this section. Such a basin would have a length of approximately 6b, measured from the beginning of the flared wingwalls to the downstream end of the basin slab.

Each range of velocity variation discussed above includes the effect of changes in basin geometry and variations in F_t. For any one basin geometry and at a given section, the general tendency of the ratio of measured velocity to mean channel velocity was to increase slightly as the Froude number F_t was increased. Much

larger variations in the ratio of measured velocity to mean channel velocity at a constant value of F_t were experienced as the basin geometry was changed. The ratio of measured velocity at the centerline to mean channel velocity for all arrangements except 46030 has been plotted versus F_t for values of L_x/b of 2, 3, and 4 in Figures III.28, III.29, and III.30 respectively. It is not the purpose of these graphs to define a function between the plotted variables, but rather to provide a graphical comparison of velocity reduction of the various geometric arrangements. Also, the variation of the ratio of centerline velocity to mean channel velocity vs. the ratio L_x/b, at a value of F_t of 2.1, has been plotted in Figure III.31 for the two arrangements which yielded the approximate extremes of the velocity ranges given in the foregoing paragraphs. This data shows that the absolute value of the centerline velocity for arrangement 60045 is more than that for arrangement 40030 at $L_x/b = 4.0$ since the ratio of the respective mean velocities is approximately 1.2.

At any given value of F_t and L_x/b, the general trend found was for lower values of the ratio of measured velocity to mean channel velocity to exist for basin arrangements with $\theta = 30°$. The highest values were obtained for arrangements 60045 and 66045. At the section $L_x/b = 4$, measured velocity for these two arrangements was in the order of 3.5 to 4 times the mean channel velocity. For many erodible channels, such order of velocity might help to create a situation of excessive scour if channel protection were ended at the section of $L_x/b = 4$.

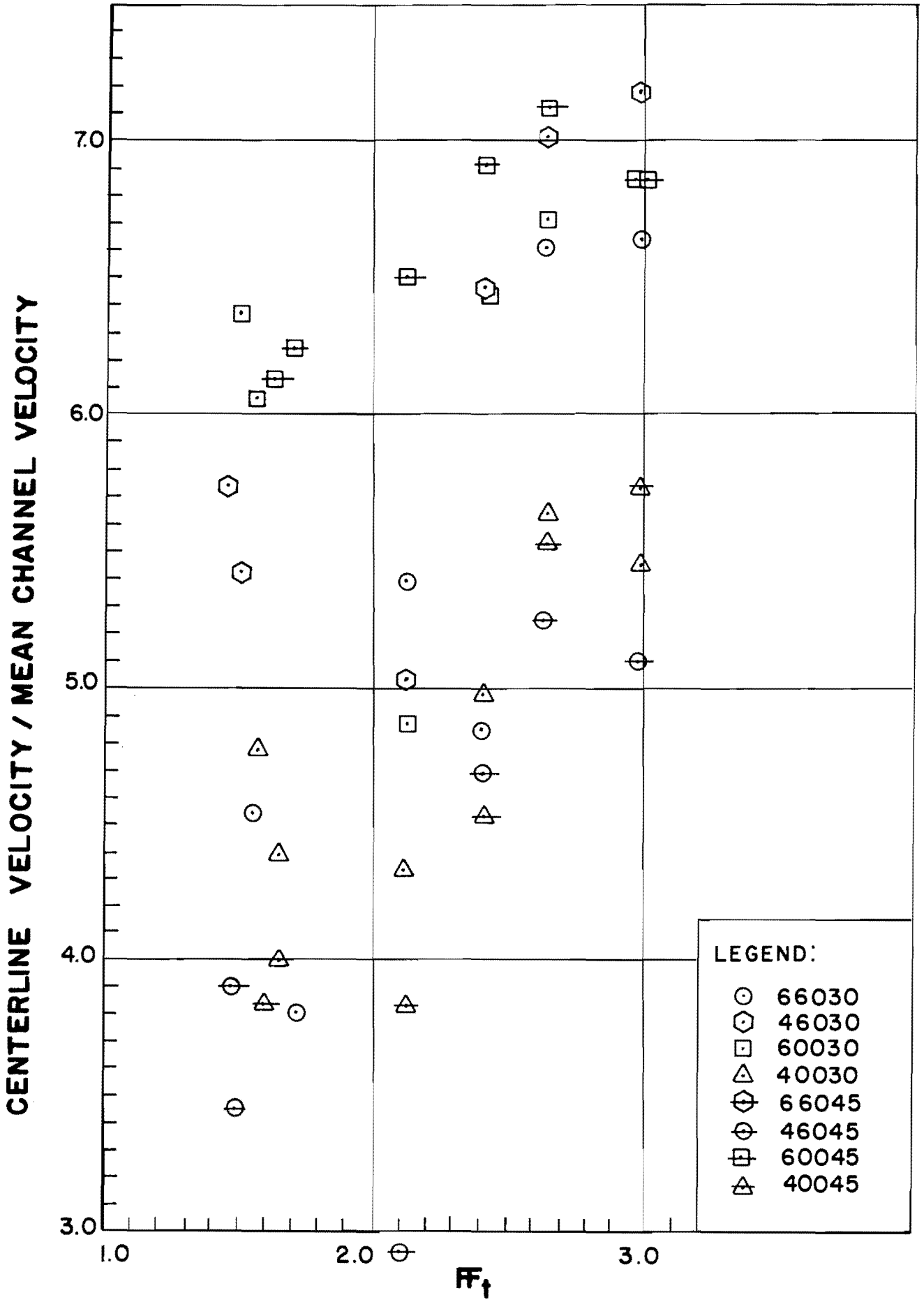

FIGURE III.28 - (V_{ℓ}/V_m) vs. F_f FOR VARIOUS BASIN ARRANGEMENTS AT $L_x/b = 2$

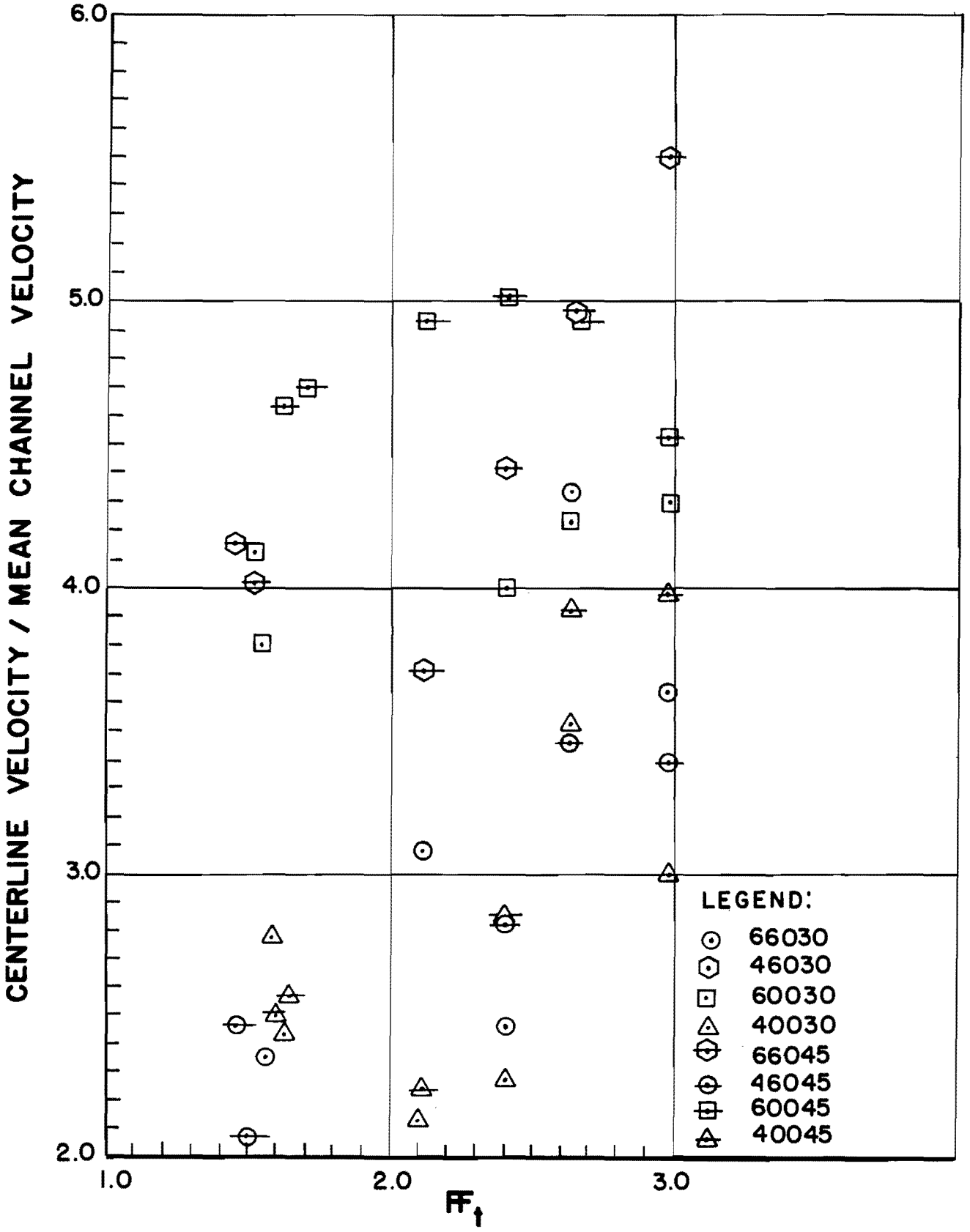

FIGURE III.29 - (V_{ℓ}/V_m) vs. F_f FOR VARIOUS BASIN ARRANGEMENTS AT $L_x/b = 3$

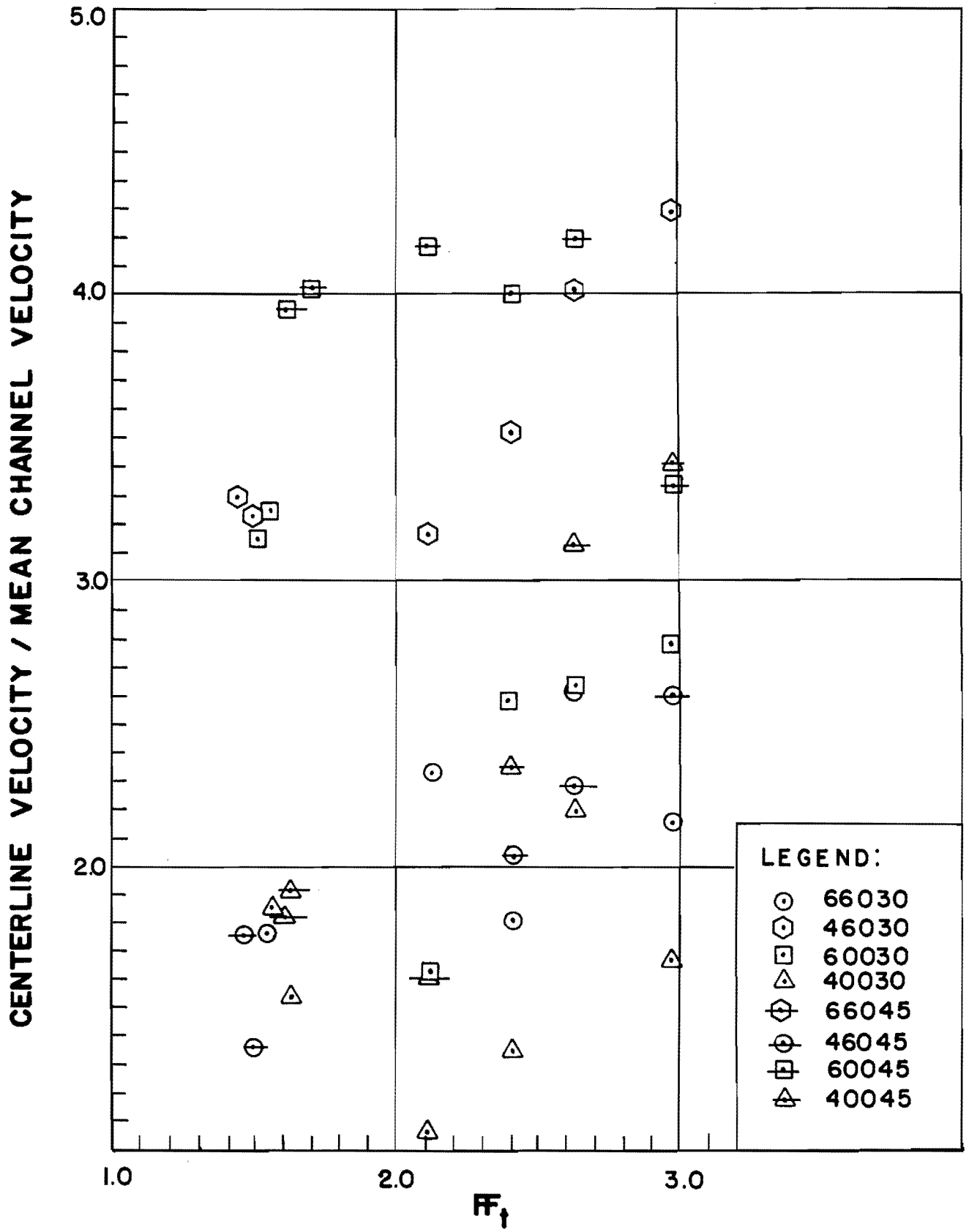

FIGURE III.30 - (V_ℓ / V_m) vs. F_t FOR VARIOUS BASIN ARRANGEMENT AT $L_x / b = 4$

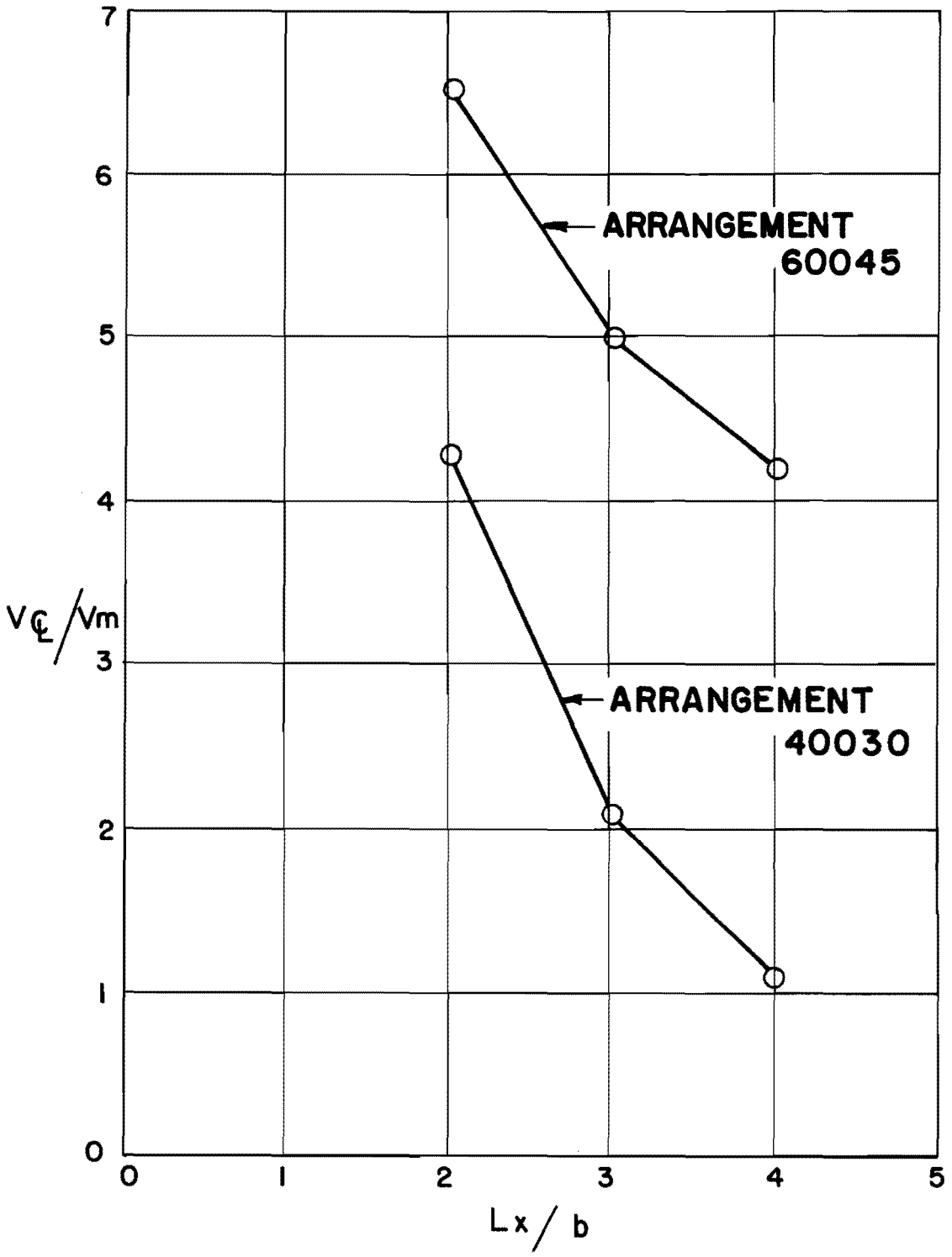

FIGURE III.31 - EXTREME VALUES OF $V_{\mathbb{C}}/V_m$ vs. L_x/b AT $F_t = 2.1$

It must be noted that in most cases of $L_x/b = 4$, points removed only a short distance from the centerline yield much lower velocities than that found at the centerline. This situation suggests that if the flow in the region of the centerline can be slowed down by some suitable method, the required length of protected channel bottom would be considerably reduced.

Water Surface Profiles

In order to determine the degree of angular uniformity and depths of flow in the basin, measurements on the free surface were made along several radial lines. For basins with $\theta = 30°$, measurements were made along lines 15° and 30° from the centerline, and along the centerline. For basins with $\theta = 45°$, measurements were taken on lines 15°, 30°, and 45° from the centerline, and on the centerline.

Generally it was found that at any given section, the flow depth at the centerline was higher than depths at the intermediate lines. For points between x/y_t of about 2 and the downstream end of the flared wall region, depths along the intermediate lines varied between 50 and 75 percent of depths along the centerline, at given transverse sections. In all cases, it was found that flow depths decreased as the flow progressed downstream to the point of formation of the hydraulic jump, which was held near the end of the flared walls throughout the depth measurements.

Along the flared wingwalls, a high wave formed in all cases immediately downstream of the basin entrance. The height of the wave varied approximately within the range of 0.45z to 0.55z. The

lower part of this range corresponds to arrangements with $\beta = 60^{o}$, the upper part to those with $\beta = 0$. For each value of β, slightly lower values of the wave height were found for arrangements with $\theta = 30^{o}$ than for those with $\theta = 45^{o}$. The section at which the wave crest occurred also varied as the angle θ was changed. The distance x to the section where the maximum wave height occurred was from 1.2z to 1.3z for $\theta = 30^{o}$. For $\theta = 45^{o}$, it varied within the range of 0.8z to 0.9z. Several representative surface profiles along various radial lines are shown in Figures III.32 and III.33.

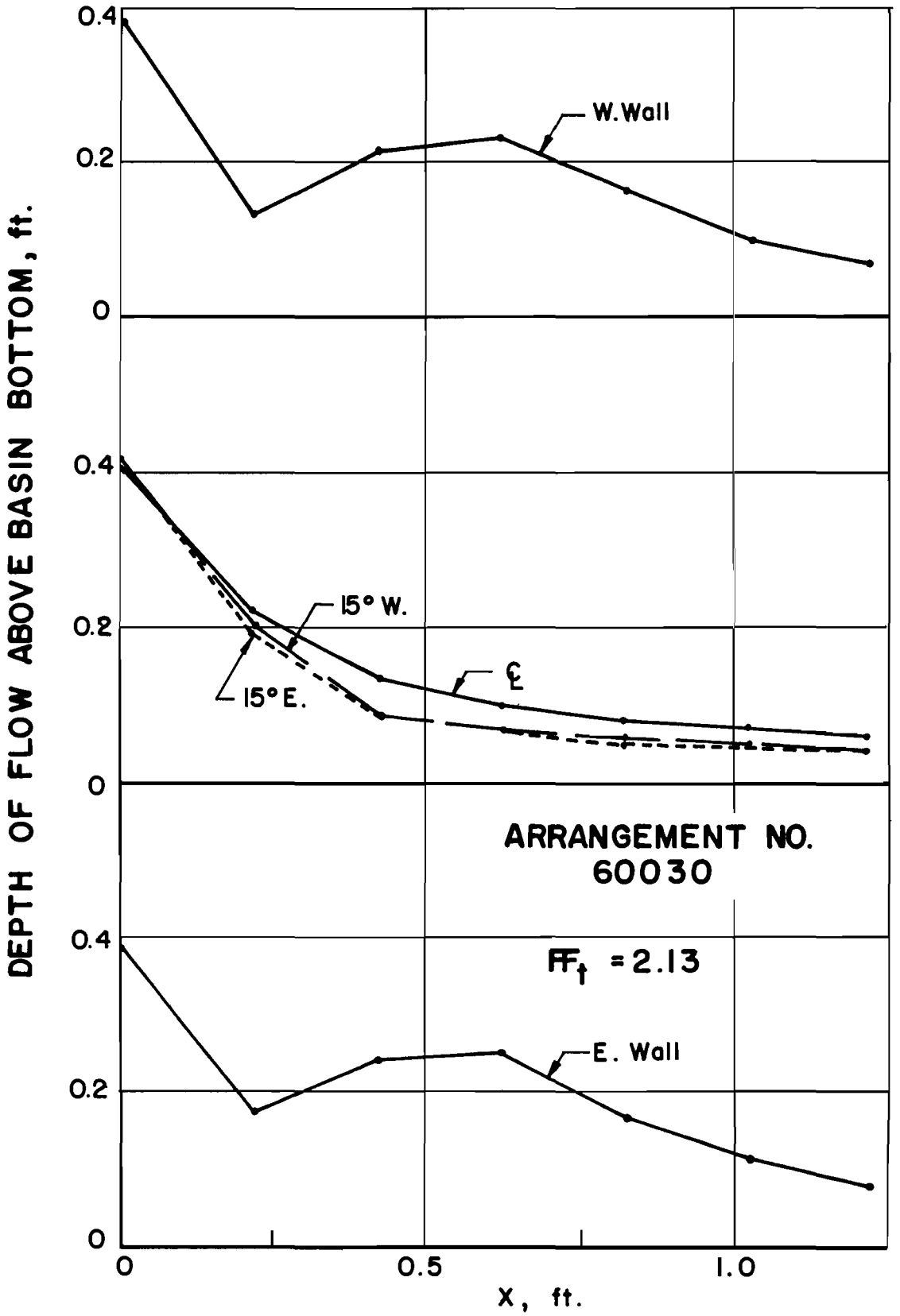

FIGURE III.32 - WATER SURFACE PROFILES OF FLOW IN STILLING BASIN

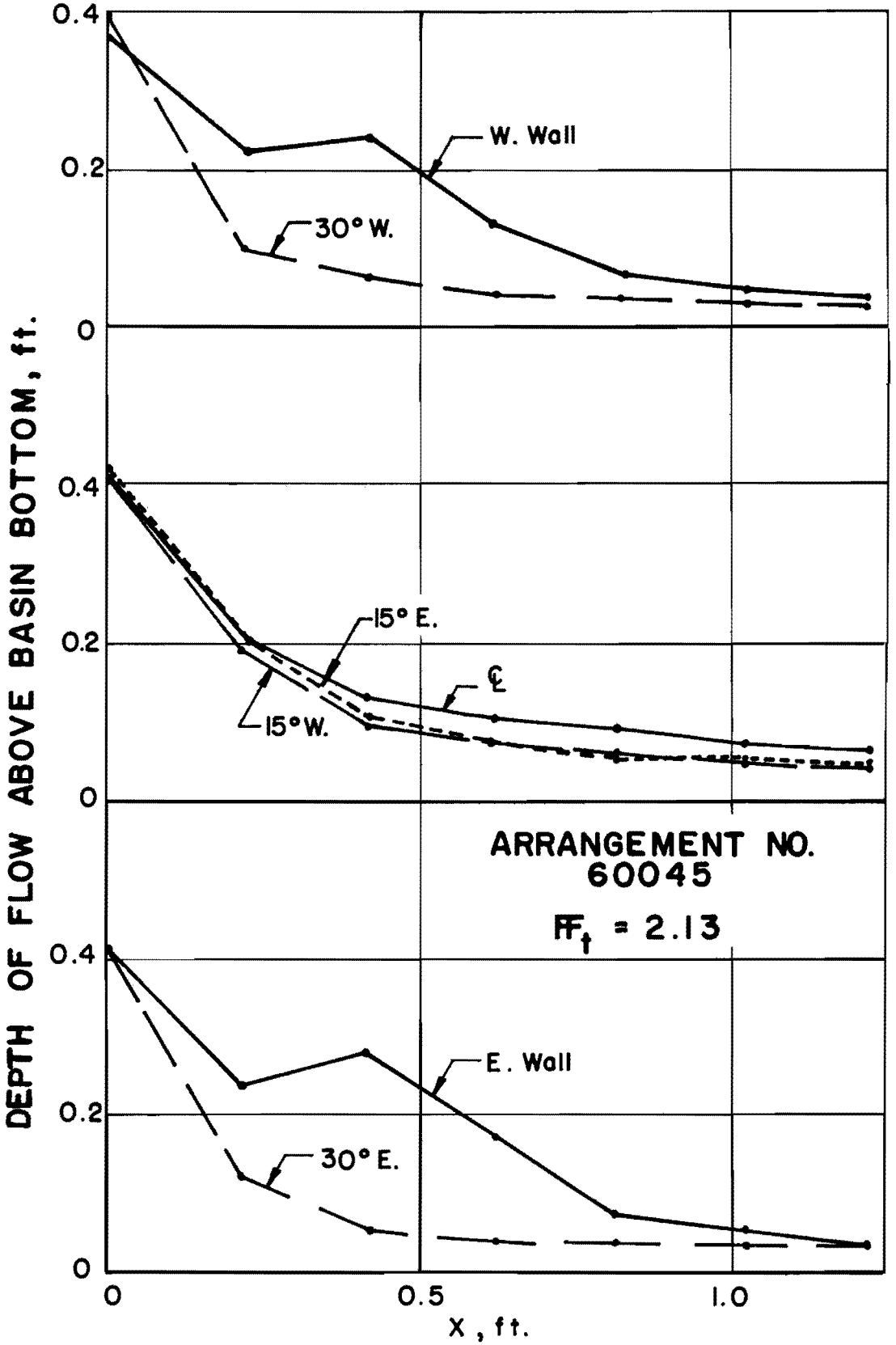

FIGURE III.33 - WATER SURFACE PROFILES OF FLOW IN STILLING BASIN

Chapter IV

CONCLUSIONS

Since the present investigation has been an exploratory study of a new type hydraulic sturcture, the results obtained herein have provided basic knowledge of its performance characteristics regarding hydraulic jump stability, absolute tailwater requirements, and efficiency of stilling action as measured by reduction of velocity near the channel bottom. Results have also indicated the degree to which the initially parallel flow is converted to radial flow by the different geometric configurations used in the present study.

The stability of the hydraulic jump, defined by the decrement of relative tailwater depth required for the jump to move a certain relative distance downstream, was found to be greatest for the geometric arrangements with the largest value of L/b, the relative length of the flared wingwall region. This behavior corroborates the observation that a higher degree of jump stability is attained in the region with flared wingwalls than in the parallel channel.

The two basin arrangements which displayed the highest degree of stability were 60030 and 66030, followed by 46030 and 40030. The entrance channel bottom angle β did not appear to have any distinct influence on the jump stability characteristics of

the stilling basin. From a construction point of view, the entrance bottom with $\beta = 0$ is the preferable choice since it would be simpler and thus more economical to construct.

The different basin geometric arrangements were also ranked according to the absolute tailwater depth required for the jump to be held within a certain region. The lowest tailwater requirements were found for Arrangement 60045, followed by 66045. When the jump was held in the region near the entrance channel drop, the next two arrangements with lowest tailwater requirements were 46045 and 40045. When the jump was allowed to occur farther downstream, the third and fourth lowest tailwater requirements were given by Arrangements 60030 and 66030.

From a point of view of hydraulic design aimed at holding the hydraulic jump within the stilling basin, the most attractive configurations appear to be Arrangement 60045, for cases where the parameter B/b is in the order of 6, and Arrangement 40045 for cases where the value of B/b is in the order of 4.

Velocity measurements near the channel bottom were made in order to estimate the efficiency of stilling action and the angular uniformity of the radial flow. Such measurements indicated that velocity reduction is adequate near the sides of the channel, but along the centerline, for most cases additional reduction in velocity would be desirable. At the section $L_x/b = 4$, measured centerline velocities ranged from 1 to 4 times the mean velocity in the downstream

channel. It is estimated that in most instances a prototype structure may be safely operated at velocities in the lower portion of this range, without excessive scour immediately downstream of the basin.

The geometric arrangements for which the best stilling action was obtained were those with $\theta = 30^{\circ}$. Although these arrangements required higher tailwater than those with $\theta = 45^{\circ}$, they are recommended for use in cases where tailwater is sufficiently high, and topography is such that the entrance channel drop may be accommodated. The required length of the stilling basin would vary, depending on the characteristics of the channel bed and on the desirability of using riprap or other bed protection downstream of the stilling basin. The minimum distance required to reduce the velocity near the bottom to approximately $1V_m$ is in the order of 6b, measured from the beginning of the flared wingwalls. The length of the stilling basin structure may be less than 6b, especially in cases where bed protection is provided downstream of the stilling basin. Such length would be comparable to or slightly greater than that specified for most existing designs, which require sills, baffle blocks, impact walls, etc. The prospect for improving the performance or reducing the length of the present structure by means of simple sills or end sills remains to be determined. Even if a greater length is required for the present structure, the advantages of simple construction and debris free operation would seem to justify its use where conditions are favorable.

Chapter V

SUGGESTIONS FOR FUTURE STUDY

The field for future study is very wide; one needs only to consider the limited ranges of variables investigated and the limited parameters which were held constant to realize the numerous variations which may still be the object of future studies.

One geometric combination which was held constant was that of r, z, and α. The angle α may affect the degree of spreading considerably, which in turn may modify the distribution of velocity in the region of the jump. Since velocity distributions across the channel width were found to be lacking in uniformity, an entrance channel with a larger angle α should be investigated. Such a change in α would require a change of either r or z. It is felt that r should not be decreased in order to avoid any lower pressures on the bottom, therefore, z could be varied within reasonable limits.

Another variation which may be investigated in the interest of more uniform velocity distribution is the addition of a rise in the channel bottom at or near the downstream end of the flared basin wingwalls. Besides the possibility of providing better velocity distribution, such a rise would lower the tailwater depth required to hold the jump in the basin.

One phase which should also be investigated is the adaptability of the present structure to circular pipe culverts. The structure may be connected to a circular pipe at some point along the entrance channel, and its performance characteristics under such conditions investigated. The connection between the circular pipe and the rectangular entrance channel should occur either at the point of curvature (P.C.) of the bottom, or some distance upstream from it. Such a distance may become a new significant variable to be investigated.

BIBLIOGRAPHY

1. Argue, J. R., "New Structure for Roadway Pipe Culverts," Journal of the Institution of Engineers, Australia, Vol. 32, No. 6 (June, 1960.)

2. Blaisdell, F. W. and Donnelly, C. A., "The Box Inlet Drop Spillway and Its Outlet," Transactions, ASCE, Vol. 121, pp. 955-986 (1956.)

3. Blaisdell, F. W., "The SAF Stilling Basin," U. S. Soil Conservation Service, Report SCS-TP-79 (May, 1949.)

4. Bossy, H. G., "Culvert Design Manual," Bureau of Public Roads (Unpublished material.)

5. Bradley, J. N. and Peterka, A. J., "The Hydraulic Design of Stilling Basins: Small Basins for Pipe or Open Channel Outlets," Proceedings, ASCE, Journal Hydraulics Division, Vol. 83, No. HY5, Paper No. 1406 (1957.)

6. Chow, V. T., Open-Channel Hydraulics, McGraw-Hill Book Co., New York (1959.)

7. Davis, W. B., "Transition Phenomena in Radial Free Surface Flow," M. S. Thesis, Massachusetts Institute of Technology (1958.)

8. Keim, S. R.,"The Contra Costa Energy Dissipator," Proceedings, ASCE, Journal Hydraulics Division, Vol. 88, No. HY2 (March, 1962.)

9. Kunz, K. S., Numerical Analysis, McGraw-Hill Book Co., New York (1957.)

10. Morris, H. M., Applied Hydraulics in Engineering, The Ronald Press Co., New York (1963.)

11. Sadler, C. D. and Higgins, M. S., "Radial Free Surface Flow," M. S. Thesis, Massachusetts Institute of Technology (1963.)

12. Vallentine, H. R., Applied Hydrodynamics, Butterworth and Co. Ltd., London (1959.)

APPENDIX

Appendix

FREE SURFACE POTENTIAL FLOW NEAR BOUNDARY INTERSECTION

The solution of this problem was obtained by performing several transformations of the flow pattern. Throughout such operations, the flow was transformed from its physical pattern, called the z-plane, to a pattern of uniform flow, known as the w-plane. Following are the transformations made and sketches of the pattern of flow obtained for each plane.

z-plane

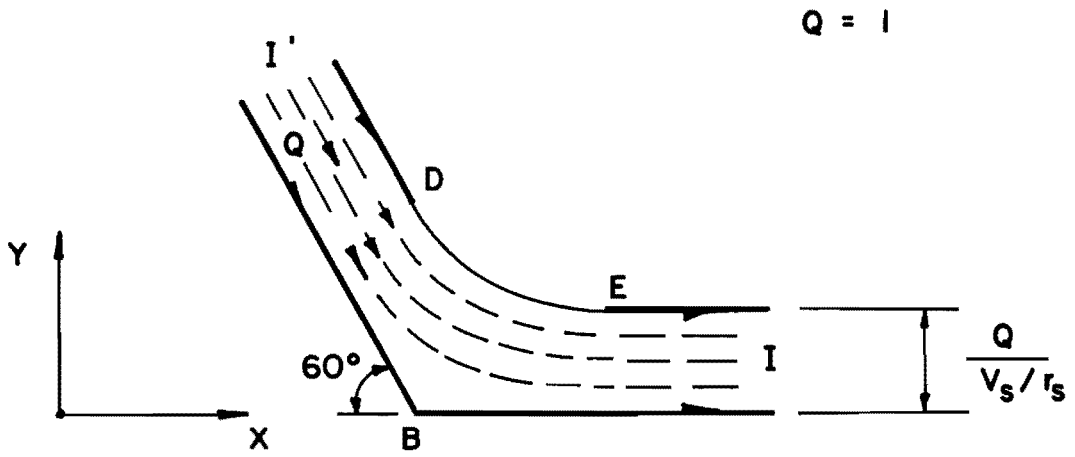

V_s = Free streamline velocity

V_u = Uniform velocity of confined region of flow

$r_s = V_s/V_u \quad > 1$

(i) z-plane to ζ -plane

$$\zeta = \left|\frac{1}{V}\right| e^{i\alpha'}$$

where:

V = Velocity of flow at any point

α' = Angle formed on the z-plane by a horizontal line and the velocity vector at any point of the flow field

In order to simplify numerical operations, without altering the proportions of the flow, let the free streamline velocity $V_s = 1$.

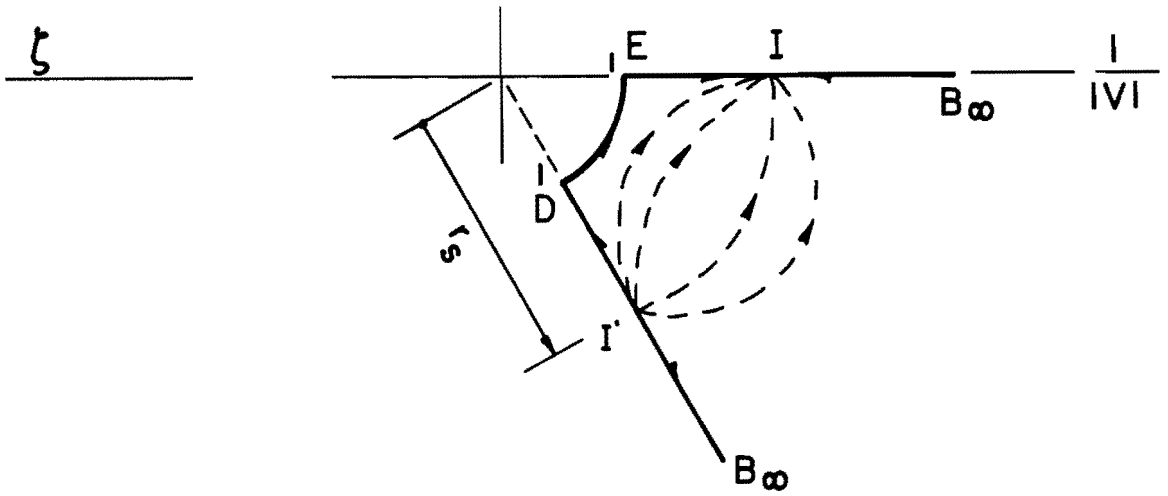

(ii) ζ -plane to ζ' -plane

$$\zeta' = \ln \zeta = \ln\left|\frac{1}{V}\right| + i\alpha'$$

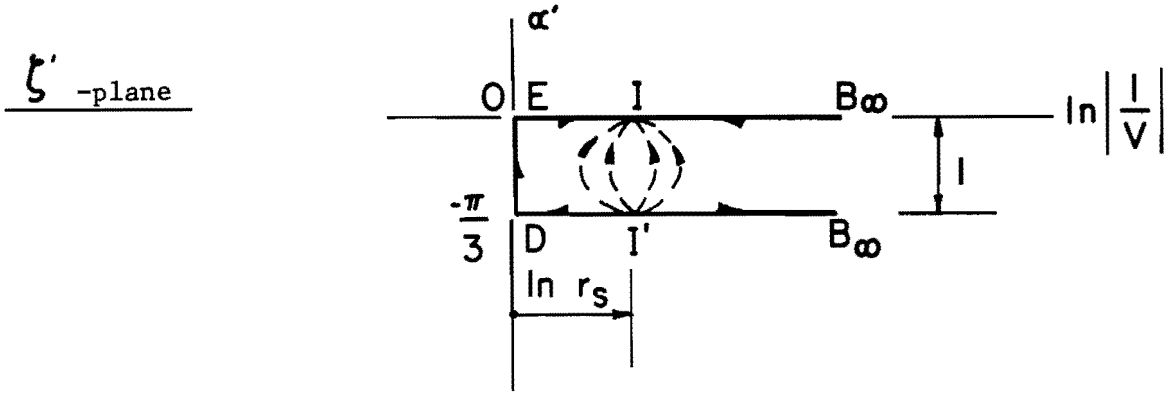

(iii) ζ' - plane to t-plane

$$t = \cosh \frac{\pi}{l} (\zeta' - \zeta_1')$$

is the transformation for a horizontal semi-infinite strip with its lower finite vertex at ζ_1'.

For the present case, $\zeta_1' = -i\,\pi/3$ and $l = \pi/3$, therefore:

$$t = \cosh \frac{\pi}{\pi/3} (\zeta' + i\,\pi/3) = \cosh (3\zeta' + i\,\pi)$$

t-plane

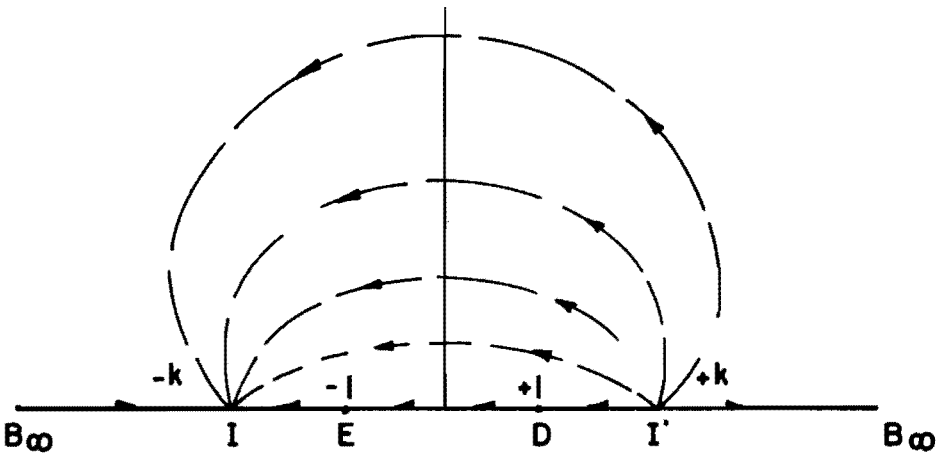

The pattern in the upper half of the t-plane is found to be a source at t = +k, and a sink at t = -k. The value of k may be obtained by considering the source at I' thus:

At I', $\zeta' = \ln r_s - i\,\pi/3$

$$t_{I'} = k = \cosh (3 \ln r_s - 3\,i\,\pi/3 + i\,\pi) = \cosh (3 \ln r_s) = \frac{r_s^3 + 1/r_s^3}{2}$$

(iv) t-plane to w-plane

The equation for the pattern in the t-plane is:

$$\omega = (Q/2\pi)\ln(t-k) - (Q/2\pi)\ln(t+k)$$

Since Q = 1

$$\omega = \frac{1}{2\pi}\ln(t-k) - \frac{1}{2\pi}\ln(t+k) = \ln\left(\frac{t-k}{t+k}\right)^{1/2\pi}$$

w-plane

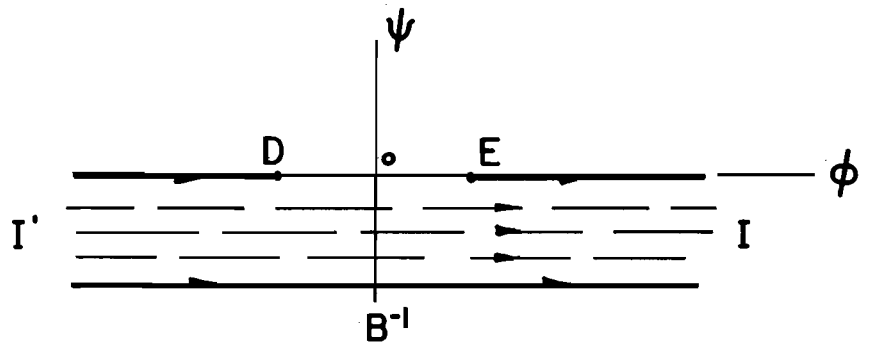

From the equation for w:

$$d\omega = \frac{1}{2\pi}\left[\frac{dt}{(t-k)} - \frac{dt}{(t+k)}\right] = \frac{1}{2\pi}\left[\frac{1}{(t-k)} - \frac{1}{(t+k)}\right]dt$$

Along the free streamline:

$|V| = 1$ and ψ = constant, so that $d\psi = 0$

$$d\omega = d\phi = \frac{d\phi}{ds}\,ds = V\,ds$$

$$\therefore\ d\omega = ds$$

where s is measured along the free streamline

Also along the free streamline:

$$\zeta = i\,\alpha'$$

$$t = \cosh(3\zeta' + i\pi) = \cosh(3i\alpha' + i\pi) = \cosh[i(3\alpha' + \pi)]$$
$$= \cos(3\alpha' + \pi) = -\cos 3\alpha'$$

$$dt = 3 \sin 3\alpha'\, d\alpha'$$

$$ds = dw = \frac{1}{2\pi}\left[\frac{1}{-\cos 3\alpha' - k} - \frac{1}{-\cos 3\alpha' + k}\right] x\ 3 \sin 3\alpha' d\alpha'$$

$$dx = ds \cos\alpha' = \frac{3}{2\pi} \sin 3\alpha' \cos\alpha' \left[\frac{1}{\cos 3\alpha' - k} - \frac{1}{\cos 3\alpha' + k}\right] d\alpha'$$

$$dy = ds \sin\alpha' = \frac{3}{2\pi} \sin 3\alpha' \sin\alpha' \left[\frac{1}{\cos 3\alpha' - k} - \frac{1}{\cos 3\alpha' + k}\right] d\alpha'$$

$$dx = \frac{3}{2\pi} \sin 3\alpha' \cos\alpha' \left[\frac{2k}{\cos^2 3\alpha' - k^2}\right] d\alpha' \qquad (A.1)$$

$$dy = -\frac{3}{2\pi} \sin 3\alpha' \sin\alpha' \left[\frac{2k}{\cos^2 3\alpha' - k^2}\right] d\alpha' \qquad (A.2)$$

Equations (A.1) and (A.2) were integrated numerically by Kutta's third-order rule (9). Results yielded corresponding x/y_u and y/y_u coordinates of the free streamline at given values of α'. After coordinates of the free streamline were calculated, thus establishing the upper boundary of the flow, stream function values were determined at nodes of a rectangular grid system covering the

required flow field. Stream function values were calculated numerically by Liebmann's method of relaxation (9). Streamlines were graphically interpolated on the grid system to yield the solution presented in Figure I.6.